UNIVERSITATEA DE MEDICINĂ ŞI FARMACIE “IULIU HAŢIEGANU”CLUJ-NAPOCA

ŞCOALA DOCTORALĂ

CLUJ-NAPOCA 2022

DOCTORAL THESIS

Innovative nanomaterials as building blocks of (bio)sensors

Candidate	**Gheorghe Melinte**
PhD coordinators	**Prof.Dr. Cecilia Cristea**
	Prof.Dr. Giovanna Marrazza

UMF
UNIVERSITATEA DE MEDICINĂ ȘI FARMACIE
IULIU HAȚIEGANU
CLUJ-NAPOCA

UNIVERSITÀ
DEGLI STUDI
FIRENZE

Acknowledgements

I would like to express my very great appreciation to Professor Cecilia Cristea and Professor Giovanna Marrazza, my research supervisors, for their valuable and constructive suggestions during the planning and development of this research work. Their continuos support can be seen in every aspect of this thesis, from the ingenuity of the research work to the high impact of the journals that published the results.

A very special thanks go to Oana for always finding the right words to keep me motivated to continue no matter how difficult the situation was, for helping me understand better every aspect of the work and for always being a mentor worth following.

I would also want to thank Dr. Bogdan Feier, Dr. Mihaela Tertiș and Dr. Andreea Cernat for always being open to help me, both with scientific advices and numerous life lessons that helped me become a more mature scientist and human.

Special thanks are also given to the committee for evaluating and improving my thesis.

I want to thank to all my colleagues from the Cluj research group, starting with the more experienced ones: Prof. Dr. Radu Oprean, Prof. Dr. Ede Bodoki, Dr. Ioana Tiuca, Dr. Bogdan Iacob, for their advices and wisdom, and to the younger ones: Iulia, Adi, Magda, Florina, Ani, Ale, Denisa, for making the hours spent in the laboratory passing fast and with joy. I want to give special thanks to the entire staff of University of Florence for helping me with any minor or major problems I had during this co-joint thesis, with special thanks to Prof. Dr. Papini. I felt like home in Florence, and for that I have to thank Tiziana with whom a pandemic lockdown passed in a moment and my Italian improved significantly and to all my colleagues from the lab: Giulia, MariaGrazia, Naomi, Ilaria and all the others I did not manage to name here, they stopped being just colleagues, they became friends.

My family had a very important role in choosing this career path and I want to thank them for that and for their constant support during these years.

Finally, I want to thank Andreea for being there for me and for supporting any decision I made during this PhD. She was the most loving and supportive person, constantly improving my moral, and encouraging me throughout these years.

Publications

List of ISI Publications as 1st author

1. **Gheorghe Melinte,** Oana Hosu, Cecilia Cristea, Giovanna Marrazza, *Ara h1 peanut allergen detection using a labelled electrochemical aptasensor based on GO-COOH@bimetallic composite platform.* Food Chemistry 2022, 134074, https://doi.org/10.1016/j.foodchem.2022.134074, (IF: 9.231, Q1) **(Personal contributions, Chapter III.3)**

2. **Gheorghe Melinte#,** Oana Hosu#, Cecilia Cristea, Giovanna Marrazza, *DNA sensing technology a useful food scanning tool,* Trends in Analytical Chemistry 2022, 154, 116679, https://doi.org/10.1016/j.trac.2022.116679 (IF: 14.908, Q1) **(State of the art, Chapter IV.3)**

3. **Gheorghe Melinte**, Oana Hosu, Geanina Ştefan, Diana Bogdan, Cecilia Cristea, Giovanna Marrazza, *Poly-L-Lysine@gold nanostructured hybrid platform for Lysozyme aptamer sandwich-based detection*, Electrochimica Acta. 2022, 403, 139718, https://doi.org/10.1016/j.electacta.2021.139718 (IF: 7.336, Q2) **(Personal contributions, Chapter II.2)**

4. **Gheorghe Melinte**, Giulia Selvolini, Cecilia Cristea, Giovanna Marrazza, *Aptasensors for Lysozyme detection: Recent advances*, Talanta, 2021, 226, 122169, http://doi.org/10.1016/j.talanta.2021.122169 (IF: 6.557, Q1) **(State of the art, Chapter II.2)**

5. **Gheorghe Melinte**, Andreea Cernat, Aurora Petica, Oana Lazar, Marius Enachescu, Liana Anicai, Cecilia Cristea, *Electrochemical non-enzymatic detection of glucose based on 3D electroformed copper nanostructures*, Materials, 2020 13(12), 2752, https://doi.org/10.3390/ma13122752 (IF: 3.623, Q1) **(Personal contributions, Chapter I.1)**

6. **Gheorghe Melinte,** Andreea Cernat, Maria-Bianca Irimes, Szabolcs János Györfi, Mihaela Tertis, Maria Suciu, Liana Anicai, Robert Sandulescu and Cecilia Cristea, *Selective Detection of Folic Acid Using 3D Polymeric Structures of 3-Carboxylic Polypyrrole*, Sensors 2020, 20, 2315, https://doi.org/10.3390/s20082315 (IF: 3.576, Q1) (**Personal contributions, Chapter III.1)**

7. **Gheorghe Melinte#**, Oana Hosu#, Cecilia Cristea, Giovanna Marrazza, *Electrochemical fingerprint of Arsenic (III) by using hybrid nanocomposite*

based platforms, Sensors 2019, 19(10), 2279, https://doi.org/10.3390/s19102279 (IF: 3.275, Q1) (**Personal contributions, Chapter II.1)**

List of ISI publications as first author with equal contributions

8. Oana Hosu[#], **Gheorghe Melinte**[#], Geanina Ștefan, Magdolna Casian, Cecilia Cristea, *Towards selective tetracycline recognition in wastewater based on gold nanovoids@aptamer sensing*, *Electrochimica Acta*, submitted ([#] Equal contribution) **(Personal contributions, Chapter III.2)**

9. Anca Florea[#], **Gheorghe Melinte**[#], Ioan Simon, Cecilia Cristea, Electrochemical *Biosensors as Potential Diagnostic Devices for Autoimmune Diseases, Biosensors*, 2019, https://doi.org/10.3390/bios9010038 ([#]Equal contribution) (IF: 3.240, Q2) **(State of the art, Chapter I.2)**

10. Mihaela Tertiș[#], **Gheorghe. Melinte[#],** Bianca Ciui, Ioan Șimon, Rareș Știufiuc, Robert Săndulescu, Cecilia Cristea, *A novel label-free electrochemical magnetoimmunosensor for human interleukin-6 quantification in serum*, Electroanalysis, 2018, http://doi.org/10.1002/elan.201800620 ([#]Equal contribution) (IF: 2.851, Q2) **(State of the art, Chapter I.2)**

List of ISI publications as co-author

11. Gabriela Andreea Filip, Marcela Achim, Paula Mihalte, Maria Olimpia Miclaus, Cecilia Cristea, **Gheorghe Melinte,** Bogdan Gheban, Dana Maria Munteanu, Oana Cadar, Ioan Simon, Ovidiu Pana, Lucian Barbu Tudoran. *Design, in vitro bioactivity and in vivo influence on oxidative stress and matrix metalloproteinases of bioglasses in experimental skin wound*, Journal of Trace Elements in Medicine and Biology, 2021, 68, 126846, http://Doi.org/10.1016/j.jtemb.2021.126846 (IF: 3.849, Q3)

List of non-ISI publications as co-author

12. Giulia Selvolini, A-M Drăgan, **Gheorghe Melinte**, Cecilia Cristea, Giovanna Marrazza, *A smart colorimetric sensor for the enzymatic detection of L-lactate in screening analysis*. Proceedings 2020, 60(1), 35, https://doi.org/10.3390/IECB2020-07020

Table of Contents

ABBREVIATIONS

$[Ru(NH3)_6]^{3+}$	Hexaaminoruthenium
6-MCH	6-mercapto hexanol
AA	Aminoacid
Aac	Ascorbic acid
AuNPs	Gold nanoparticles
AuNSs	Gold nanostructures
AuNVs	Gold nanovoids
AuE	Gold electrode
AuSPE	Gold screen-printed electrode
BSA	Bovine serum albumin
CNTs	Carbon nanotubes
CV	Cyclic voltammetry
DEA	Diethanol amine
DMF	*N,N*-dimethylformamide
DPV	Differential pulse voltammetry
E.U.	European Union
EDC	1-ethyl-3-(3-dimethylaminopropyl) carbodiimide
EIS	Electrochemical impedance spectroscopy
FA	Folic acid
FDA	Food and Drug Administration
$Fe(CN)_6]^{3-/4-}$	Ferri-ferrocyanide
FRA	Frequency response analyser
GCE	Glassy carbon electrode
Glu	Glucose
GO	Graphene oxide
IL-6	Interleukin 6

IUPAC	International Union of Pure and Applied Chemistry
Lyz	Lysozyme
MES	2-(N-Morpholino)ethanesulfonic acid
MIP	Molecularly imprinted polymers
MNPs	Metallic nanoparticles
MPA	Multiple pulse amperometry
MWCNTs	Multi-walled carbon nanotubes
NHS	N-hydroxysuccinimide
PANI	Polyaniline
Poly-L-Lys	Poly-L-Lysine
PS	Polystyrene latex beads
PtNPs	Platinum nanoparticles
PVP	Polyvynilpyrrolidone
QD	Quantum Dots
Rct	Transfer charge resistance
Rf	Roughness factor
RSA	Real active surface area
RSD	Relative standard deviation
s-ALP	Streptavidin alkaline phosphatase
SELEX	Selection Evolution of Ligands by EXponential enrichment
SPCE	Screen-printed carbon electrode
ssDNA	Single-stranded DNA
SWCNTs	Single-walled carbon nanotubes
SWV	Square wave voltammetry
TET	Tetracycline
TRIS	Tris(hydroxymethyl)aminomethane
U.S.	United States
UA	Uric Acid
WHO	World Health Organisation

INTRODUCTION

In the last couple of years, the science of nanomaterials and nanotechnology has seen a significant development towards nanoscale biosensing with very low limits of detection, high versatility and the ability to detect different biophysical signals that can be associated with the presence of health or pollution markers.

This capability of detecting molecules that can be associated with the presence of a disease or level of contamination represents an essential tool that impacts the general population's well-being by increasing life quality and expectancy. Even though science has improved so much over the last decades in this direction, the general analysis methods are still using expensive lab equipment, long-lasting procedures and a high number of operations that can be performed only by specialized people. Devices that can be used *in situ* by untrained people, that have a lower cost of production and short analysis time while preserving good analytical performances are highly preferred. However, their development is much more complex, and some challenges like the lack of selectivity, reproducibility and sensitivity must be overcome.

The development of electrochemical sensors is a good alternative to the traditional methods. The modification of electrodes with different nanomaterials has been extensively studied as they can generate platforms with many applications and reduce the disadvantages of unmodified electrochemical cells.

Nanomaterials like metallic particles, polymers or carbon nanotubes can be used to increase the electrochemical area of the electrode and, therefore, offer higher electric signals that enable the detection of lower levels of target analytes. At the same time, an optimised deposition procedure will increase the signal to noise ratio and decrease the variations in the signal acquisition, leading to better reproducibility of the sensor.

The lack of selectivity can be overcome by the immobilisation of biomolecules (peptides, enzymes, proteins, antibodies, aptamers) that can selectively recognise and bind the target analyte. These molecules are called bioreceptors, and the electrochemical sensor is called a biosensor. Besides selecting the best bioreceptor to bind the analyte, its immobilisation at the electrode surface is an important step that one must achieve. For this, nanomaterials with specific reactive groups (-COOH, -NH_2) or a very reactive surface (gold, platinum) that can form bonds with the bioreceptor can be used as immobilisation platforms.

The main objective of this thesis research was to develop various electrochemical platforms suitable for electroanalytical applications using different designs and strategies. For this, several nanomaterials were used as building blocks to increase the analytical performances, like conductive polymers, noble MNPs, or metallic wires. Their syntheses represent one of the most important parts of the research. Different shapes and sizes of MNPs and polymers were synthesised and optimised in order to offer the best analytical performances possible and characterised by electrochemical and different surface characterisation tools.

The applicability of the developed platforms was proven in bioanalytical sensing. Target analytes with important roles in the medical and environmental fields were chosen to be detected from complex matrixes, simulating the *in-situ* conditions. To establish a good selectivity, bioreceptors like aptamers were immobilised on the nanostructured platforms prior to the interaction with some of the targets (tetracycline, lysozyme, ara H1 allergen). In contrast, for the targets such as glucose, folic acid, and arsenic, optimal electrochemical testing conditions were chosen in order to increase the platform selectivity toward the analytes.

State
of
the art

I. Electrochemistry and electrochemical sensors/biosensors: Fundamentals

1. Electrochemical (bio)sensors

International Union of Pure and Applied Chemistry (IUPAC) define a chemical sensor as a device that transforms chemical information, ranging from the concentration of a specific sample component to total composition analysis, into an analytically valuable signal[1]. It usually has two main interconnected parts: a recognition system also called a receptor, and a physicochemical transducer[2]. A sensor is characterized by its sensitive response to a specific chemical or physical modification, being completely unresponsive to other medium variables. The sensitivity of a sensor is indicated by the degree of variation of the output signal relative to the change in the measurable chemical or physical signal. The selection of a sensor should be realized based on such essential features as selectivity[3], sensitivity, accuracy, calibration range, resolution, cost-effectiveness, and repeatability, as well as prevailing environmental conditions[4].

An electrochemical sensor stands for the sensor where the transducer is an electrode surface. Some essential advantages derive from this, like (i) the use of the electron for signal acquisition which is considered a green model for analytical applications, with no or little waste generation, (ii) the ability of miniaturization to develop portable devices, (iii) the short analysis time, and (iv) the low production costs compared with other chemical sensors[5].

According to IUPAC, sensors containing biological or biomimetic recognition systems are called biosensors[1]. The use of a bioelement as a recognition system leads to a high selectivity for the target analyte mainly because of the specific interaction between the analyte and the receptor. More importantly, the specific interaction prevents signal interference from other matrix components, which could modify the sensors response[6]. There are two main categories of biosensors, classified by the biorecognition process. The first type of biosensors is the catalytic biosensors that use as recognition elements enzymes, whole cells, bacteria, fungi or even animal or plant tissues. The second category is the affinity biosensors, in which the bioreceptor is capable to selectively and reversibly bind a specific ligand. In this category, we can find nucleic acids, antibodies, molecularly imprinted polymers (MIPs) or peptides (Scheme 1) [7].

A good biosensor is evaluated according to some of its important characteristics like the selectivity and the specificity for the target; the higher it is, the most reliable is the result of the analysis and the more effective is the biosensor to identify and measure the desired analyte with very low interferences from the matrix[8]. Another important aspect is the sensitivity of the biosensor; a high sensitivity means that with minimal changes in the analyte concentration, a significant change in the output signal from the sensor is observed[8,9]. It is also essential to analyse the repeatability or the precision of the biosensor; the closer the analytical results between several repetitions, the higher the precision is obtained. Last but not least, the accuracy of the biosensors shows how close the results are to the absolute value. All these are crucial aspects in obtaining a highly performant biosensor[10].

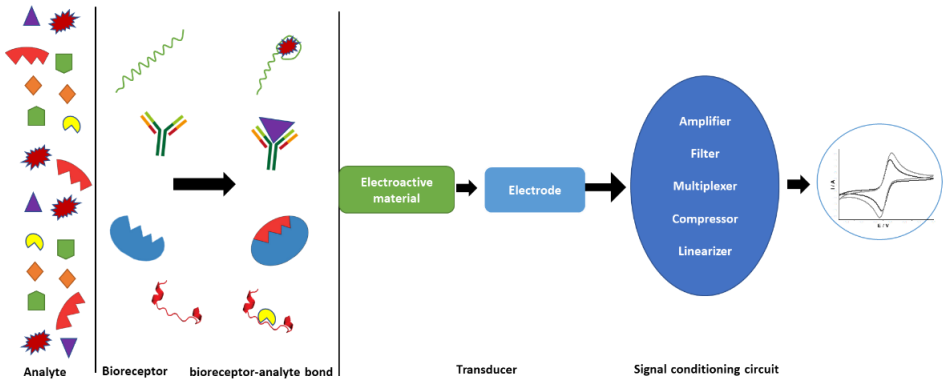

Scheme. 1 *Schematic representation of an electrochemical biosensor*

2.Bioreceptors

The recognition element, also called a bioreceptor, is one of the most important elements involved in the construction of an electrochemical biosensor. It is the element that offers the selectivity much needed for the detection from real samples with complex matrices[11]. The success of a biosensor significantly relies on the way the analyte interacts with the bioreceptor. This interaction has to be strong, selective and fast enough to be achieved while maintaining or even increasing the interaction between the recognition element and the sensor surface while maintaining its biological stability[12,13].

2.1 Enzymes

The enzymatic biosensors contain an enzyme as a biorecognition element in contact with the transducer. The enzyme reacts selectively with its substrate. Due to the

natural specificity of enzymes, enzymatic biosensors often show excellent selectivity to the target in practical applications. Enzymatic biosensors can measure the catalysis or the inhibition of enzymes by the substrate. In this way, the biosensor detects produced or consumed species, respectively. Commonly, only one enzyme is used in enzymatic biosensors, but progress in this field has seen combinations of enzymes to obtain multienzyme systems in the same assay for enhanced selectivity or even sensitivity[14,15]. According to the development method, enzymatic biosensors can be classified into four generations: one of the first enzymatic biosensors was developed by Updike and Hicks for the detection of glucose. They used Glucose (Glu) oxidase as a bioreceptor, immobilized on an oxygen electrode and polyacrylamide film[16]. These are the first-generation Glu biosensors.

The second-generation biosensors were developed by coupling enzymes with redox mediators such as ferrocene, methylene blue or other electroactive molecules. The third-generation brings a modification of the electrode material using one of the following electrode modifiers: quantum dots (QDs), graphene, polymers, and metallic nanoparticles (MNPs). The 4th generation comprises the nanocomposite enzymatic biosensors and combines the materials from the 3rd generation and their composites to enhance the electron transfer characteristics associated with the nanomaterials[17].

Even though enzymes offer very high selectivity for the target analyte, some challenges are difficult to overcome when developing an enzymatic biosensor, such as the stability of the enzymatic activity that can be easily influenced by the medium and storage conditions and the difficulty of the enzyme immobilization at the transducer surface while keeping its activity[18].

2.2 Peptides

In the last decade, synthetic peptides have been identified as interesting biorecognition elements for biosensor construction. Peptides are short chains of aminoacids (AA) (10-50) that can bind a specific target. An increased number of peptides linked in a peptide chain is called a protein. Short peptides, up to 10 AA residues, can be easily obtained by fast and cost-effective synthetic methods, having good biocompatibility, chemical and conformational stability compared to proteins and offering a short response time in electrochemical detection assays[19].

Peptides are probably the most versatile devices in the progress of supramolecular and flexible frameworks. Due to their tuneable Physico-chemical properties, specific peptides are able to fold in compact structural motifs shaping nanosized architectures in monolayers, tubes, bilayers, strips, micelles and fibres[20,21]. Through the rigidity of their secondary structure, peptides have the remarkable ability

and recognition flexibility to sterically adapt to any target molecule and form different types of non-covalent bonds[22].

Due to their ability to interact with the target molecule using different binding sites, like N-terminus, SH-groups or hydrogen bonds, peptide-based biosensors exhibit high selectivity[23]. The proper utilization of peptides as biorecognition molecules is critically connected with their attributes: their nature (hydrophobic, hydrophilic, etc.), isoelectric point, storage conditions, peptide character and solubility in different buffers to optimize the appropriate conditions for biosensor application[24]. All these chemical and physical properties of peptides offer them a series of advantages in electrochemical biosensing. They have better stability than proteins against denaturation, they are very easy to modify, and versatile towards electrode immobilization and interaction with the target analyte. In addition, they retain a high affinity for the target as the protein they derive from[25].

Even though the good sensitivity recommends the use of peptides, in the world of electrochemical biosensors there is still work to be done in order to fully take advantage of the peptides. Most of the published biosensors report platforms that were not characterized in biological samples taken from patients and in the presence of multiple interferences. There are also studies to be conducted in order to prove the repeatability, reproducibility and stability of peptide-based biosensors[26].

2.3 Molecularly imprinted polymers

MIPs are realized by generating specific recognition sites in polymer backbones to mimic a biological receptor. The identification of the target molecule resembles a "lock and key" model, in which MIPs act as the lock that is complementary in size, shape and functional groups orientation to the target molecule, the key[27].

MIPs are synthesized using a template-assisted approach: functional monomers form a complex with the template, represented by the target analyte, and then, using an appropriate solvent and crosslinkers, the polymerization begins. Next, the template is removed by extensive washing steps in order to break the template-monomers interactions, allowing the polymer to maintain specific recognition sites, complementary to the template in size, shape and position of interacting functional groups[28]. The selectivity of MIPs depends on the molecular level associations between the polymer and the target. The interactions between monomers and templates can be studied prior to synthesis through computational modelling, which can dictate or be dictated by synthesis choice and can help choose the most suitable type of synthesis as well as the monomer used for polymerization[29]. The electrochemical polymerization of

the monomer is very convenient since it is easier to control the shape and thickness of the polymer around the target molecule[29].

2.4 Antibodies

Biosensors that use an antibody as a bioreceptor are called immunosensors. They combine the power of antibodies as sensitive and specific sensing elements and an appropriate physico-chemical transduction mechanism to convert the recognition events into readable signals for directly identifying and capturing the target analyte[30]. Furthermore, the use of immunosensors is a widely spread procedure because of their sensitivity, excellent selectivity, simple assembly, autonomous operation, low cost, quick response, and user-friendly measurement mode[31].

Above all, it is known that the antibody-antigen complex can be dissociated using an appropriate reagent. For example, concerning the detection of pesticides, immunosensors allow the possibility to create reusable devices, which are very useful for continuous monitoring of real samples or on-field analysis. The experimental procedure of immunosensors can be summarized in two steps: molecular recognition of the target and transduction process[32].

There are two antibody types, monoclonal and polyclonal antibodies, depending on the epitope. Monoclonal antibodies are more specific for a single epitope, diminishing the chance of cross-reactivity. Polyclonal antibodies can bind multiple epitopes on an antigen, showing a heterogeneous immunological response. The choice of the antibody is performed in accordance with the specificity needed for the assay[33]. When developing an immunosensor, it is imperative to have a stable procedure. A small variation in the antibody structure can lead to very high differences of affinity between the antibody and its antigen[34] . Also, changes in temperature, pH or buffer solution can create a high electrochemical signal difference, leading to false analysis results[35].

The use of antibodies in electrochemical biosensors can cause changes in potential, current, ion concentration, conductance, capacitance or impedance signals, and each one can be quantified using electrochemical techniques. In general, electrochemical immunosensors are compact, inexpensive, robust, have fast response times and can be mass-produced using a very low volume of analytes. Therefore, immunosensors have been applied in a wide range of applications, especially in the detection of high molecular mass biological molecules, like biomarkers for different pathologies[36,37].

2.5 Nucleic acids

Aptamers are short and single-stranded DNA or RNA sequences, selected *in vitro* using a technique called SELEX (Selection Evolution of Ligands by EXponential

enrichment) from synthetic oligonucleotide libraries that contain up to 10^{15} different sequences. They are able to bind different kinds of target molecules, like, oligonucleotides, proteins, biomarkers or even very small proteins[38].

Aptamers have better properties compared with antibodies, like a smaller size, 20–25 fold smaller, conferring them better access to biological compartments, with great applications in sensors for diagnosis where are mostly used as biorecognition element in aptasensors desgin[39]. They also have higher stability in different medium conditions, a higher detection range, with limits of detection down to femtomolar lever, a prolonged shelf life, acceptable cross-reactivity and can be obtained using efficient and cost-effective processes. They can be also easily modified, giving the possibility to obtain various labelled probe elements[40].

As a bio-recognition element, aptamers can be used directly linked to the transducer, both as single-target or multitarget probe (labelled or label-free). Another possible approach is given by the possibility to use aptamer-target interaction to indirectly activate on-off devices in which the interaction with the analyte or the aptamer itself inhibits certain reactivity. Moreover, aptamers are subjected to significant conformational change caused by the interaction with the analyte that can be used as a recognition parameter when combined with appropriate transducers[41,42].

An aptasensor usually consists of the aptamer-based sensing layer, which is synthetically synthesized and immobilized on a substrate. This immobilization is very important in order to assure a high reactivity, appropriate orientation, accessibility and stability of the surface-confined aptamer probe as well as for minimizing non-specific adsorption events[43].

3. Immobilization techniques

The immobilization method employed to link the bioelement to the transducer is extremely important in order to obtain a good performance of the biosensor. The immobilization method should be chosen in order to assure an, appropriate orientation of the bioreceptor, a high accessibility to the target analyte, high reactivity and stability of the surface-confined bioreceptor probe as well as for minimizing non-specific adsorption events[44].

For example, the bioelement can be linked via self-assembly monolayers formed by the receptor directly on the substrate, or they can be directly adsorbed onto the electrode. Both methods are simple procedures but they do not allow a controlled orientation of the recognition element for the proper binding target analyte.

Additionally, fouling of the electrode surface may occur. Thus, methods that allow a controlled, oriented immobilization of the bioelement are preferred[26].

For this, several methods can be used for probe immobilization including covalent binding, noncovalent binding, or chemisorption. Covalent binding is usually carried out by modifying a linker group or a natural group (–NH_2 and –COOH) on an end of the bioreceptor, and the group reacts with the corresponding group on the substrate, such as –COOH, –NH_2, and –CHO[45] . As a non-covalent binding, avidin–biotin reaction is a typical example and one of the most widely used method because of its good stability and very high specificity[46]. Another non-covalent binding method used mostly for the immobilization of aptamers is the Au-SH reaction. In this case, the DNA probe is modified at one end with a SH group, typically a $(CH_2)_6$-SH group, and let to react overnight with a gold-based surface, like a gold electrode or gold nanoparticles (AuNPs) deposed on a glassy carbon surface[47].

In conclusion, there are many bioreceptor immobilization methods, each one with its advantages and disadvantages. A proper immobilisation method must be chosen depending on the bioreceptor and target analyte, the immobilization surface, and the expected final result (faster analysis, lower limit of detection (LOD), higher specificity).

II. Electrochemical detection methods

1 Electroanalytical techniques

In electrochemical sensing, the transduction element is an electrochemical cell usually formed from a working electrode, a reference electrode and a counter electrode. The electrochemical reaction that happens at its surface is measured in terms of an electric signal. Depending on the way the electric signal or read-out is generated, there are a series of electrochemical techniques that are mostly used. Some of them are voltammetric techniques (cyclic voltammetry (CV), differential pulse voltammetry (DPV)), amperometric techniques (chronoamperometry, multipulse amperometry) or impedimetric techniques (electrochemical impedance spectroscopy (EIS)[48] .

1.1 Cyclic voltammetry

In a CV technique, the electrochemical current is measured with respect to the potential applied at the working electrode and the working potential is swept with a particular scan rate measured in V s^{-1}. The potential is applied between the working and reference electrodes, whereas the current is measured between the working and counter electrodes. The electrochemical current, measured in amperes is plotted on the x-axis versus the working electrode potential y-axis obtaining a cyclic voltammogram. As the potential reaches the highest set value during measurements, it reverses back to its initial potential. This is the reason it is called cyclic voltammetry. The cyclic experiment can be repeated several times[49]. Therefore, CV is performed by cycling the potential applied and measuring the resulting electrochemical current generated during the oxidation and reduction process of redox species. During redox reactions, the electrons are transferred from analytes to electrodes or from electrodes to analytes (Figure 1A)[50].

Apart from the qualitative and semi-quantitative analysis, it is used to study the electrochemical properties of an analyte in solution or of a material that is filmed onto the electrode surface. CV could be also used to calculate various other parameters, such as diffusion coefficient, redox potential for the analyte, electrochemical area of the electrode, surface concentration of immobilized biomolecules and can be coupled easily with other techniques[49].

1.2 Differential pulse voltammetry

DPV is one of the most widely used electrochemical techniques due to its high sensitivity and rapidness. In this technique, a series of potential pulses of fixed amplitudes (10–100 mV) are superimposed onto a slowly changing base potential, and

the resulting current difference is measured and plotted against the base potential. The obtained peak current is used to measure the concentration of an analyte[49].

This procedure is reducing at a minimum the background current called capacitive current that in CV often reduces the resolution of the oxidation&reduction peak, also called the Faradaic current, the one interested in analysis. This advantage leads to higher sensitivity and therefore to smaller quantities of analyte detected. Using low step potentials, DPV leads to better peak-to-peak separation and enables simultaneous analysis of multiple redox-active analytes with narrow oxidation&reduction peak potentials[51]. One disadvantage arises from the low scan rates used, which increases the time needed for analysis, making it slower than a typical CV. Also, it may be considered an irreversible or destructive technique since it only changes the potential in one direction leaving the analyte either oxidized or reduced. As in the case of CV the results are represented in a voltammogram in which the current is plotted versus the potential (Figure 1B) [52].

1.3. Chronoamperometry

The name of the technique, chronoamperometry, stands for the measurement of the current (hence "amp") that is recorded over time (hence "chrono")[53] and it is an amperometric technique in which constant potentials are applied for a period of time, potentials that are higher or equal to the open circuit potential. The voltage is initially held at a resting potential (E1), where neither oxidation nor reduction of any of the analytes of interest can occur. The current that can be read at E1 shows that the technique has a background current that must be taken into consideration because it can significantly influence the Faradaic current. The voltage is then stepped to a value where clear oxidation or reduction of the analyte of interest can occur (E2). By maintaining E2 for a sufficient period of time the analyte is consumed and the current decreases. It generates a graph in which the anodic or cathodic measured current vs time reveals the anodic or cathodic processes that are happening at the electrode surface(Figure 1C) [54,55].

The main advantage of amperometric techniques is the ability of monitoring the current over time at a fixed potential. Therefore, every modification that appears in the current value is directly related to a concentration change or apparition of a new analyte. Also, due to the fact that most analytes that are electrochemically active have different oxidation/reduction potentials, chronoamperometry offers a good selectivity in complex matrixes. Nevertheless, if two analytes have close oxidation/reduction potentials, the separation is very difficult to be made in chronoamperometry, this being one of the most important limitations of the technique. Amperometric approaches are applied where rapid dynamic changes in the concentration of analyte occur[56].

1.4 Multi pulse amperometry

In multiple potential steps amperometry or multiple pulse amperometry (MPA), the initial voltage applied (E1) is where no oxidation or reduction of the analyte can occur just as in chronoamperometry. For the next step, the voltage is stepped to additional voltages (E2-E5). When stepped to these varying voltages, the duration that each voltage is applied can also be varied and the number of times each potential line is applied can also be set. Considering the last part, the total time of the procedure can be determined. The duration that a potential step is applied is critical to ensure that the measured response is faradaic. By reducing the time of pulses, different applications arise, from analyte detection to the formation of electrodeposition and polymerization centres.

Multiple potential amperometry allows for the detection of multiple analytes within a single measurement. By subtracting the current responses obtained at varying voltages, the difference in the current response may allow users to understand the oxidation or reduction of one analyte in a mixture[55].

1.5 Electrochemical impedance spectroscopy

EIS is an electrochemical method that is based on the application of a fixed voltage (or current if a galvanostatic impedance is performed) at the working electrode surface, and the analysis of the voltage response as a function of the frequency change. It cannot be performed using a traditional potentiostat, it needs a special module called frequency response analyser (FRA), and it can be performed in 2- or 3-electrodes configuration, depending on the absence (2-electrodes) or the presence (3-electrodes) of a reference electrode, whose potential is known and fixed. The frequency switch is usually performed in a wide range, from MHz down to mHz, higher frequencies needing a shorter analysis time, time that is increasing with the need to apply smaller frequencies[57] .

The EIS data is usually represented using two types of plots. The first one and most used in biosensors development is called the Nyquist plot and represents the impedance (Z), Z'' as a function of Z' in the complex plane (Figure 1D). Even if not always observed in the published literature, it is a good practice to employ isometric axes in this type of graph: this is particularly useful in order to immediately detect the possible presence of non-ideal capacitive behaviour. Compared with the other representation, the Bode plot, this one is more compact, even if the frequency dependence is not evident. The Bode plots represent 2 overlayed graphs reporting Log(Z) and the phase angle (θ) as a function of the logarithm of frequencies[58].

EIS is mostly used to characterize different surfaces or modifications performed at the electrode surface. From the Nyquist plot, the transfer charge resistance (R_{ct}) is read and correlated with the modifications that appeared on the working electrode. In the biosensing field, it is used in order to see the amount of bioreceptor immobilized, the R_{ct} generally increased with the increase of bioelement amount immobilized. The main disadvantage of this technique is the lack of selectivity. Since all the analyses have to be performed using a redox probe, usually $[Fe(CN)_6]^{3-/4-}$, it is difficult to interpret if the change in R_{ct} is due to a specific interaction between a bioreceptor and its target or by an unspecific adsorption of an element. Therefore, EIS is only on rare occasions used to detect an analyte[59].

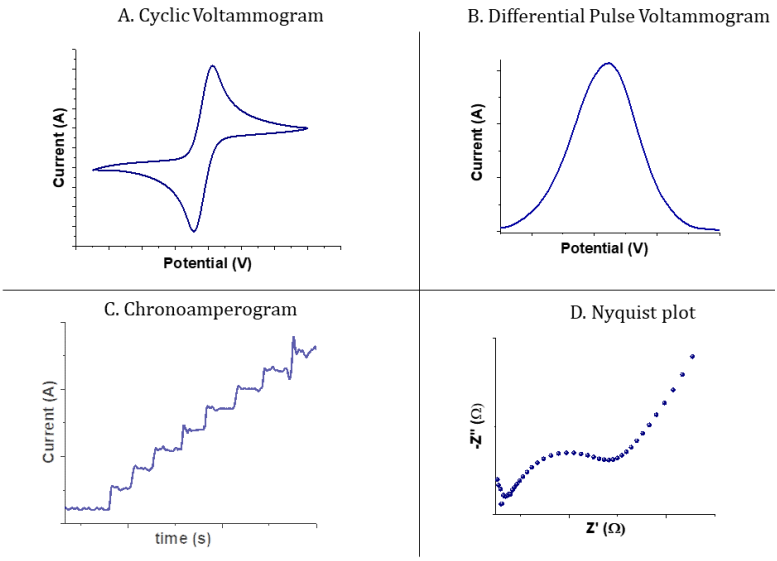

Figure 1. *Visual representation of the results obtained using:* ***A****. Cyclic voltammetry,* ***B****. Differential Pulse Voltammetry,* ***C****. Chronoamperometry,* ***D****. Electrochemical Impedance Spectroscopy*

2. Analytes detection

Probably the simplest approach used in electrochemical sensors is the direct detection of the desired analyte. For this to be possible, the analyte needs to have some specific properties. The most important of them are derived from their structure. The analyte has to have a structure that can be easily involved in redox reactions and moreover, it needs to contain functional groups, that can be oxidized or reduced by using just the electric current generated during electrochemical measurements[60].

Even though this is the simplest approach, there are still many challenges that have to be overcome in order to obtain a reliable analysis result. Most of the time the analyte concentration is very small and on unmodified electrodes the electron transfer has to be improved in order to be able to see the result of the electrochemical reaction[61]. Moreover, what makes the measurement even more difficult is the coexistence of several interfering compounds in complex matrixes that can have an electrochemical signal at the same potential range as the desired analyte leading to selectivity problems[62]. In order to decrease the possibility of interference of the target analyte with other compounds, it is beneficial to modify the electrode with materials that can specifically catalyse analytes redox processes, for example, modifying its oxidation potential[63].

Other parameters have to be considered during detection protocol like the scan rate in voltametric analysis, not too high in order not to miss the oxidation point of the analyte or not too low when the oxidation peak might be too small to be read. Also, for amperometric measurements, the time of analysis is important; the analyte is most of the time subjected to environmental factors and might be affected. Even though selectivity problems are oftentimes very difficult to be overcome, there are molecules of high importance from the analytical and medical point of view that have been successfully analysed in complex matrixes using electrochemical sensors. Direct detection of ascorbic acid[64], uric acid[65], or dopamine[66] has been reported in studies being detected alone or simultaneously with other targets[67].

The number of analytes that can be detected using direct detection methods is still very low, most of the biological molecules like biomarkers, proteins, DNA sequences or drugs with high molecular mass are not electrochemically active and therefore the electrochemistry had to adapt and find new strategies. In order to overcome the selectivity problems, biosensors have been developed, enabling indirect detection using labelled biosensors and label-off biosensors [68].

2.1. Label-free biosensors

An electrochemical label is an electrochemically active molecule that attached to a bioreceptor, an enzyme or another molecule is interacting with the desired analyte. The role of the label is to offer an electrochemical signal that can be directly correlated with the presence/absence and the concentration of the analyte[69]. But labelling a bioreceptor is time-consuming, expensive and requires very complex procedures that are difficult to reproduce. Moreover, the labelling process can affect the bioactivity of the bioreceptor and therefore it can decrease its interaction with the target[70].

An alternative may be represented by the label-free biosensors, in which no molecule of interest is labelled with a redox moiety, and the detection is based only on the intrinsic properties of the molecules crafted on the electrode surface and the phenomena occurring during the biochemical reactions on a transducer surface[71]. However, their most significant downside is the lack of an amplification mechanism and the fact that they rely only on the binding event, and therefore they require a bioreceptor with a good affinity and increased specificity. As a result, it is challenging to develop label-free biosensors with low LODs and very high specificity[72].

Label-free biosensors have a series of advantages compared with labelled biosensors that arise from their development method. The latest generations provide real-time quantification of products from biomolecular reaction, making it possible to record live a biochemical reaction, allowing kinetic monitoring of parameters of the ligand—receptor recognition and interaction[71]. In the absence of the labelling process, the cost of developing is smaller and the use of organic compound is considerably reduced. In the absence of a specific label there is the opportunity to detect very small molecules, the opportunity to create multiplex biosensors[73]. Probably the most important advantage is that all the molecules involved in the detection (bioreceptor, analytes, ligands) are in their natural form and the biological reaction is not influenced by their structure modification[74].

EIS is the electrochemical technique mostly employed in label-free biosensors. By measuring the charge transfer resistance, or impedance, every modification arising at the electrode surface can be observed. In this case, the difference between the impedances obtained before and after the bioreceptor-analyte interaction can be correlated with the analyte concentration. The main downside of EIS in this case is the lack of selectivity, and therefore in order to have a reliable detection in complex, the interaction between the bioreceptor and analyte has to be very specific and strong and the unspecific adsorption has to be reduced to minimum[75].

In the case of label-free biosensors, the electrochemical signal is offered by a redox probe that in this case is added in the detection solution. Potassium ferri-ferrocyanide ($[Fe(CN)_6]^{3-/4-}$) is usually used in EIS. It is a common negatively charged redox probe, which cannot get close to the DNA-modified electrode surface due to the electrostatic interactions, thus an increase in charge transfer resistance can be detected with the increase of electrode modification layers [76]. Other redox probes can be used for the label-free detection. Positively charged hexaaminoruthenium salt $[Ru(NH_3)_6^{3+}]$ can be used when the biomolecules are negatively charged in order to reduce the electrostatic repulsion and it is used mostly in DNA sensors[77]. Measuring the conductivity of the biosensor in CV or DPV might be an alternative to EIS studies, offering

an increased number of redox probes that can be used besides the one mentioned above: methylene blue[78], thionine[79], diaminophenazine[80] or Prussian blue[81].

2.2. Labelled biosensors

Electrochemical labelled biosensors require more complex procedures during their development because of the extra step of labelling but if this part is optimized and efficient the labelled biosensors offer a higher specificity compared with the label-free ones, the electrochemical signal change occurring only due to the interaction between bioreceptor and the target[82].

The most common type of biosensors are the ones in which the bioreceptor is directly modified with the label and the signal of the label is measured before and after the interaction with the target. In most cases the bioreceptor is a peptide modified at its C-terminus[83], aptamer or a ssDNA modified at their 3' or 5' end, depending on the way the molecule is immobilized on the electrode surface[84].

There are two main modalities of label binding, each one with different behaviour. On one side, there is the possibility of covalent labelling. In this category we can add those devices that are using a sensing mechanism based on the analyte-induced refolding of bioreceptor bearing a covalently attached redox probe. This approach is the simplest and between the most effective method to construct labelled electrochemical aptasensors[85].

In general, this sensor design couples a target-induced conformational change in the labelled molecule leading to a change in electron transfer ability between a distal-appended redox marker and an electrode surface. Such aptasensors can lead to an increase or a decrease of the electrochemical signal after the bioreceptor-analyte interaction leading to a *signal-on* or *signal-off* mode biosensor, respectively[86]. The main advantages of this approach are the simple reagentless protocol, fast target-induced conformational changes in the aptamer that allows real-time analysis and the reduced unspecific response in complex media due to conformational changes that appear only in the presence of the target. However, there are some limitations of this approach like the sensitivity that is limited by the ability of the redox probe to reach the electrode surface or the ability to obtain a stable bioreceptor 3D structure that is not influenced by temperature, pH or ionic strength[87].

The other approach is based on non-covalent binding of the redox probe. They interact with the bioreceptors through electrostatic binding or intercalation, and this property has been used to design electrochemical biosensors without a redox probe attached. This approach has been mostly used in genosensors construction, where the redox probe is intercalated between the two strands of a hybridized DNA and it is

released after the interaction with the target[88]. It has the advantage over the first approach that a high load of intercalated redox probes leads to a higher sensitivity. However, the process is longer since they cannot be operated in a single-stop protocol[87].

The most widely used redox probes are methylene blue, ferrocene, horseradish peroxidase, or some nanocomposite complex containing metals like Au, Ag, and Cu or carbon-based materials like graphene oxide, for enhancing the electrochemical signal[89].

Another approach that can be used in developing electrochemical biosensors with indirect detection is the binding using covalent bonds of other molecules that in the end will produce a reaction with electrochemical signal generation. In this case, not only the bioreceptor can be modified, but also the analyte can perform covalent bounds with the molecules that will help generate the electrochemical signal. The most representative method for this category is the enzyme-linked array[90]. For example, the bioreceptor can be modified with a biotin group, and streptavidin alkaline phosphatase (s-ALP) can further bound, taking advantage of the specificity and sensitivity of the biotin-streptavidin bond. In the final step, the alkaline phosphate will hydrolyse a phosphate substrate like 1-Naphtil Phosphate to α-Naphthol, whose oxidation will generate the electrochemical signal[91]. Other enzyme-linked assays that are widely used are based on the Horseradish peroxidase coupled with 3,3′-diaminobenzidine[92] or with hydrogen peroxide/hydroquinone[93].

Depending on factors like linear range needed, the complexity of the matrix, miniaturization, time needed for analysis, and the necessity of in situ detection, different electrochemical detection techniques can offer the needed advantages. Therefore, an intensive literature study must be performed before choosing a protocol for electrochemical biosensors development.

III. Materials used in electrochemical sensors

One of the biggest challenges in biosensors development is to obtain a very selective method that in the same time offers a good signal enhancement for a low detection limit. Most of the times this process starts from a platform with no selectivity like graphene electrodes for electrochemical techniques that must be modified with different materials[94].

According to their shape, nanomaterials involved in biosensing are divided in 4 main categories: Zero dimensional (0D) nanomaterials, 1D nanomaterials, 2D nanomaterials and 3D nanomaterials[95]. 0D nanomaterials like nanoparticles[96], QDs[97] or nanoclusters[98] are usually used thanks to their physiochemical properties as signal enhancement materials in small molecules detection[99]. In the category of 1D nanomaterials, most often used are nanotubes[100], nanowires[101] and nanorods[102]. They distinguish from other categories of materials by their high density within a small area improving in this way the sensitivity of the biosensor[103]. 2D nanomaterials are an improvement of the previous category. They are usually solid crystalline materials that can form strong interlayer interactions[104]. In addition, they can form interactions with other layers of different nanomaterials, obtaining in this way better physiochemical properties and new optical and electrochemical features, extremely helpful in DNA sensing[105]. The last and most recent category, 3D nanomaterials and composed from a combination of 0D – 2D materials. Most often they are developed by combining different conventional nanomaterials with nanocomposite, or by the self-assembly of different nanoparticles systems[106].

1. Electroconductive polymers

The discovery of electroconductive polymers in 1958 lead to a new era in the polymer science field and gave new opportunities in electrochemistry. Later in 1977, a vast stride was taken when *Heeger and coworkers* found a remarkable conductivity in polyacetylene doped with iodine[107].

Good electric conductivity acquired through redox processes is the flagship property of polymers containing extended conjugated π-electron systems. Moreover, by using an optimized deposition with a very good reproducibility, the presence of polymers on the surface of electrochemical sensor creates a regulated porous surface that allows the incorporation of different nanomaterials and decreases the standard deviation of the analysis[108]. Polyheteroaromatics polymers, such as polypyrrole, polyaniline (PANI) and their derivatives have attracted a lot of attention lately because of their possible application in electrochemical sensors[109]. The generation and

immobilization of polymers on an electrode substrate can be obtained using different methods like:

A. Electropolymerization
B. Chemical polymerization
C. Organic solvent polymerization and deposition
D. Layer by layer deposition(110).

1.1 Polyaniline

PANI [H–$(H_4C_6NH)_n$–H] can be considered one of the first synthetic polymers and it is still widely used in electrochemical sensors and biosensors due to its low cost and relatively easy polymerization procedure[111]. PANI is usually prepared by polymerizing aniline in strong acid solutions like H_2SO_4 or $HClO_4$, and it can be polymerized either chemically or electrochemically. The acid medium is favourable to the electroconductivity of PANI thanks to a higher doping. A higher pH will lead to low doping levels and therefore to a smaller conductivity[112].

Thanks to the facile, inexpensive fabrication, adequate ion exchange capacity, and other conspicuous criteria like acceptable bioactivity and eco-friendly, PANI is widely applied as a substrate for bioreceptors immobilization in electrochemical biosensors development[113].

1.2 Polypyrrole

After PANI, Polypyrrole [H–$(H_2C_4NH)_n$–H], is considered one of the most used class of conductive polymers. In comparison with other conductive polymers, polypyrrole is adapted to more types of dopant ions to conduct the doping-undoping process during its polymerization, achieving higher doping level and higher conductivity. It also exhibits higher redox reversibility compared with PANI which allows it to be used in a broader range of potentials and for a higher number of electrochemical analysis[114].

Applications of polypyrrole electrodes to analytical sensor technologies and the development of biomedical devices are still among the main interests in the world of science. Polypyrrole is regarded as an environmentally friendly polymer. It is quite stable and undergoes reversible-redox switching in aqueous environments[110].

1.3 Poly-L-Lysine

Poly-L-Lysine (Poly-L-Lys) is another conductive polymer, not as popular PANI or Polypyrrole but still a conductive polymer that offers very good water solubility, high biocompatibility, good versatility and an increased stability. Moreover, it can be easily

prepared by electropolymerization of L-Lysine in phosphate buffer using CV, obtaining a very reproducible polymer[115].

The porous structure of the polymeric film that is obtained during the electropolymerization process, allows the incorporation of nanomaterials that can boost its already good conductivity. A good example would be the electrodeposition of gold nanostructures (AuNSs) inside the polymer matrix. In this way, the electrocatalytic properties of the polymer are greatly enhanced and the overall properties of the electrode surface as well[116].

2 Metallic composites

MNPs are nanosized metals with a size range of 10–100 nm. The development of novel MNPs with different structures, shapes and dimensions has attracted the attention of the scientific world more and more often in the last years. Their unique properties make MNP an ideal tool in electrochemical sensors development. Among these specific characteristics, high electrical conductivity, large surface-to-volume ratio, increased biocompatibility and the ability to increase the catalytic activity of the electrochemical platform provides a huge space for MNPs in improving the overall sensor performances[117].

2.1 Gold nanoparticles

Among metallic particles, AuNPs have a significant role and are probably the most used MNPs in electroanalytical device development. They offer very good biocompatibility, a good surface to volume ratio and the highest conductivity observed in MNPs. Furthermore, due to their superior stability and complete recovery in electrochemical redox processes, AuNPs have been used as bioreceptors immobilization platforms and as catalyst in electrochemical biomedical applications. Their excellent conductivity and catalytic effect open the possibility of creating miniaturized sensing devices and create new ways for fast in situ detections[118].

There are several methods of synthesis, each one with different characteristics and parameters to optimize in order to obtain the most suitable AuNPs. Chemical reduction is one of the mostly used methods. It includes the reduction of a gold salt, usually $AuCl_4^-$ in an acidic medium, in the presence of a reduction agent like sodium citrate or sodium tetraborate. This method produces monodispersed spherical AuNPs in the range of 10–20 nm in diameter and allows a good control of their shape size and distribution and offers a high monodispersity of the nanoparticles[119]. Another method is the electrochemical one; in this case, the AuNPs are directly electrodeposited on the surface of the working electrode. Usually, the gold is electroreduced from its $AuCl_4^-$ salt

using CV or amperometric methods. Adding different ligands in the electrodeposition solution, additional advantages, like the development of different structures, increase of hydrophilicity, increase of electroactive surface area or the ability to specifically interact with a particular target are accomplished [120].

Apart from the electrocatalytic point of view, AuNPs possess many advantages in biosensors development. The covalent interaction between gold and thiol groups is a robust and specific interaction and has the advantage that thiolated aptamers can be immobilised by self-assembling, which guarantees suitable stability, surface coverage and maintenance of the same binding affinity as that shown in solution[43]. Moreover, the gold surface promotes the single-stranded DNA (ssDNA) binding by non-covalent bonds, such as electrostatic interaction and hydrophobic forces, especially with purine and pyrimidine rings of the DNA bases[121].

2.2 Platinum nanoparticles

Platinum nanoparticles (PtNPs) are attractive for various electrochemical applications due to their size and shape-dependent chemical and electronic properties. In many ways, similar to AuNPs, these nanoparticles have the advantage of both the dimensional and functional characteristics of their surface and inorganic domains, which transforms to enhance their specific physical properties. Their size can provide a large surface-area-to-volume ratio and, as the particle size shrinks, the population of surface atoms increases significantly. By the exploitation of these properties, PtNPs offer feasible alternative platforms to AuNPs to address a wide variety of applications in the biosensing field[118,122].

Regarding the methods of syntheses, PtNPs can be obtained using similar procedures as for AuNPs, chemical or electrochemical reduction of H_2PtCl_6. Considering these similarities, AuNPs and PtNPs can be synthesized together, amplifying each-others advantages by synergistic effects. This combination of nanoparticles can lead, if the right ratios of $HAuCl_4$ and H_2PtCl_6 are used, to increased specificity of the biosensors. The addition of PtNPs can increase the antifouling effect of the platform and decrease the unspecific adsorption, the main disadvantage of AuNPs, by obtaining particles with a lower water contact angle[123].

2.3 Other metallic particles

Metallic composites with different structures and sizes like wires or rods have become an interesting field for researchers because they can provide a larger surface to volume ratio compared with nanoparticles. Metallic composited can be synthesised using template-assisted techniques such as electrochemical deposition. This is probably the most effective method because of the significant advantages of low cost, high aspect

ratio, variable diameter, large surface area and controllable properties by changing the temperature, applied voltage, pH value, and electrolyte[124].

A widely used category of metallic composites in electrochemical sensors are the Cu based electrodes. They are particularly attractive due to their catalytic ability and ready availability representing suitable materials for direct electrochemical detection of several analytes, including Glu, hydrogen peroxide or nitrate. Moreover, due to an excellent electron transfer along a one-dimensional direction, the Cu electrodes have been reported to be highly sensitive to glucose oxidation[125].

Cu electrodes have a porous surface that allows them to be dopped or modified with different nanostructures that can increase their sensing abilities. Nanoporous metallic foams are a good example. They are 3D structures of pores with nano-ramified walls that have a wide pore size distribution and porosities higher than 50%. Allowing the fast diffusion of active species through the material, they provide an increased surface area for electrochemical reactions. They also combine these properties with those characteristics of metals, such as good electrical conductivity and easiness of malleability[126]. There are several methods of synthesis in order to obtain nanoporous metallic foams, mostly used being the hard template synthesis. In this case, the metal is deposed chemically or electrochemically in template voids. In the end, the template is dissolved in a proper solvent or burnt, without affecting the surface[127]. Metals that are mostly used as Cu electrodes nanoporous metallic foams modifiers in electrochemical sensors are Ni[128], Mo[129] or Au[130].

3 Carbon-based nanomaterials

Carbon-based nanomaterials have some advantages compared with metal-based nanomaterials. Their price is lower, so they are more affordable; carbon offers a high surface area, thus the possibility of immobilization of a high amount of biological compound. They are also very versatile, and a high number of structures can be obtained with specific characteristics[131].

Depending on the shape, dimension and carbon structure, there are many types of carbon-based materials that used in electrochemical sensing. Each type has its own characteristics, advantages and disadvantages. Most often met in the scientific literature are the graphene sheets that are 2D materials with a 0.3μm thickness and very good conductivity[132]. Carbon nanotubes (CNT) are another type of carbon-based materials. CNT consists of a monolayer of graphite in a cylindrical format that has a very good conductivity and biocompatibility. CNTs can be classified according to the number of layers of existing coaxial cylinders in single-walled carbon nanotubes (SWCNTs) or multi-walled carbon nanotubes (MWCNTs)[133]. Fullerenes are spherical and hollow

carbon molecules in which each carbon atom forms three simple bonds of 120° with other atoms in sp2 hybridization[134]. There are also the graphene oxides (GO) that are composed of a single polymerized layer of carbon atoms closely packed into a 2D honeycomb lattice and characterized by the ample presence of various oxygen-containing groups. These nanomaterials can be found in their oxidized or reduced form[135].

3.1 Single-walled carbon nanotubes

SWCNTs have a great analytical potential as materials for electrode modification. The use of SWCNTs in electrochemical sensors development has seen a significant increase during the last decade. They are used mainly because of their excellent electrocatalytic activity, very good promotion of electron transfer, enhancement of the sensitivity of voltammetric methods and excellent compatibility with a high number of different nanomaterials. There are also properties like high thermal resistance and increased mechanical strength that not only separates them from other carbon-based materials but enlarge their application possibilities.

It has been demonstrated that the surfaces of CNTs can be easily modified in numerous ways, either by covalent or non-covalent functionalization, by introducing various organic functional groups and providing a strong physical adsorption area. Furthermore, the functionalization using covalent or non-covalent binding is mandatory in order to minimize the π–π stacking interactions between the tubes and the van der Waals forces that can negatively influence SWCNTs dispersion in water and the development of electrochemical sensors[136].

3.2 Graphene

Graphene is a type of nanomaterial composed of a single-atom-thick sp^2-bonded carbon configuration arranged hexagonally, which has crystallinity, electrical properties, and various physical and chemical properties. These properties encompass outstanding thermal and electrical conductivity, increased theoretical specific surface area, high optical transmittance, robust flexibility, lightweight, and exceptional mechanical strength[137]. From the graphene category, mostly used are the graphene oxide which are maintaining their oxidised (GO) form and the reduced graphene oxide (rGO), which are having slightly modified electrochemical properties. This thesis presents a study where only the oxidised graphene oxides were used.

GO is a carbon composed material that is prepared by using graphite paste and strong oxidizing agents. This oxidizing process is able to produce numerous oxygen groups like hydroxyl or carboxyl, groups that do not act only as catalytical active canters in the electrochemical process but they also offer good anchoring sites for covalent or

non-covalent immobilization. By optimising the oxidation process, an exact number and exact positions of the anchoring groups can be obtained. Therefore, GO can represent a very useful tool in electrochemical biosensing by being a suitable platform for homogenous immobilization of bioreceptors[138].

Apart from the above-mentioned characteristics, and the general characteristics of carbon-based materials, GO distinguish themselves by having distinctive properties like greater hydrophilicity due to the high number of reactive oxygen groups, easily controllable electronic properties, wider potential window and negligible residual current[139]. Despite these extremely important properties of GO, there is an important disadvantage of using this compound and it consists in the formation of some structural defects and vacancies that break the sp^2 network and dramatically decrease the electronic conductivity. For this reason, GO tends to be rather an insulating material. But its structure allows its functionalization with other conductive materials resulting in a combination of effects, by maintaining the ability of GO of binding bioreceptors and increasing its conductivity. For this, materials like MNPs or polyelectrolytes have been previously used and cited in the literature[140,141].

IV. Target molecules

1. Targets from environmental analysis

1.1 Arsenic

Arsenic is one of the top 20 most abundant minerals in the earth's crust and one of the top 15 most abundant minerals in the human body. It was a mineral of great use in agriculture, electronics, metallurgy and even medicine. It is well known that its inorganic forms are very toxic, with As(V) even more toxic than As(III). But, if it is used in its organic forms like monomethylarsonic acid or dimethylarsinic acid, arsenic toxicity is greatly decreased[142].

The intoxication with arsenic can be acute or chronic. The acute cases are extremely rare since there must be ingested a very high amount of arsenic. In the second case, poisoning incurred from chronic exposure to constant levels of arsenic is referred to as arsenicosis[143]. Among the symptoms that can be observed first are skin lesions and hard patches on the palms of hands and soles of feet. Later after a longer exposure, skin and internal organ cancers can appear as well as diseases of blood vessels in the legs. Diabetes can also be observed after a long exposure together with high blood pressure. Arsenicosis severity is highly dependent on the dose and number of years of exposure to analyte[144].

The World Health Organization (WHO) considers arsenic as one of the top 10 chemicals of major public health concern and therefore they pay significant attention to arsenic levels, especially in public water. In the Guidelines for drinking-water quality issued by WHO, arsenic received a major part where recommendations and evidence of possible arsenic exposure can be found. In order to reduce arsenic exposure, the current recommendation states that there should be less than 10 $\mu g\ L^{-1}$ of arsenic in drinking water. Unfortunately, since there are no ways to remove the arsenic from water, this value is only provisional, and the main activity that is recommended is to keep the concentrations as low as possible, preferably under the value from the guideline[145].

Moreover, since there are very few measures that can be taken in order to decrease the concentration of arsenic in water, there are many regions around the world where the WHO guidelines values are exceeded. Among others, contaminated areas include Argentina, Bangladesh, China, India, Mexico, Myanmar, Nepal, Pakistan, Vietnam, and parts of the USA[144]. Specifically, contamination of aquifers in Bangladesh is

deemed the most serious. Studies showed that around 28-62% of the population is subjected to a high amount of arsenic ingestion from public water and nearly 20% of deaths are due to arsenic chronic poisoning, in some parts of Bangladesh, arsenic levels in water rise up to 2500 μg L^{-1}[146]. In Europe, where the limit of Arsenic in water is set by European Council Directive 98/83/EC to the same amount of 10 μg L^{-1}, the most affected country seems to be Italy, where in the Viterbo area, values of up to 295 μg L^{-1} of Arsenic could be found[147].

Concluding, it is of upmost importance to have fast, accurate and miniaturised devices that can detect arsenic in situ in public waters with very low costs and that can be operated by unqualified personnel.

2. Relevant targets for medical analysis

2.1 Glucose

Glu is the most common monosaccharide with many important roles in the human body, being involved in most major metabolic pathways. Once got in the bloodstream, Glu can be used either directly for energy or stored in the liver muscles and tissues as glycogen. Glu regulation in the blood is made by hormones such as insulin created by pancreatic β-cells and glucagon released by α-cells also in pancreas[148]. The rate of Glu absorption is extremely important in order to allow glucose to play its important role in human metabolism. It is dependent on the provision and digestion of carbohydrates in the upper gastrointestinal tract, as well as effective sensing and transport of glucose and other monosaccharides by the intestinal mucosa[149].

Glu exhibits its roles best when it is in the normal range of concentration in blood (80-120 mg dL^{-1}). An increased concentration or a decreased one will create metabolic disruptions[150]. When Glu is accumulated in blood in quantities higher than 120 mg dL^{-1}, hyperglycaemia sets in and the main reason it appears is that glu fails to be stored in the liver and muscles. On the opposite side, when there are problems with Glu absorption and the value of glycemia is less than 70 mg dL^{-1} hypoglycaemia sets in. Persistent hypoglycaemia is a deadly disease and it can affect kidneys and other vital organs[151].

Glu blood levels play a very important role in the medical field. Diabetes, a common endocrine disorder caused by the deficiency of insulin, leads to a major health problem that contributes to the worldwide deaths. According to WHO, diabetes is predicted to be the world's 7th leading cause of death by 2030. It is already one of the most common diseases, with an increasing number of patients every year. WHO statistics anticipate that by 2035, 592 million people will be affected. Just in 2015 around

1.6 million people were reported dead from causes directly related to diabetes, while in 2012 2.2 million deaths were registered with causes due to high glycemia[152].

The importance of daily glycemia monitoring is undeniable and the necessity of fast, simple and accurate devices for its detection is increasing with each year. Glu is an electroactive substance having the ability to be oxidised using a specific potential and that allows its direct detection using electrochemical sensors and the number of publications and developed methods is increasing every year(Figure 2)[153].

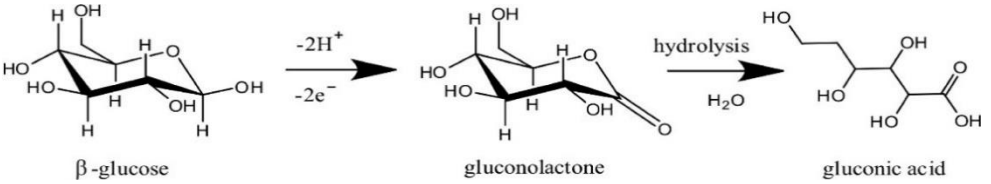

Figure 2 *Steps involved in the oxidation of Glu*

2.2 Folic acid

Folic acid (FA), also called pteroylglutamic acid or Vitamin M or B9, is the oxidized and the most active form of the vitamin B complex. It is rarely found in food, and therefore it must be taken from vitamin complexes. Moreover, there is a distinction between food folate and FA, a distinction that is important because the two forms have different bioavailabilities[154]. Both substances are metabolically inactive and require a series of enzymatic processes to become active. Conversion to dihydrofolate and tetrahydrofolate catalysed by dihydrofolate reductase is the first step, followed by conversion to l-methylfolate by methylene-tetrahydrofolate reductase. This conversion allows gut absorption and liver transfer and storage of this active metabolite. In general, the food born FA has a bioavailability down to 50% lower than the synthetic one[155].

One of the most important roles of FA is to reduce the risk of neural tube defects like spina bifida and anencephaly that can be developed from the failure of neural tube closure during the third and fourth weeks of pregnancy. FA can prevent their apparition by providing the methyl-group required of one carbon transfer pathways, fundamental in amino acid metabolism. It also helps DNA synthesis and methylation by being a methyl group donor. Both roles are extremely important for foetal development[156].

A supplementation with 400 μg FA during the periconception period is highly recommended to prevent neural tube disease development. Today, at least 82 countries have a legislation to mandate nationwide mandatory fortification programs in which at least one industrially milled cereal grain product (e.g., wheat flour, maize, or rice) are fortified with FA[157,158].

One of the main issues when FA necessary dose is taken from food and in some cases even for the synthetic FA capsules and solutions is that the substance is very sensitive to medium changes and it can easily be oxidized and degraded.

2.3 Tetracycline

Tetracycline (TET) is a widely employed antibiotic in human and veterinary medicine and has been widely investigated, especially in veterinary samples. Probably the most prominent type of tetracyclines class, it is absorbed in small amounts through the animal intestinal tract and mainly accumulates in veterinary wastes and environmental samples[159,160].

It has demonstrated several adverse effects, such as antibiotic resistance, liver damage, allergic reactions in hypersensitive individuals, change in gut flora, vision problems, and tooth discoloration in infants[161]. In the last years, TET has been widely used in livestock in order to assure the fast and healthy growth of the animals leading to large TET residues in animal-derived food as well as in the waste water derived from the animal's sacrifice, all in all leading to the appearance of TET-resistant bacteria isolates in the environment[162].

As a result, the European Union (E.U.) has established maximum residue levels (MRL) for TET in milk products (100 μg kg^{-1}), eggs (200 μg kg^{-1}), liver (300 μg kg^{-1}) or kidneys (600 μg kg^{-1}). In the U.S. Food and Drug Administration (FDA) has also established MRLs that are more or less similar to the ones proposed by the E.U. 400 μg kg^{-1} in milk, 6000 μg kg^{-1} in the liver and 2000 μg kg^{-1} for the muscle samples[163].

Therefore, a fast, non-expensive and reliable detection method would be necessary. In the last years, electrochemical sensors have attracted increased attention in TET detection. Milk samples are commonly investigated for TET levels using biosensors, while honey as a possible food matrix has also been analysed for TET, as it is often added in the production process of honey to treat bacterial bee brood infection in apiculture[164].

3. Relevant targets for food analysis

3.1 Lysozyme

Lysozyme (Lyz), also known as muramidase or N-acetylmuramic hydrolase, is a small protein with a molecular weight of 14.3 kDa, monomeric, stabilized by disulphide bonds made between the eight-cysteine residues[165].

Also called the human's body own antibiotic, Lyz exhibits its antibacterial effect thanks to a cleavage made by its catalytical effect on the β (1-4) – bond between the N-

acetylmuramic acid and N-acetylglucosamine residues of bacterial wall, that determines the peptidoglycan integrity[166].

In the human body, Lyz can be found in almost all body fluids, but the highest activity is in tears, where the enzyme is about 120 times more active than in serum[167].

Due to its antibacterial activity, Lyz is applied in the food industry, especially as a food preservative. Particularly, Lyz is applied in wine industry in order to stabilize the wine and stop the fermentation instead of sulphites, with an allowed limit set by the E.U, to 50 g hL^{-1}[168]. Moreover, it is added in some cheese as well as in beer as prevention for butyric bacteria, in meat and shrimps to extend their shelf-life[169].

Although widely applied in the food industry, Lyz can potentially trigger adverse reactions in sensitive individuals. It has an allergenic activity demonstrated by using the skin-pick test. Early asthmatic response appears on allergic patients. Serum specific IgE antibodies to Lyz were detected, proving its allergic activity[170]. Even in trace amounts, Lyz can be toxic with symptoms such as weakness, lethargy, and dishevelment or non-toxic. The allergic reactions are immune-mediated adverse reactions that are mediated by IgE and they can become severe adverse reactions[171]. They can occur from mild urticaria to anaphylactic shock that can cause the death of the patient. In order to prevent this kind of adverse reaction, individuals with a history of allergenic sensibility must avoid interaction with the allergen and the food containing it[172].

Therefore, it is necessary to develop reliable analytical methods to guarantee consumers protection and to improve food production in terms of hazard analysis of critical control, points risk assessment and good manufacturing practice[173].

3.2 Peanut allergens

Peanuts (Arachis hypogaea) are among the most common food products with allergic reaction-induced, being often introduced in human dietary due to their essential protein, fat, iron, zinc, and niacin (vitamin B3). The most allergenic proteins responsible for peanuts allergy are from the Ara h family: Ara h 1, 2, 3, and 6 [174].

Ara h1 is the most prevalent peanut allergen. It is considered one of the most severe, life-threatening food sensitivities since it triggers the highest frequency of severe and fatal reactions, even in trace amounts. It accounts for between 35 and 95% of allergic reactions in peanut allergy patients[175].

Since the allergenic reaction happens extremely fast, there is almost no possibility to prevent the allergen reaction from happening, so the best way is avoidance of possible peanut-based foods. Currently, in the U.S. there are 32 million people having food allergies which roughly means 1 in 10 adults[176]. Moreover, there has been a 377%

increase in the diagnosed anaphylactic food-induced reactions between 2007 and 2016[177]. The E.U. created a list of major 14 food allergens which must be labelled on the pre-packed food products as deliberate ingredients (Ref:CX/FL93/5)[178,179].

Even though it is quite easy to avoid direct contamination, there is a possible risk of ingesting the allergen from products that generally do not contain peanuts, but that were contaminated during the manufacturing process, from product mislabelling or just from economical purpose adulteration[180].

Thus, it is extremely important to develop fast, accurate and easy-to-use analytical methods to determine Ara h1 allergen from food products that might contain traces of peanuts.

Personal contributions

I. Polymer-based electrochemical platforms

1. Poly-Pyrrole electrochemical sensor for direct detection of Folic Acid (Study 1)

1.1 Introduction

FA is a vitamin with important functions for the human body, such as the development and healthy growth of the foetus. FA cannot be stored in the human body. Because of that, regular intake of dietary products or vitamin supplementation is necessary for a healthy lifestyle, as much as it is necessary to monitor the levels of FA in the body fluids in case of deficiency or in the case of pregnancy[155]. Therefore, it is necessary to develop in situ quantification methods that can be applied for biological samples, drug and food control.

In this study, cone-like carboxylic functionalized polypyrrole was synthesised via the electrochemical polymerisation by CV of 3 carboxylic pyrrole in the presence of $LiClO_4$ and polyvinylpyrrolidone, on a screen-printed carbon electrode (SPCE) (Scheme 2).

The developed platform was used for the preconcentration of FA using DPV at the electrode surface, followed by CV for its detection. The importance of the sensor's specificity was not neglected and evaluated using dopamine, serotonin and ascorbic acid as possible interferents. In order to assess the potential applications of the sensor, it was tested in spiked human serum samples and pharmaceutical FA tablets and the obtained results were compared with a validated spectrophotometrically method.

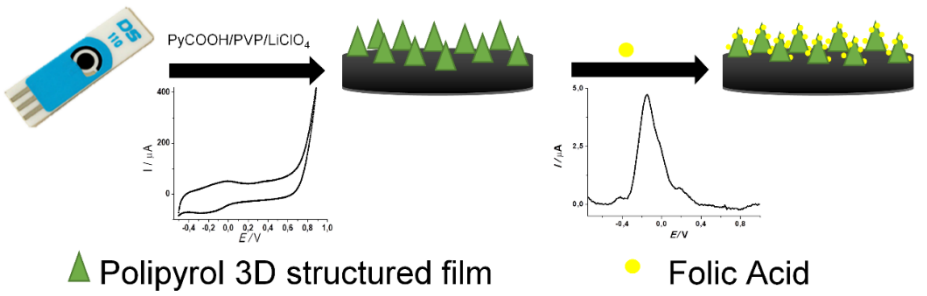

Scheme. 2 *Schematic representation of the FA sensor development*

1.2 Materials and Methods

All the reagents were purchased at an analytical grade and were used without further purification. Potassium ferrocyanide ($K_3[Fe(CN)_6]$), potassium ferricyanide ($K_4[Fe(CN)_6]$), 3-carboxylic pyrrole, $LiClO_4$, Na_2HPO_4, NaH_2PO_4 polyvynilpyrrolidone (PVP) were all bought from Sigma Aldrich (Germany). FA was purchased from Toronto Research Chemicals (Canada). For real sample analysis, human serum was purchased from Thermo Scientific (Germany) and the pharmaceutical tables (Acifol, 5mg) from a local pharmacy. All solutions were prepared using Milli-Q water.

SPCE from Methrom Dropses (Netherlands) was used as an electrochemical cell, with a working electrode surface of 12.56 mm^2, a silver pseudoreference and a carbon auxiliary electrode. CV was employed in the electropolymerization of the 3-carboxylic pyrrole by adapting a previously published procedure[181]. Practically, 50µL of a 0.1M monomer in 0.1M $LiClO_4$ and 9 mg mL^{-1} PVP solution was dropped on the SPCE and using CV (-0.5 – 1.1V, 100 mV s^{-1}, 10 scans) it was polymerized to 3-carboxylic poly-Pyrrole (PPy-COOH). The modified electrodes were characterised electrochemically using CV and EIS in a 5 mM $Fe(CN)_6]^{3-/4-}$ in 20 mM PBS pH 7.4 solution.

Before the detection of FA, a pretreatment in DPV was performed. Basically, a 50 µL of FA solution containing different concentrations was dropped on the electrode surface, and the potential was scanned from -0.8 to 1 V with a scan rate of 20 mV s^{-1}. Next, the detection of FA was achieved by CV in the same solution. The potential was scanned three times between -0.8 and 1V, with a scan rate of 50 mV s^{-1}.

In order to assess the sensitivity of the proposed sensors, it was tested in FA standard solutions prepared in 20 mM PBS buffer pH 7.4 as follows: 2.5 µM, 5 µM, 12.5 µM, 25 µM, 50 µM, 100 µM, 150 µM, and 200 µM.

The real samples analysis was performed on commercial human serum and on pharmaceutical tablets. The commercial human serum was diluted with 20 mM PBS pH

7.4 at a 1:100 ratio and then spiked with standard solutions of FA in the range 5 – 200 μM.

For the pharmaceutical tablets of declared 5 mg FA, the following protocol was used: 10 tablets were weighed and ground until a fine, homogenous powder was obtained. 100 mL of 20 mM PBS pH 7.4 were added and then ultrasonicated for 90 minutes, followed by a filtration process using 0.45 μm and 0.2 μm Phenex microfilters. Next, the samples were spiked with an internal standard of FA in order to achieve a theoretical concentration of 100 μM.

The stability of the platform towards the detection of FA was evaluated by performing successive tests on the same electrode using a 100 μM standard solution of FA. The stability in time was assessed after 1, 3, 10, and 30 days after the elaboration of the platform. Each experiment was performed on a new electrode.

All electrochemical experiments were performed using Autolab PGSTAT30 and Autolab PGSTAT302N potentiostats equipped with an EIS module, and Nova 1.10 software was used for data processing.

SPECORD250 PLUS (Analytical Jena, Germany) spectrophotometer fitted with deuterium and tungsten lamps was used for the spectrophotometric analysis and WinAspect software for the data acquisition.

1.3 Results and discussions

1.3.1. Electrochemical Deposition and Characterization of the PPy-COOH Morphology

The electrochemical deposition of 3-carboxylic pyrrole was performed by CV using 0.1 M $LiClO_4$ as electrolyte solution and PVP as surfactant and shape modifier. 10 potential scans were applied -0.5 V to 1.1 V at 50 mV s^{-1}. From Figure 3A, a peak couple that is increasing in intensity with the increase of the CV scan number, corresponding to the growth of the backbone was observed. The anodic (0.07 V) and cathodic (-0.07 V) peaks linked to the deposition of the polymeric structures suggest the growth of the conductive layer on the electrode carbon surface. The anodic peak suffered a slight shift from 0.05 V to 0.08 V during the 10 scans and the cathodic one a shift from -0.033 V to -0.1 V mainly because the polymeric structures did not reduce the electron transfer rate, despite the increase of polymerization signal suggesting the formation of a conductive polymeric surface[182].

In order to prove the electropolymerisation of PPy-COOH, we carried out the deposition in the absence of the surfactant (Figure 3B), observing that the peak heights

were significantly lower compared to the deposition in the presence of PVP. The deposition was also evaluated in the absence of the monomer. No characteristic peaks for the electrochemical polymerisation were formed, confirming that observed peaks correspond only to the electrochemical generation of the PPy-COOH.

The concentration of 3-carboxylic pyrrole was also optimised. As it can be seen in Figure 3C, there is an increase in peak oxidation/reduction peak height from 0.05M (black line) to 0.1M (red line). However, by the increase of the monomer concentration to 0.25M (green), an increase in the capacitive current was observed, which could block the signal attributed to the electrochemical oxidation of FA.

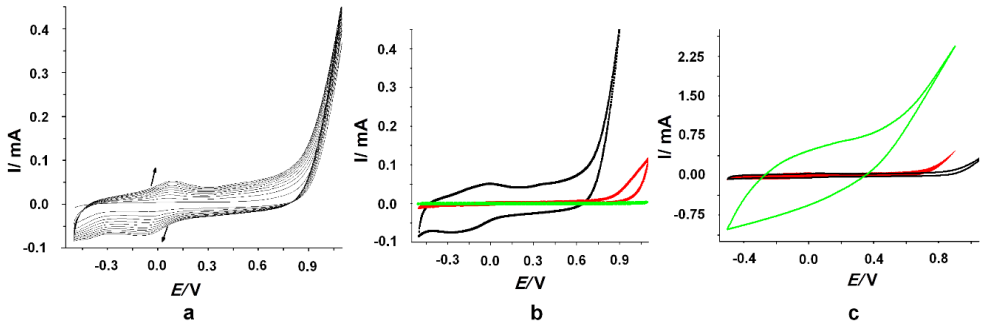

Figure 3 A *Electrochemical deposition of 3-carboxylic polypyrrole in 0.1 M $LiClO_4$ with 9 mg mL^{-1} PVP;* ***B*** *10^{th} cycle for the electrochemical polymerisation of 3-carboxylic pyrrole in the presence of 9 mg mL^{-1}PVP in 0.1M $LiClO_4$ (black line), only in 0.1M $LiClO_4$ (red line) and in 0.1M $LiClO_4$ and 9 mg mL^{-1} PVP in the absence of the monomer (green line);* ***C*** *10^{th} cycle for the electrochemical polymerization of 3-carboxylic pyrrole 0.05 M (black line), 0.1 M (red line) and 0.25 M (green line) in the presence of PVP in 0.1M $LiClO_4$*

1.3.2 Platform Characterisation

The platforms were assessed by electrochemical and microscopic methods. The PPy-COOH structures were tested in the presence of a 5 mM $[(Fe(CN)_6]^{3-/4-}$ in 20 mM PBS pH 7.4 solution as a redox probe in order to evaluate the conductivity properties before and after the electropolymerisation, and after the detection of FA, as well (Figure 4A). A slight decrease in the average current intensity was observed after the polymerisation suggesting a reduction of the electron transfer rate due to the different morphologies that partially covered the working electrode. After the interaction with a 100 µM FA solution, an increase in the oxidation/reduction peak intensities was observed. This might be due to a change caused either to the polymerisation or adsorption of FA[183].

The interfacial charge-transfer phenomena were assessed step by step on the unmodified SPCE, after the deposition of the polymeric structures and after the testing

of FA by EIS experiments in a 5 mM $[Fe(CN)_6]^{3-/4-}$ solution in 20 mM PBS pH 7.4 (Figure 4B).

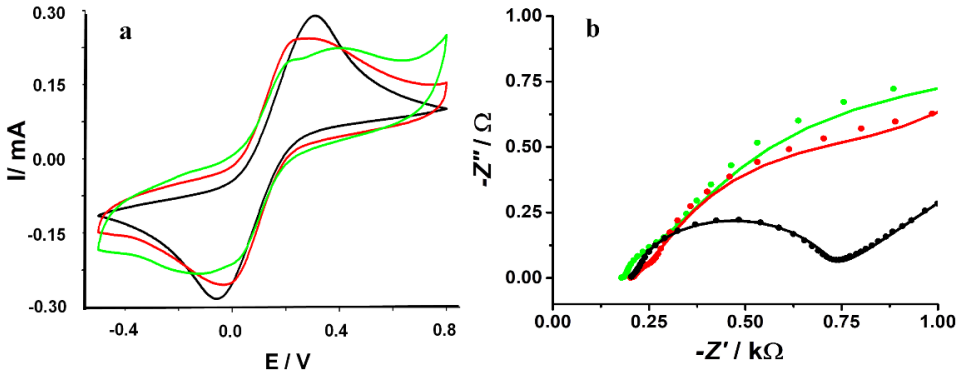

Figure 4 a *CV and* ***b*** *EIS graphs performed in 5 mM $[Fe(CN)_6]^{3-/4-}$ for the unmodified SPCE (black line), after the electrochemical generation of the PPy-COOH structures (green line) and after the detection of 100 μM FA (red line).*

A dramatic decrease of R_{ct} after the deposition step from 508 Ω to 55 Ω was observed. This confirmed the CV results that showed an improvement in the electron transfer. The second semicircle in the Nyquist plot represents the generation of the polymeric structures. After the FA addition, a new resistance decrease could be observed, again confirming the CV results.

1.3.3 Folic Acid determination

The electrochemical behaviour of the analyte on the 3D PPy-COOH modified SPCE was studied. First, a conditioning DPV procedure was performed in order to preconcentrate FA and then a CV procedure for its determination.

An anodic peak was observed during the DPV analysis at -0.2 V, and it was linked to the electrochemical oxidation of the polypyrrole backbone (Figure 5A). The DPV anodic pretreatment performed using a low scan rate enabled the oxidation of FA molecules at the electrode surface leading to an activation of the redox process of FA. Also, dehydrofolic acid was generated by CV when the potential was firstly scanned in the anodic direction.

In Figure 5B an anodic peak at -0.5 V can be observed and associated to the electrochemical oxidation of FA. Its apparition only on the platform in the presence of PVP proves the affinity of this platform for FA oxidation. The 3D morphologies have an

important effect on the detection of FA since only the interaction with the polymeric structures enabled the reversible oxidation of 5, 8-dihydrofolic acid at -0.5 V.

The intensity of the anodic peak correlated with the electrochemical oxidation of 5,8-dihydrofolic acid increased proportionally with the increase of the concentration of the analyte from 2.5 µM to 200 µM (Figure 5C). Therefore, a linear range in this domain was obtained with a calibration curve calculated as: I (µA)= 0.0245*[FA] (µM) +0.731 and a LOD of 0.8 µM was calculated as the signal/noise ratio of three (S/N=3) (Figure 5D).

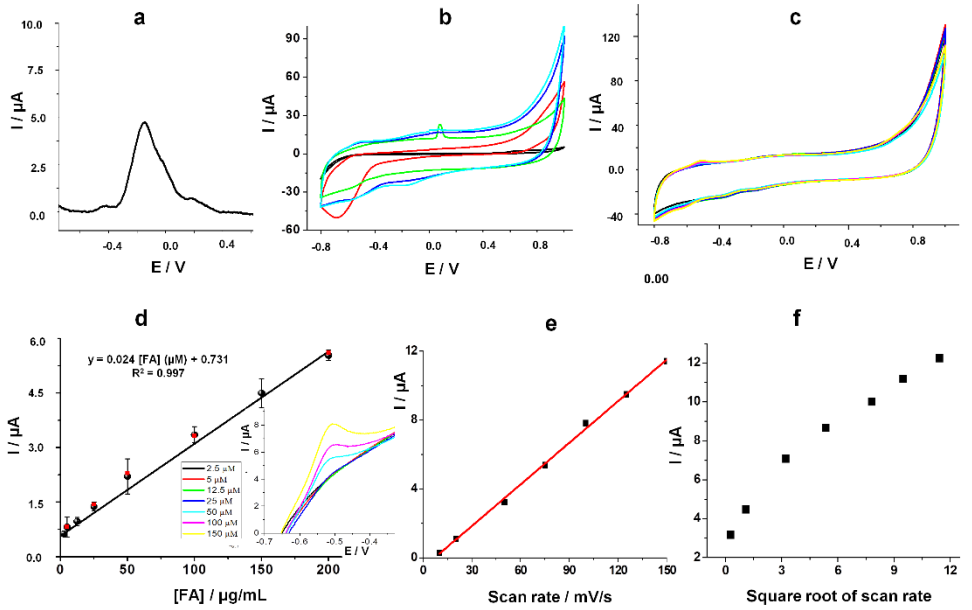

Figure 5 A *Preconditioning by DPV in 0.1 mM FA in 20 mM PBS pH 7.4;* ***B****: CV in 100 µM FA on the unmodified SPCE (black line), with 3-carboxylic pyrrole polymerised in 0.1M $LiClO_4$ (red line), with 0.1 M $LiClO_4$ and 9 mg mL^{-1} PVP (green line), with 3-carboxylic pyrrole polymerised in 0.1M $LiClO_4$ and 9 mg mL^{-1} PVP (blue line), with 3-carboxylic pyrrole polymerised in 0.1 M$LiClO_4$ and 9 mg mL^{-1} PVP kept 5 minutes under nitrogen prior the analysis (light blue line).* ***C:*** *CV for different concentrations of FA standard solutions in 20 mM PBS pH 7.4 on the modified surface (black plots), FA standard solutions in 1:100 commercial human serum in 20 mM PBS pH 7.4;* ***D:*** *Calibration curve for different concentrations of FA; Inset: magnification of the anodic peak at -0.5 V/Ag;* ***E:*** *Influence of the scan rate on the current intensity corresponding to the oxidation peak at -0.5V/Ag;* ***F:*** *Influence of the square root of the scan rate on the current intensity*

FA is a molecule with a structure that facilitates the adsorption on the surface of the electrode thanks to its p-aminobenzoic acid moiety and the high differences in the

graphite-based working electrode surface. A current intensity increase with the increase of the scan rate is further confirming the adsorption of FA on the polymeric surface (Figure 5E). When plotting the current intensity against the square root of the scan rate, no linear correlation was observed, underlining that the electron transfer is not diffusion-controlled, which means that FA molecules remain adsorbed on the electrode surface (Figure 5F).

1.3.4 Stability, specificity and applications

The assessment of intra-assay stability of the sensor was performed by making repetitive tests on the same electrode with different standard solutions of 100 μM FA. Between the assays, the electrode was thoroughly rinsed with ultrapure water. After the second test it was registered an increase in the signal of 40% and after the third test an increase of 52% (Figure 6A).

In time stability was evaluated by performing analysis using different sensors tested on a specific number of days after their preparation (1, 3, 7, 10, 30 days) and using 100 μM FA. The sensors were stored at 4°C while waiting to be tested. Excellent recovery of the signal was obtained in comparison with the data obtained on the first day (Figure 6B), with less than 2.5% difference in each case, suggesting that the sensor remains stable for up to one month, stored at 4°C and it can be used directly, without any pretreatment.

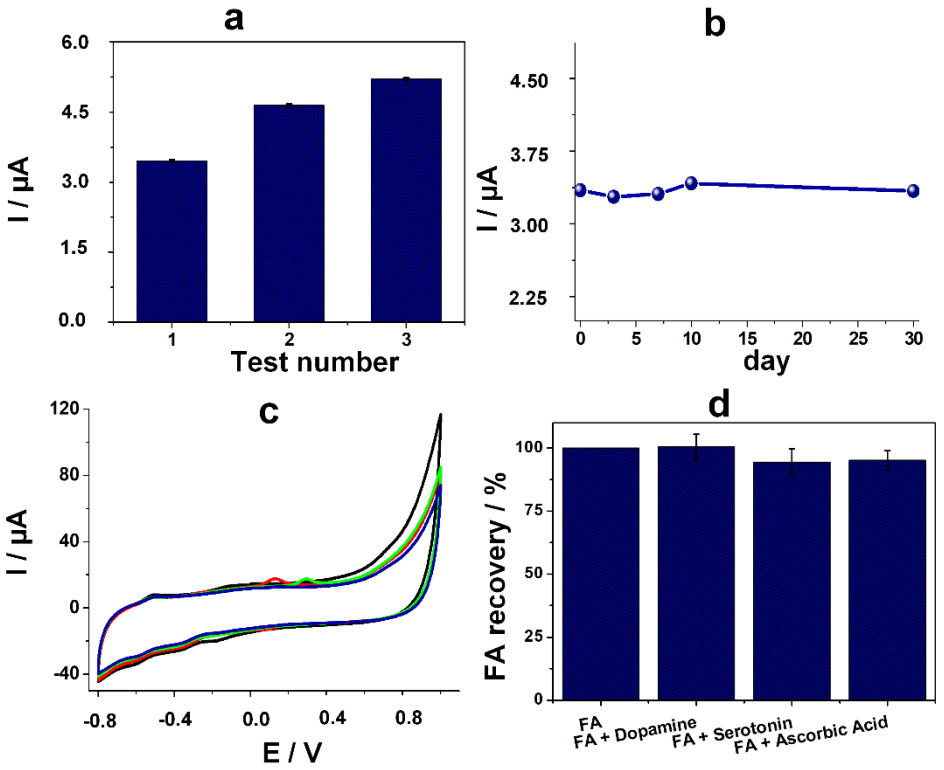

Figure 6 A *Current intensity (µA) obtained after performing tests on the same electrode using a 100 µM FA solution;* ***B*** *Current intensity (µA) corresponding to the electrochemical oxidation of 5, 8-dihydrofolic acid after 1-30 days in the presence of 100 µM FA;* ***C*** *CVs of a 100 µM FA (black line) and 25 µM interfering agent in 20 mM PBS pH 7.4: dopamine (red line), serotonin (green line), and ascorbic acid (blue line);* ***D*** *Recoveries for the current intensity (µA) of the anodic peak correlated with the electrochemical oxidation FA in the presence of 100 µM FA and of 25 µM interfering agents: dopamine, serotonin and ascorbic acid*

The selectivity of the sensor for FA specific detection was assessed in the presence of analytes commonly found in real samples like dopamine, serotonin and ascorbic acid; 25 µM of interfering agents and 100 µM FA were used in the detection solution. It can be easily observed no decrease in the anodic peak current intensity in the presence of any of the interferents (Figure 6C). The oxidation peaks of the analytes were observed at 0.1 V for dopamine (red line), at 0.3 V for serotonin (green line) and at 0.1 V for ascorbic acid (blue line), peak potentials that do not interfere with the electrochemical signal of FA. This difference in the oxidation peak potentials allows their simultaneous analysis without any other modification of our platform. The average recoveries of the signal corresponding to the oxidation of FA in the presence of

dopamine, serotonin and ascorbic acid were 100.49% (Relative standard deviation (RSD) 4.98%), 94.52% (RSD 5.13%), 95.12% (RSD 3.74%), respectively (Figure 6D).

Regarding the applications of the developed sensor, analyses were performed in diluted commercial serum and commercially available FA tablets solutions. In the first case, human serum samples were diluted 1:100 with 20 mM PBS pH 7.4 and then spiked with FA to achieve concentrations in the range of 0 - 200 μM.

In the absence of the target analyte, no anodic peak was observed, while with the increase of FA concentration in the determination solution, the characteristic oxidation peak started to appear. Very good recoveries for the current intensity of the anodic peak: 101.9% (RSD 2.44%) were observed. Moreover, the current intensities of the anodic peaks were plotted in the calibration curve obtained with the FA standard solutions and the obtained results indicated an average recovery of the concentrations of 106.0% (RSD 16.7%).

Table 1 . *Summarized Data for the Electrochemical Detection of FA in Real Samples*

Commercial serum spiked with FA			**Pharmaceutical tablets (5 mg)**			
	Recovery			Recovery		
[FA] (μM)	I (%)	[FA] (%)	[FA] (μM)	I (%)	Calculated [FA] (%)	Amount of FA in tablets (%)
25	104.1	115				
50	104	120.8	50	88.2	99.5	101.9
100	98.9	105.6	100	98.3	104.4	102.4

In the second case, the pharmaceutical tablets, the FA was first extracted in 20mM PBS pH 7.4 and then the samples were analysed and compared with a UV-VIS control method. The intensity of the signal corresponding to FA electrochemical oxidation was plotted in the calibration curve and the corresponding concentrations of the samples were calculated. The average recovery for the calculated concentrations was 102.1% (RSD 3.2%, 5 samples) and for the amount of FA in a tablet, the average recovery was 100.2% (RSD 3.3%, 5 samples). The results obtained were summarised in Table 1. In order to compare the electrochemical data with the UV-VIS data, a statistical t-test was

applied and the results indicated that there is no significant difference between the two series (0.142 >0.05). Also, the ANOVA test showed a F value of 1.27161, larger than 0.05, confirming that there is no significant difference between the two series.

1.4 Conclusions

In this study, a carboxyl groups modified polymer was used in the development of an electrochemical platform suitable for the selective detection of FA. After a simple two steps protocol that included a pretreatment step and a FA detection one, the sensor was able to detect and quantify FA in pharmaceutical samples and biological liquids in a large concentration range between 2.5 -200 μM. The applicability of the sensor was confirmed by spectrophotometric analysis. This sensor represents a promising first step in the development of a point of care device for the detection of FA in pharmaceutical and biomedical samples.

II. Polymer – noble metallic particles based electrochemical platforms

1. Gold-Platinum/poly-aniline nanostructured platform for arsenic fingerprinting (Study 2)

1.1 Introduction

Arsenic is considered to be one of the most toxic elements that can be found in nature, with an increased carcinogenic effect, thanks to its ability to mutate DNA sequences that lead in the end to aberrant gene expressions[184]. Since there are many regions worldwide (Bangladesh, Argentina, China, India, Italy) in which the amount of arsenic found in water is much higher than the limit of 10 μg L^{-1} imposed by WHO, therefore, fast, cost-effective and reliable detection methods are needed[146].

Currently used methods for its detection in water samples are atomic absorption and emission spectrometry, mass spectrometry and, nonetheless, high-performance liquid chromatography methods[185]. Although these methods present good LODs and high specificity, there are some limitations that could be mentioned: the complex equipment and skilled personnel, long time sample preparation, and most important they are not suitable for *in situ* detection and routine analysis.

In this study, a sensitive electrochemical sensor for arsenic analysis in water samples is presented. For this, an electrochemical platform based on a mixed PANI film and bimetallic composite Au-PtNPs. PANI, as one of the most promising conducting polymers, has an important role in increasing the conductivity with a low cost of production and a decreased production time[186–188]. The electrochemical detection of arsenic was achieved by measuring the oxidation potential of the analyte by means of square wave voltammetry (SWV) on SPCE, showing a good potential for *in situ* detection.

1.2 Materials and Methods

1.2.1 Reagents

50mM Sodium arsenite ($NaAsO_2$), LiCl, 11M Aniline ($C_6H_5NH_2$) and 30% hydrochloric acid (HCl) were purchased from Merk (Germany), 97% H_2SO_4 solution, KCl, perchloric acid ($HClO_4$), tetrachloroauric acid ($HAuCl_4$), hexachloroplatinic acid (H_2PtCl_6 $K_3[Fe(CN)_6]$, $K_4[Fe(CN)_6]$, were purchased from Sigma-Aldrich. Heavy metal solutions were prepared using Cu(II), Pb(II), Hg(II) standard solutions of analytical grade, from

Flucka (Italy). All the solutions were prepared using ultrapure water from a Mili-Q System (Milipore, Italy, 18 MΩ cm^{-1}).

1.2.2 Electrochemical analysis

Autolab potentiostat *PGSTAT302*, using NOVA 1.10 and 1.11 was used for all the electrochemical experiments. SPCE with a 3mm diameter working electrode, a Ag^{+}/AgCl pseudo-reference electrode and a graphite counter electrode were purchased from EcoBioServices (Florence, Italy).

For the platform development and electrodes modification standard solutions of 2mM $HAuCl_4$ in 0.5M H_2SO_4, 40µM H_2PtCl_6 in 0.5M H_2SO_4, 1mM H_2PtCl_6 in 0.5M H_2SO_4 and 2.5mM $C_6H_5NH_2$ in 50 mM $HClO_4$ were prepared.

Aniline was deposited through an electropolymerization procedure[189,190] by dropping a 50µL drop of a 2.5mM $C_6H_5NH_2$ in 50 mM $HClO_4$ onto SPCE and cycling the potential between 0.4 – 0.8 V, 10 times and a 50 mV s^{-1} scan rate. $HAuCl_4$ and H_2PtCl_6 deposition was performed using chronoamperometry on SPCE and PANI modified SPCE by applying a fixed potential of – 0.2 V for 130s from solutions containing:

- 0.2mM $HAuCl_4$ in 0.5M H_2SO_4;
- 2mM $HAuCl_4$ in 0.5M H_2SO_4;
- 4µM H_2PtCl_6 in 0.5M H_2SO_4 (a);
- 1mM H_2PtCl_6 in 0.5M H_2SO_4 (b);
- Combination of these

Determination of the electroactive surface area/bare SCPE geometric area (3 mm diameter) of the developed platform was performed in a 5 mM $[Fe(CN_6)]^{4-/3-}$ in 0.1M KCl solution at different scan rates (25-150 mV/s), and a potential range between -0.5 and 0.8 V.

The electrolyte effect was analysed by performing SWV in 0.1 M KCl in HCl pH=2, 6 M LiCl in 0.1 M H_2SO_4 and 0.1 M HCl all containing different concentrations of arsenic obtained by diluting 50mM $NaAsO_2$ water solution in the electrolyte chosen for the experiment. SWV conditions were: conditioning potential (E_{cond}) +0.7 V for 30s, deposition potential (E_{dep}) -0.5- -0.3 V for 60-240s, equilibration time (t_{eq}) 30s, scan rate 45mV s^{-1}, step potential 0.003V, frequency (f) 15 Hz. For the measurements the platform was immersed in 5.0 mL of solutions. Stirring was used during the accumulation step and the deposition period using a Methrom 728 stirrer. $E_{dep,}$ deposition time were optimized and the best electrolyte solution was chosen during the experiments.

Multiple measurements were performed using the same platform and the same electrolyte solution by increasing the concentration of As(III) and by washing the platform with 50µL of a 0.1M HCl solution 3 times, between measurements.

1.3 Results and Discussions

1.3.1 Platform development

Figure 7A presents a comparison between the % of electroactive surface area/bare GSPE geometric area for the platforms with the best electroactive areas. The histograms represent the electroactive area of the modified electrodes, as seen in Table 2, which was calculated using the Randles–Sevcik equation (1):[191]

$$i_p = (2.69 \times 10^5)n^{3/2}ACD^{1/2}\,v^{1/2} \quad (1)$$

Table 2 . *Metallic salts and PANI modification of SPCE in order to obtain a hybrid platform for the As(III) detection*

Platform design		Experimental conditions	
		Solution concentration	**Electrodeposition parameters**
(I)	AuNPs/SPCE	2 mM $HAuCl_4$ in 0.5 M H_2SO_4	– 0.20V for 130 s
(II)	PtNPsi/SPCE	4 µM H_2PtCl_6 in 0.5 M H_2SO_4	– 0.20V for 130 s
(III)	PtNPsii/SPCE	1 mM H_2PtCl_6 in 0.5 M H_2SO_4	– 0.20V for 130 s
(IV)	Au-PtNPs/SPCE	2 mM $HAuCl_4$ + 4 µM H_2PtCl_6 in 0.5 M H_2SO_4	– 0.20 V for 130 s
(V)	PANI/SPCE	2.5 mM $C_6H_5NH_2$ in 50 mM $HClO_4$;	CV: -0.40– 0.80 V vs Ag/AgCl, 10 scans, 50 mV s^{-1} at SPCE
(VI)	Au-PtNPs/PANI/SPCE	2.5 mM $C_6H_5NH_2$ in 50 mM $HClO_4$;	CV: -0.40– 0.80 V vs Ag/AgCl, 10 scans, 50 mV s^{-1} at SPCE
		2 mM $HAuCl_4$ + 4 µM H_2PtCl_6 in 0.5 M H_2SO_4	– 0.20 V for 130 s at PANI/SPCE

Choosing the best platform for further optimization in order to develop a sensor for As(III) fingerprinting was taken into consideration not only the obtained electroactive area but also other factors like the linearity of the calibration curve, the reproducibility of the test, the costs and time needed for the modification. The platforms that offered the best results regarding the above description are represented in Figure 7.

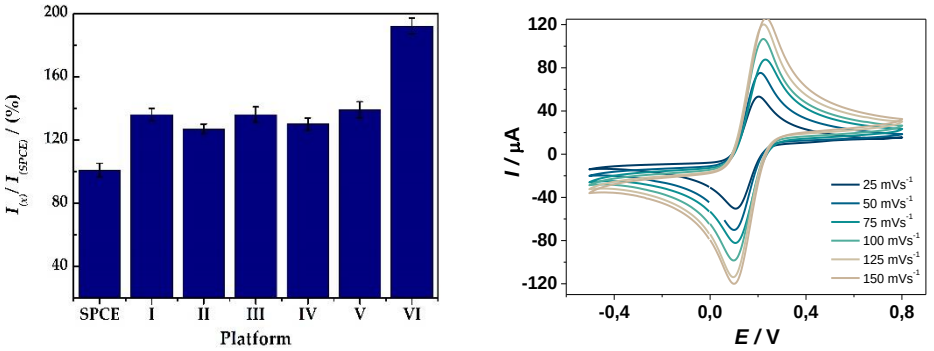

Figure 7 A. *Electroactive surface area % versus geometric area of a bare SPCE compared to SPCE modified with: (I)AuNPs, (II)PtNPs^{i}, (III)PtNPs^{ii}, (IV)Au-PtNPs, (V)PANI, (VI)Au-PtNPs/PANI.* ***B*** *Cyclic Voltammograms of the 2 mM $HAuCl_4$ + 4 µM H_2PtCl_6 in 0.5M H_2SO_4/SPCE modified electrodes in a 5 mM $[Fe(CN_6)]^{4-/3-}$ in 0.1M KCl solution using increasing values of scan rate speed: 25 – 150 mVs^{-1}*

From Figure 7A, it can be seen that the effective surface area of **(I)**AuNPs/SPCE platform is 1.33 times higher than the bare SPCE. The effect of H_2PtCl_6 concentration over the bimetallic platforms architectures was also evaluated. A higher concentrated chloroplatinic acid solution is not influencing significantly the electrocatalytic effect, the results being approximately the same for **(II)**PtNPs/SPCE (127%) and **(III)**PtNPs/SPCE (130%), respectively. Therefore, for the bimetallic platform design **(IV)**Au-PtNPs, a slightly higher effective surface area was obtained (136%), and when in combination with PANI, amplified peak currents with more reversible redox peaks were observed, which was related to around 2-fold increased electroactive surface area of **(VI)**Au-PtNPs/PANI/SPCE (192%) compared to bare SPCE. The synergistic effect of the combination of metallic particles and electroconductive polymer could be observed as **(V)**PANI/SPCE showed an increase of the electrode surface area of only 139% compared to bare SPCE proving nevertheless a small electrocatalytic effect of platform **(VI)**. Moreover, an important factor is the time needed for the platform development. For the fabrication of Au-PtNPs an amperometric procedure is applied and it takes 130s for the deposition, whereas for the electropolymerisation of aniline, a CV of 480s needs to be applied.

In order to decide which of the developed platforms is more suitable for arsenic fingerprinting, their overall characteristics were considered. AuNPs and PtNPs have proven to be very good electrical conductors, and with their incorporation in the sensors design, the electron transfer has improved. Moreover, studies have demonstrated that the PtNPs also work as atomic and molecular hydrogen generators in acidic environments and can chemically reduce the As (III) to As(0) leading to a cathodic pre-

concentration of As(0) at both the Pt sites and the Au sites[192]. Therefore, the platforms with the best overall performance chosen for further experiments were: **(IV)**Au-PtNPs/SPCE and **(VI)**Au-PtNPs/PANI/SPCE.

1.3.2 Experimental conditions optimization

In Figure 8, CVs of the platforms **(IV)** and **(VI)** in 0.1 M HCl in the presence and absence of 1 mM As(III), without any previous pre-concentration step can be observed. In the solutions free of As(III) there were no redox peaks observed for Au-PtNPs/SPCE platform, while when Au-PtNPs/PANI/SPCE was used a redox pair at around 0.38 V was obtained and explained as the oxidation/reduction of PANI. In the presence of As(III) both platforms showed a peak around 0.1 V that can be assigned to electrooxidation of As(0). The peak current intensity for **(VI)**Au-PtNPs/PANI/SPCE was 11.6 μA, while for **(IV)**Au-PtNPs/SPCE a lower current intensity was obtained (1.94 μA), platform **(IV)** showing, therefore, a better sensitivity towards As(III) detection **(VI)**.

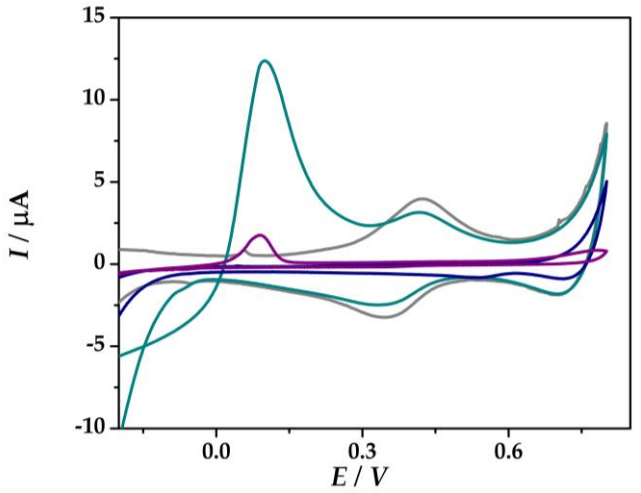

Figure 8 *CVs recorded in 0.1 M HCl at* ***(IV)****Au-PtNPs/SPCE (blue) and in the presence of 1 mM As(III) in (purple),* ***(VI)****Au-PtNPs/PANI/SPCE (grey) and in the presence of 1 mM As(III) (dark cyan) at 50 mV* s^{-1}

Several electrolytes (6.0 M LiCl in 0.1 M H_2SO_4 **(i)**, 0.1 M KCl in HCl pH=2.0 **(ii)**, and 0.1 M HCl **(iii)**) were tested towards As(III) fingerprinting using the optimised platforms. Parameters like the As(III) deposition time (t_{dep}) and potential (E_{dep}), electrochemical method, the response and the linearity of the developed platforms towards As(III) were studied and optimised using all solutions (i-iii).

Firstly, electrolyte **(i)** was tested for arsenic fingerprint. In Figure 9A, the peak currents intensities obtained for a 3 μM As(III) electrolyte (i) at the platform **(IV)**Au-

PtNPs/SPCE can be observed. Pre-concentration times of 120 s (A) and 240 s (B) and potentials of -0.35 V and -0.50 V, respectively, were optimised. It can be observed that at t_{dep} = 120 s pre-concentration time there is a great difference in the peak current values when applying E_{dep} = -0.35 V (45.54 μA) compared to E_{dep} = -0.5 V (6.66 μA). For longer cathodic pre-concentration time (t_{dep} = 240 s), an increase in the peak current intensity (27.64 μA) was obtained for E_{dep} = -0.5 V, whereas for E_{dep} = -0.35 V a slightly decrease down to 34.54 μA was observed. Even though higher peak current intensities were obtained at -0.35 V, the results were not proportional to the deposition time modification.

Next, two arsenic concentration solutions were tested, 3 μM and 30 μM As(III) in electrolyte **(i)**. After t_{dep} = 120 s, no relevant results were obtained as for the higher concentration of As (III), lower intensity peaks were observed. After 180s, better analytical responses of 36.1 μA and 48.0 μA were obtained for the two As(III) solutions. The results demonstrated higher electrocatalytic effect of the **(IV)**Au-PtNPs/SPCE platform when the potential was applied for t_{dep} = 240 s by comparing the peak current intensity ratio (a 2-fold increase) obtained in 3 μM and 30 μM As(III) solution (Figure9B).

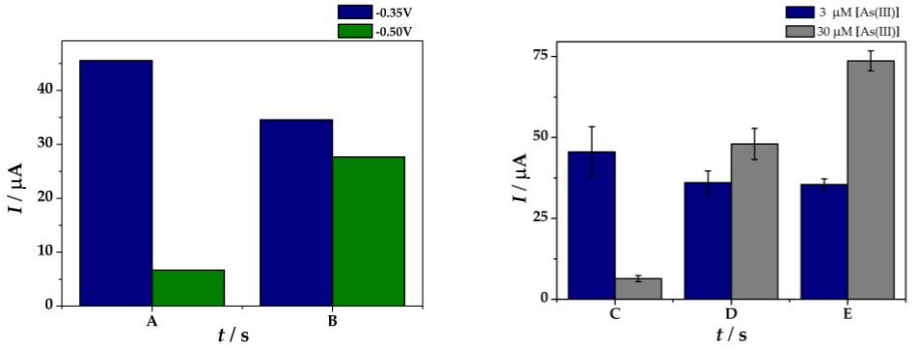

Figure 9 *Peak current intensities obtained by means of SWASV measurements at* ***(IV)****Au-PtNPs/SPCE from solutions containing 3 μM As(III) (blue) and 30 μM As(III) (grey) in 6.0 M LiCl in* H_2SO_4 *0.1 M by potential-assisted cathodic pre-concentration of :* ***A*** t_{dep} *= 120 s (A) and 240 s (B) at* E_{dep} *= -0.35 V (blue) and* E_{dep} *= -0.50 V (green); and* ***B:*** t_{dep} *= 120 s (C), 180 s (D), 240 s (E) at* E_{dep} *= -0.50 V*

As the fingerprint of As(III) in the electrolyte **(i)** offers only satisfactory results, in order to increase both sensitivity and reproducibility of the sensors, another electrolyte solution was used, namely 0.1 M KCl in 0.1 M HCl pH=2.0 **(ii)**.

Figure 10A shows the peak current intensities for **(IV)**Au-PtNPs/SPCE in 3 μM As(III) solution in the electrolyte **(ii)** with a t_{dep} = 120 s at E_{dep}: -0.35 V and -0.5 V. A

higher peak height was obtained when -0.5 V was used for the deposition of As(0 (22 μA) compared to -0.35 V (4.11 μA).

In the next step, the cathodic potential-assisted deposition time was optimised as it plays an important role in the sensitivity and reproducibility of the obtained sensors (Figure 10B). The electrochemical experiments were conducted at **(IV)**Au-PtNPs/SPCE in solutions containing 3 μM and 9 μM of As(III), respectively. The parameters of the cathodic pre-concentration of As(0) were E_{dep} of -0.50 V and t_{dep} of 120, 180, and 240 s, respectively. Increased values of the As(0) anodic stripping peaks are observed in correlation with the increase in the deposition time from 120 s to 180 s from a solution containing 3 μM As(III). When comparing the results obtained in 9 μM As(III) solution, little changes after 180 s cathodic pre-concentration (121.35 μA) could be observed, proving the low sensitivity of the sensor. When 240 s deposition time was used, an increase in the peak currents up to 59.35 μA and 112.92 μA from solutions of 3 μM As(III) and 9 μM As(III) solution in 0.1M KCl in 0.1M HCl, were obtained. Even though better sensitivities were observed, a high RSD of over 10% proves the sensors have a low reproducibility in this electrolyte.

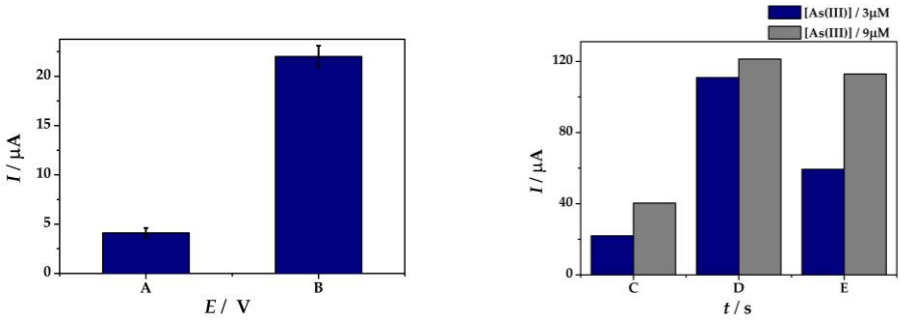

Figure 10 *Peak current intensities obtained by means of SWASV measurements at* ***(IV)****Au-PtNPs/SPCE from solutions containing 3 μM As(III) (blue) and 9 μM As(III) (grey) in 0.1 M KCl in 0.1 M HCl (pH=2.0)* ***(ii)*** *using a cathodic pre-concentration* ***A:*** *potential (E_{dep}) of -0.35 V (A) and -0.50 V (B) at t_{dep} = 120 s; and* ***B:*** *time (t_{dep}) of 120 s (C), 180 s (D), 240 s (E) at E_{dep} = -0.50 V*

After the optimisation steps, it can be concluded that -0.5 V was the best potential for the preconcentration of As(III) in both electrolytes tested. Regarding the time of the deposition, even though better sensitivities were obtained after t_{dep} = 240 s in electrolytes **(i)** and **(ii)**, the high %RSDs suggest that a reduced time could be more useful for future possible *in situ* analysis.

In order to be able to have a very reliable arsenic detection, all steps optimised during the development steps must be analysed, and the most suitable parameters used.

The oxidation peaks obtained at platform **(IV)** with a 3 μM As(III) in 6.0 M LiCl in 0.5 M H_2SO_4 **(i),** 0.1 M KCl in 0.1 M HCl pH 2.0 **(ii)**, and 0.1 M HCl **(iii),** were considered. An electrochemical reduction of As(III) was performed as pre-concentration at a E_{dep} of -0.50 V for 120 s. Regarding the platforms, number **(IV)** showed the highest electrocatalytic effect in the presence of As (6.66 μA) in the electrolyte **(i)** vs (5.07 μA and 2.76 μA) electrolytes **(ii)** and **(iii)**.

Nevertheless, when the concentration of arsenic is reduced to trace levels, the sensitivities in electrolytes **(i)** and **(ii)** are drastically reduced compared to the electrolyte **(iii)**. Considering that electrolytes **(i)** and **(ii)** exhibit an oxidation peak only at high levels of As(III) makes the electrolyte **(iii)** the best solution for As(III) fingerprinting at the developed platform. Nevertheless, the overall sensor fabrication and analysis time was 5 minutes for platform **(IV)**Au-PtNPs/SPCE, and 12 minutes for platform **(VI)**Au-PtNPs/PANI/SPCE, respectively; thus, proving its high efficiency as a possible future disposable sensor for arsenic sensing.

1.3.3. Analytical performances

A linear calibration curve for the electrochemical detection of arsenic was obtained for the platform **(IV)** Au-PtNPs/SPCE by plotting the As(III) oxidation peak (μA) versus its concentration (ppb) (Figure 11). For this, a SWV procedure was used, and concentrations of As(III) in the range 2.5 – 15 ppb were tested in 0.1 M HCl as electrolyte. A linear range between 2.5 ppb and 15 ppb As(III) with a sensitivity of 0.207 μA ppb^{-1} was obtained. The LOD, calculated on the basis of the 3*standard deviation ratio of sensitivity[191], was 0.627 ppb, with a limit of quantification of 2.5 ppb.

When platform **(VI)** Au-PtNPs/PANI/SPCE was tested using the optimized conditions, a calibration curve in the range of 0.1 – 1.25 mM As(III) with the following equation I(μA) = 6.116 [As(III)/mM] + 6.129; R^2 = 0.994. This could be probably due to the incorporation of the deposited As(0) into the PANI matrix and the lower catalytic effect of the noble particles.

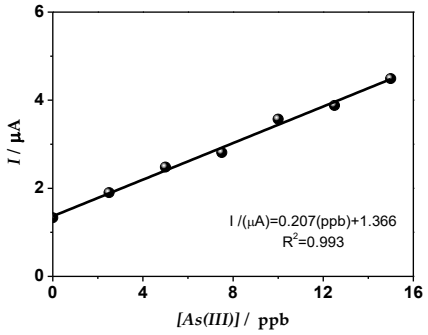

Figure 11 *Calibration curve for As(III) detection using 2.5, - 15 ppb As(III) in 0.1M HCl solution, using the 2 mM AuNPs with 4 μM PtNPs/SPCE sensor as the immobilisation platform (E_{dep} -0.5 V for 60 s)*

1.3.4. Specificity studies

Rarely As(III) can be found in water or sand samples alone, it is mainly found in complex matrixes. Most often, it is found alongside other metals like Cu(II), Pb(II) or Hg(II). All these metals can easily interfere with As(III) detection.

Platform (**IV**) was used for interference studies and SWASVs of different 0.1M HCl solutions containing Hg(II), Cu(II), Pb(II), As(III) or without any metal were performed. A specific peak for As(III) was found at a 0.20 V potential, close to which the Hg(II) (0.25 V) and Cu(II) (0.26 V) solutions could show a specific signal (Table 3). Even though this could mean an important interference from them, the low oxidation current intensity that was observed prove that the risk of interference with the As(III) detection is rather small.

Table 3 *SWASV signal for As(III), Cu(II), Pb(II), Hg(II) solution in 0.1M HCl using a ΔE 0 – 0.6V, and a deposition time of 60s at a Edep of -0.50 V*

Metal	E / V	I / μA
As(III)	0.20	8.93
Cu(II)	0.26	0.96
Pb(II)	0.47	5.67
Hg(II)	0.25	1.87

It was thus shown that using the optimised Au-PtNPs/SPCE platform, the detection of As(III) was performed even in the presence of other metallic ions.

1.4 Conclusions

A novel and easy to use nanohybrid platform based on a mixed film of PANI and Au-PtNPs bimetallic composite was optimised for the electrochemical fingerprinting of As(III). Taking advantage of PANI's low cost of production, easy and fast synthesis and good electrochemical features, it was used in a hybrid platform together with Au-PtNPs. In order to find the best protocol for As(III) detection, 3 electrolyte solutions were evaluated. Arsenic was detected with a good LOD on both a polymeric and polymer-free platform after the optimisation of the cathodic preconcentration and stripping parameters by square wave anodic stripping voltammetry at modified screen-printed carbon-based electrochemical cells. The study had proven the applicability of these sensors for As(III) *in situ* detection by a disposable and low-cost analysis method.

2. Gold /Poly-L-Lysine modified carbon electrodes for Lysozyme aptasensing (Study 3)

2.1 Introduction

Lyz is an enzyme present in multiple organisms where it plays various vital roles. One of the most important relies on its antibacterial activity, being also called the body's own antibiotic. Despite its proven utility, Lyz can potentially trigger allergic reactions in sensitive individuals, even in trace amounts, thus, the need for continuous monitoring of Lyz in products rich in Lyz, like wine or egg white, is of high importance[43].

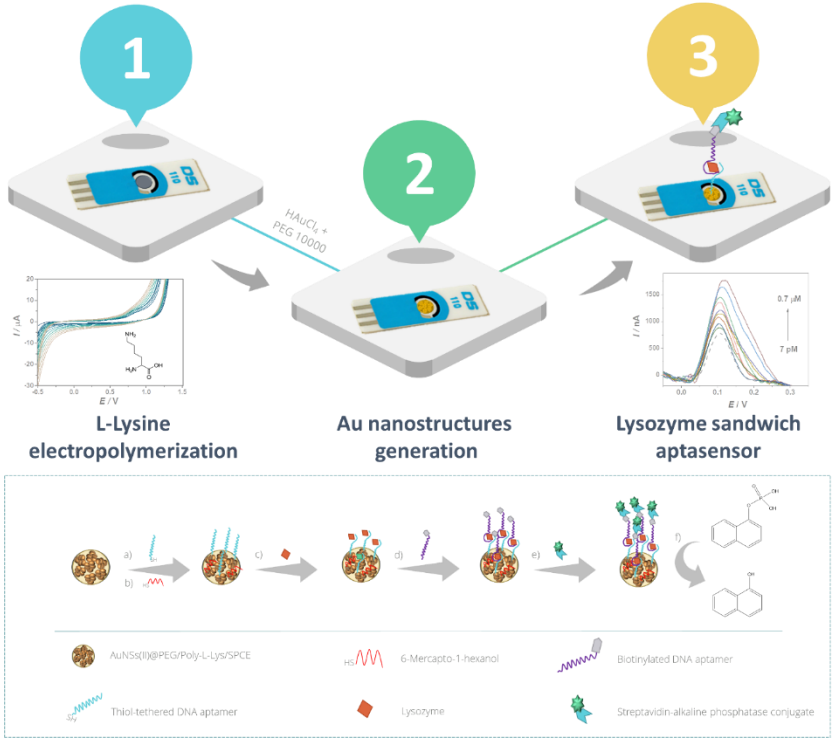

Scheme 3 *Schematical representation of the AuNS/Poly-L-Lysine based aptasensing of Lysozyme*

An electrochemical platform based on Poly-L-Lys and AuNSs was developed in this work (Scheme 3). On a first step, L-Lys was electropolymerized at SPCE followed by the electrodeposition of AuNSs from a mixture of $HAuCl_4$ and PEG 10 000. Next, once the platform was fully optimised and characterised by electrochemical and surface analysis techniques, a 5' thiol-modified aptamer for Lyz was immobilised on the platform. Then, Lyz was added and the aptamer-analyte specific reaction was enabled. A sandwich assay was obtained after adding a secondary aptamer modified at its 5'end with a biotin group. s-ALP was further bound, taking advantage of the specificity and sensitivity of the biotin-streptavidin bond. In the final step of the assay, the alkaline phosphate hydrolysed 1-Naphtil Phosphate (1-NPP) to α-Naphthol. Lyz was detected and quantified by using a DPV procedure and the oxidation of the redox-active α-Naphthol (Scheme 3). The assay was applied in real wine samples, and its efficiency was demonstrated by comparing the recovery values with a protein assay fluorescence kit.

2.2 Materials and Methods

2.2.1 Materials

KCl, sodium chloride (NaCl), L-Lys, disodium hydrogen phosphate (Na_2HPO_4), sodium dihydrogen phosphate (NaH_2PO_4), Tris(hydroxymethyl)aminomethane (TRIS), $K_3[Fe(CN_6]$, $K_4[Fe(CN_6]$, Lyz, diethanolamine (DEA), 6-mercaptohexanol (MCH), Glu, interleukin-6 (IL-6) s-ALP, α-naphtil phosphate (α-NPP) were purchased from Sigma Aldrich (Germany). Magnesium chloride ($MgCl_2$) was provided by Firma Chempur (Poland), H_2SO_4 and $HAuCl_4$ by Merck (Germany) and bovine serum albumin (BSA) by Glentham Life Sciences (United Kingdom).

Two Lyz specific aptamers from Biomers (Italy) were used:

5'- SH-C5- GCAGCTAAGCAGGCGGCTCACAAAACCATTCGCATGCGGC-3'

5'- Biot - ATCTACGAATTCATCAGGGCTAAAGAGTGCAGAGTTACTTAG -3'

Methrom (Netherlands) DropSens DRP110, SPCE were used. All electrochemical experiments were performed using an Autolab potentiostat with NOVA 1.11 software. A fluorescence protein assay kit was bought from ThermoFisher (the United States) and analysed using Qubit Fluorometer from the same company. Data analysis and representation were performed by using OriginPro 16 software.

2.2.2 AuNSs@PEG/Poly-L-Lys/SPCE platform development

Poly-L-Lys was electropolymerised at the working electrode of a SPCE from a 20 mM monomer solution in 50 mM PBS pH 7.4 using a CV procedure. Thereafter, the Poly-L-Lys/SPCE platform was washed three times with 150 μL TRIS buffer. Next, AuNSs were electrodeposited from a 20 mM $HAuCl_4$ solution containing 10 mM PEG 10 000 in

0.5 M H_2SO_4, using a multipulse assisted (MPA) procedure adapted from[193]: 10 potential pulses between − 1.4 V *vs* Ag/AgCl/3 M KCl for 50 ms and open-circuit potential for 1 s, followed by 0 V constant applied potential for 5 minutes.

2.2.3 Sandwich-structured aptasensor (Biot-Apt/Lyz/MCH/Apt-SH/AuNSs@PEG/Poly-L-Lys/SPCE) and enzymatic label

For the detection of Lyz, a sandwich aptasensor assay was developed. First, the 5'-SH modified aptamer (SH-Apt) was immobilised on the platform surface from a solution containing 2 μM SH-Apt in Buffer B. The immobilisation procedure was performed by drop-casting the solution on the electrode and left overnight at 4 °C in a wet atmosphere. Next, the remaining free sites of the AuNSs@PEG/Poly-L-Lys/SPCE were blocked with a 5 mM MCH in Buffer B, using a MPA procedure (− 0.2 V and + 0.5 V for 10 ms each for a total of 60 s) adapted from[194]. Lyz was incubated in a wet atmosphere at room temperature for 45 minutes, followed by a 45 minutes affinity reaction with a 1 μM biotin modified secondary aptamer (Biot-Apt) in the same reaction conditions. After all the above steps, the Biot-Apt/Lyz/MCH/Apt-SH/AuNSs@PEG/Poly-L-Lys/SPCE platform was washed three times with 100 μL Buffer B.

2.2.4 Electrochemical and morphological characterization

The biotinylated complexes formed on the sensor surface were further incubated with 7.5 μL solution containing 0.1 U mL^{-1} of streptavidin-alkaline phosphatase (s-ALP) enzyme conjugate and 10 mg mL^{-1} of BSA in Buffer C for 20 minutes. Each sensor was washed three times with 100 μL Buffer C. 50 μL of 1.0 mg mL^{-1} enzymatic substrate, 1-Naphthyl phosphate in Buffer C, were then dropped onto the sensor surface[91]. The electroactive enzymatic product, α-Naphthol, was detected after 20 minutes by cycling the potential from − 0.1 to + 0.4 V by a DPV method: 4 mV step potential, 70 mV modulation amplitude, 0.05 s modulation time, 1 s interval time, 5 mV s^{-1} scan rate.

The platforms were electrochemically characterised before and after each modification step in a 5 mM $[Fe(CN)_6]^{3-/4-}$ in 0.1 M KCl solution and EIS. The electroactive surface area determination studies were performed in a 5 mM $[Fe(CN)_6]^{3-/4-}$ in 0.1 M KCl solution at increasing scan rates: 12.5, 25, 50, 75, 100, 150, 300, mV s^{-1}.

2.2.5. Selectivity and applications

The selectivity of the sandwich-structured aptasensor was examined in the presence of various proteins and biomolecules, including 0.15 nM BSA, 0.5 nM IL-6 and 560 nM Glu in Buffer B. The aptasensor was incubated with the different interferences at high concentrations to ensure the excellent selectivity of the assay. Comparatively, a

low Lyz concentration of 7 nM was used for the experiments. All interferents were tested both alone and in mixture with Lyz.

In order to demonstrate the applicability of the developed aptasensor, three different types of wine were tested, namely: dry white wine, sweet white wine and rose wine. Fixed Lyz concentrations were spiked in the untreated wine, and a further 1:100 dilution with Buffer B was performed. At least five concentrations in the range from 70 pM to $3.5*10^5$ pM were tested, in triplicate, in each wine sample to plot three calibration curves. The recovery values were compared with a fluorescence protein assay kit from ThermoFisher. For this method, the wine samples (dry white wine, sweet white wine, rose wine) were spiked with Lyz to obtain a 35 μM concentration. These solutions were diluted at 1:20 with Qubit® assay buffer. Further, a 15 minute-reaction time was necessary before the samples were analysed by the Qubit® fluorometer.

2.3 Results and discussions

2.3.1 AuNSs@PEG/Poly-L-Lys/SPCE electrode platform development and characterisation

L-Lys was electropolymerised at SPCE from a solution of L-Lys in 50 mM PBS pH 7.4 (Figure 12A). Different concentrations of L-Lys solutions were used during the optimisation steps (10, 20, 30 mM) by varying the number of polymerisation cycles (5, 10, 15 cycles). To verify the electropolymerisation of L-Lys, the optimal CV procedure was tested in a solution free of monomer. As seen in Figure 12B two oxidation peaks for the L-Lys solution were registered at around + 0.45 and + 0.80 V, respectively. During the polymerisation process, the consumption of L-Lys monomer is observed as the anodic peak slightly decreases and shifts towards more positive values while the cathodic peak increases with the increasing number of CV cycles.

The optimisation of the poly-L-Lys deposition was realized by determining the electrocatalytic effect of the platforms towards $[Fe(CN)_6]^{3-/4-}$ redox probe by CV and EIS. For the CV characterisation the average value of anodic and cathodic peak currents were calculated for each platform. In order to assess the impact of the L-Lys monomer concentration over the polymerisation process, 3 different concentrations were used at a fixed number of 15 CV polymerisation cycles. The highest peak current intensity was obtained when a 10 mM L-Lys in Buffer A solution was used (178.5 μA) compared with bare SPCE (154.4 μA) (Figure 13A). Hence, it can be observed that no electrocatalytic effect was observed when applying the polymerisation procedure in a solution free of monomer, the signal (150 μA) being very close to the one of bare SPCE. In addition, by increasing the concentration of the monomer, a decrease of about 7 % was observed, probably due to thicker film formation, which hinders the charge transfer processes at the polymer/solution interface.

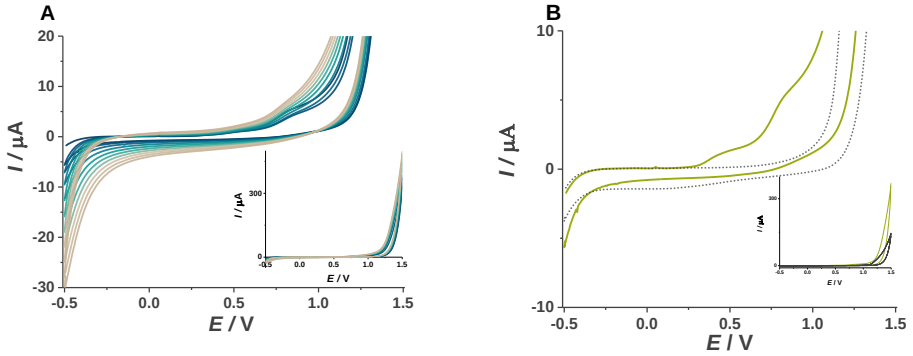

***Figure 12 A**. CVs (10 c, – 0.5 – + 1.5 V, 100 mV s–1) recorded during the polymerisation of 20 mM L-Lys in Buffer A solution; **B.** 1st cycle of polymerisation of 20 mM L-Lys in Buffer A solution (green line) and in Buffer A free of monomer solution (grey dotted line)*

The platforms were also tested by EIS in a 5 mM $[Fe(CN)_6]^{3-/4-}$ in 0.1 M KCl (Figure 13B). The Nyquist plots follow the Randles circuit described by a semicircle in the high-frequency region, characterised by kinetics at the electrode surface, and a straight line in the low-frequency region which is attributed to diffusion-controlled processes.

The electron charge transfer resistance (R_{ct}) dramatically decreased from bare SPCE to Poly-L-Lys(5 CV scans)/SPCE down to 512.9 Ω R_{ct} for L-Lys(10 CV scans)/SPCE. However, a slight increase of the R_{ct} was observed with the increase of polymerisation cycles from 10 to 15. The highest electrocatalytic effect towards the redox probe was obtained at Poly-L-Lys(10 CV scans)/SPCE platform obtained from a 10 mM L-Lys in Buffer A solution.

2.3.2 Gold nanostructures electrodeposition

The next step involved in the platform development was represented by the electrochemical deposition of AuNSs or AuNPs with respect to the method employed. Electrodeposition of gold at Poly-L-Lys/SPCE led to the formation of a more structured surface and to increased electrocatalytic properties by the formation of gold structures in the porous matrix of the polymer.

For this, a fixed concentration of 2 mM $HAuCl_4$ in 0.5 M H_2SO_4 was used and an amperometric electrodeposition method was employed. A constant concentration of 10 mM L-Lys was used for the formation of Poly-L-Lys/SPCE. After the gold deposition, a CV was performed in a 5 mM $[Fe(CN)_6]^{3-/4-}$ in 0.1 M KCl redox probe and the average oxidation/reduction peak current intensities were calculated. The results have shown an increased catalytic effect at the platform obtained from a 2 mM $HAuCl_4$ in 0.5 M H_2SO_4 electrodeposition solution (AuNPs/Poly-L-Lys/SPCE) compared with Poly-L-Lys/SPCE,

regardless of the number of L-Lys polymerisation cycles (Figure 13C). A further increase in the current intensity can be observed after the addition of 10 mM 10 000 PEG in the electrodeposition solution and the formation of the AuNSs(I)@PEG/Poly-L-Lys/SPCE. However, an increased catalytic effect was observed at AuNPs/Poly-L-Lys/SPCE and AuNSs(I)@PEG/Poly-L-Lys/SPCE platforms when using up to 10 polymerization cycles of L-Lys, but no significant difference between 10 and 15 polymerization cycles was observed.

Nevertheless, the impact of L-Lys concentration used in the formation of AuNSs(I)@PEG/Poly-L-Lys/SPCE was assessed (Figure 13D). An increase in current intensity was observed when 20 mM L-Lys in Buffer A solution was used. Therefore, 20 mM L-Lys in Buffer A solution and 10 cycles polymerization profile was chosen as optimal parameters to ensure a uniform polymer matrix for the incorporation of AuNPs.

The effect of PEG 10 000 concentration was also assessed by CV in a 5 mM $[Fe(CN)_6]^{3-/4-}$ in 0.1 M KCl at AuNSs(I)@PEG/Poly-L-Lys/SPCE (Figure 13E). An increase of the average current intensity was observed up to 10 mM (268.1 μA), followed by a sharp decrease of the average current intensity when 50 mM PEG was added in the electrodeposition solution. Up to 10 mM PEG, the formation of size-controlled gold clusters is proportional to the concentration of polyol; however, due to the high viscosity of the 50 mM PEG solution, the Au electrodeposition was obstructed.

Despite the excellent catalytic effect obtained at AuNSs(I)@PEG/Poly-L-Lys/SPCE platform compared to bare SPCE, the formation of sufficient Au sites for aptamer immobilization is of paramount importance. Based on the optimal parameters, two platforms were developed with respect to the $HAuCl_4$ concentration: AuNSs(I)@PEG/Poly-L-Lys/SPCE and AuNSs(II)@PEG/Poly-L-Lys/SPCE, formed from a 2 mM $HAuCl_4$ solution and 20 mM $HAuCl_4$, respectively.

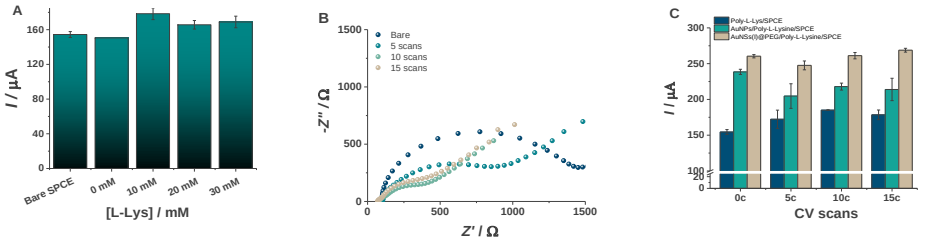

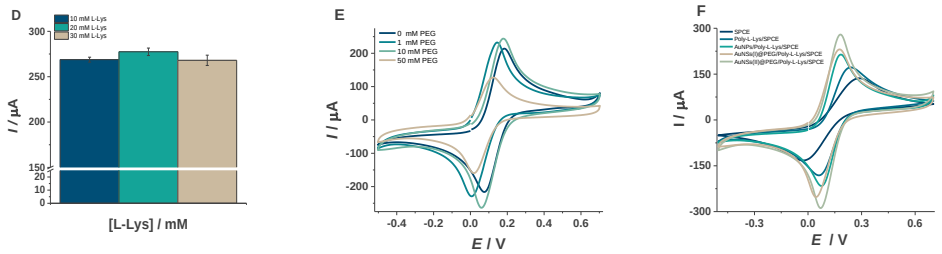

***Figure 13**. **A)** Average current intensities measured by CV and **B)** Nyquist plots obtained in a 5 mM $[Fe(CN)_6]^{3-/4-}$ redox probe in 0.1 M KCl at Poly-L-Lys/SPCE using different monomer concentration and number of polymerisation CV cycles; Average current intensities measured by CV in a 5 mM $[Fe(CN)_6]^{3-/4-}$ redox probe in 0.1 M KCl at: **C)** Poly-L-Lys/SPCE, AuNPs/Poly-L-Lys/SPCE, AuNSs(I)@PEG/Poly-L-Lys/SPCE after different L-Lys polymerisation CV cycles and **D)** AuNSs(I)@PEG/Poly-L-Lys/SPCE obtained using different monomer concentration; CVs of 5 mM $[Fe(CN)_6]^{3-/4-}$ in 0.1 M KCl redox probe measured at: **E)** AuNSs(I)@PEG/Poly-L-Lys/SPCE platform obtained using different PEG concentration and **F)** bare SPCE, Poly-L-Lys/SPCE, AuNPs/Poly-L-Lys/SPCE, AuNSs(I)@PEG/Poly-L-Lys/SPCE, AuNSs(II)@PEG/Poly-L-Lys/SPCE*

The electrochemical surface area was calculated for Poly-L-Lys/SPCE, AuNSs(I)@PEG/Poly-L-Lys/SPCE and AuNSs(II)@PEG/Poly-L-Lys/SPCE, respectively, and compared with the electroactive area of bare SPCE. Only a small increase in the electroactive area of the Poly-L-Lys/SPCE platform compared with the bare SPCE was observed, showing a uniform monolayer poly-L-Lys formation to ensure Au reduction at the electrode surface. After Au deposition, a 3.5 fold increase of the electroactive area was obtained for the AuNSs(I)@PEG/Poly-L-Lys/SPCE platform and a 3.9 fold increase for the AuNSs(II)@PEG/Poly-L-Lys/SPCE platform, respectively. This increase suggests a higher active surface, extremely important for further aptamer immobilisation, as well as a very good catalytic effect that will increase the sensitivity of the aptasensor towards the analyte.

The two gold-based platforms were also characterised by CV (− 0.2 - + 1.5 V, 0.1 V s^{-1}) in 0.5 M H_2SO_4. An anodic response appears at around + 1.1 V due to the formation of Au oxides. In the reverse potential scan, the Au oxides are eventually reduced at about + 0.65 V. By integrating the charge consumed for reducing the Au oxides formed in the positive scan, the real active surface areas (RSAs) and the roughness factors (R_f) of both platforms were calculated, by assuming that the calculated charge value for chemisorption of an oxygen monolayer on the surface of polycrystalline gold is 386 µC cm^{-2}[195,196]. The presence of a rougher surface with a much higher RSA (AuNSs(II)@PEG/Poly-L-Lys/SPCE) proves a better deposition of gold layers within the polymer matrix with very dense and heterogenous AuNSs.

2.3.3 Morphological and structural characterization

SEM and AFM images were recorded at modified electrodes at each step involved in the platform development to reveal their morphologies and link them with the electrochemical properties (Figure 14). Poly-L-Lys forms a relatively smooth surface structure, as seen in Figure 14A, with little to no irregularities compared to bare SPCE. For the electrodeposition of gold, 2 different concentrations were optically evaluated, 2mM and 20mM.

A higher concentration of $HAuCl_4$ enables the formation of uniformly organised AuNSs that form a 3D network in the polymer film (Figure 14B-C). The Au nuclei formation is first realised, followed by the development and expansion of the network. Although the procedure might seem more expensive, low volumes of $HAuCl_4$ solution are needed to realize the procedure at SPCEs.

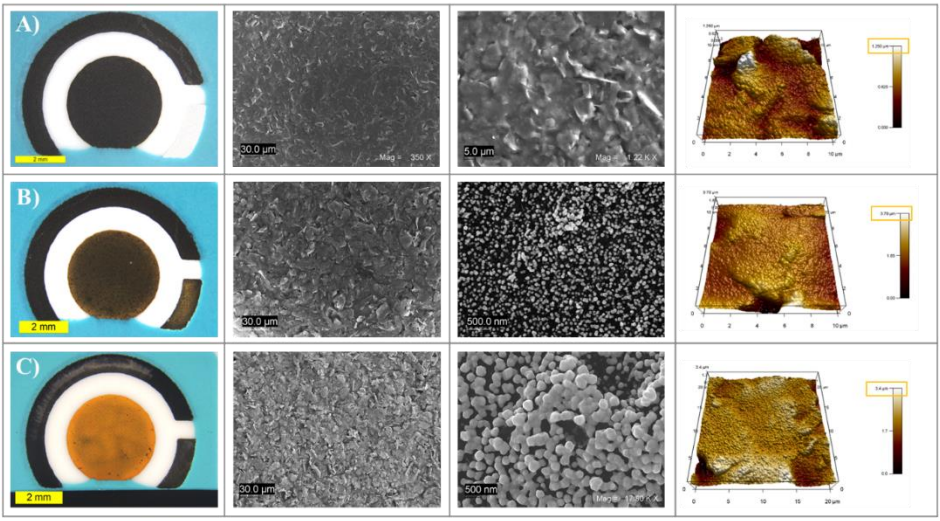

Figure 14. *Optical images, scanning electron microscopy micrographs at different magnitudes and AFM images of: A) Poly-L-Lys/SPCE, B) AuNSs(I)@PEG/Poly-L-Lys/SPCE, C) AuNSs(II)@PEG/Poly-L-Lys/SPCE*

2.3.4 Aptasensing steps development

Even though the electrochemical characterization of the developed platforms showed increased electrocatalytic effect and surface area at the AuNSs(II)@PEG/Poly-L-Lys/SPCE platform, further assessments were conducted to determine the optimal SH-Apt1 immobilization. According to these results, the optimal SH-Apt1 immobilization was conducted at the AuNSs(II)@PEG/Poly-L-Lys/SPCE platform, using a SH-Apt1 concentration of 2 µM solution which was left in contact with the modified working electrode for 18 h (overnight).

The next step is represented by the uniform blocking of remaining free Au sites on the platform, after SH-Apt1 immobilisation. A short-chain aliphatic thiol (6-MCH) was immobilised at the modified electrode by potential-pulse assisted thiol chemisorption. First, the 6-MCH concentration was optimised using a 20s MPA immobilisation procedure. A signal difference of 32 % was obtained when the 5 mM 6-MCH concentration was used. In comparison, when 0.5 mM MCH was chemisorbed, a 31.3 % result was obtained and 14% when 50 mM 6-MCH was immobilised. 60 s potential-assisted immobilisation was revealed to be more successful (46.9%). Therefore, 5 mM 6-MCH was immobilised by chemisorption for 60 s in the next steps.

The incubation time with Lyz was also optimised. Different incubation periods were tested (30-90 minutes) and the final response of the aptasensor was evaluated. The results were quantified as the current intensity difference obtained in the presence and absence of Lyz ($\Delta I/I_0$ /%). A signal difference of 17.53 % with a 15.5 % RSD was obtained after a 30 min incubation with Lyz, 46.8 % and a 7.7 % RSD after 45 minutes and 49.15 % signal difference with a 9.9 % RSD after 90 minutes. Therefore, 45 minutes Lyz incubation time was used, since the signal difference between 45 and 60 minutes is not significant, and the assay aims for fast analysis.

Finding the best interaction between the Apt2-Biot and Lyz, for the sandwich assay, is of crucial importance in the final analyte determination to have a quantitative interaction between aptamer-Lyz and to avoid any possible hybridisation with SH-Apt1 or non-specific adsorption. No difference in the detection of a 700 nM Lyz solution detection was observed when 1 and 5 μM Apt2-Biot concentrations were used. A significant change in the signal difference, compared with the 1 μM for 45 minutes incubation was observed when the 2 μM concentration was used or the time was increased to 90 minutes. Nevertheless, the standard deviation was higher in both cases, high differences being obtained between the performed analysis. For instance, when 2 μM Apt2-Biot was used for 45 minutes, a signal difference of 142 % with a STDEV of 88 % was obtained. When only the incubation time was increased to 90 minutes, for the same 700 nM Lyz concentration, a signal difference of 65 % with a SD of 47% was obtained. For the 1 μM Apt2-Biot concentration, incubated for 45 minutes, an 89% signal increase was observed with a 1.2% SD. In this case, for Lyz detection, the immobilisation of the Biot-Apt was performed using a 1 μM concentration for 45 minutes.

2.3.5 Analytical performances

A calibration curve for Lyz detection was obtained using the signal obtained in the absence and in the presence of Lyz. The signal is reported as $\Delta I/I_0$ %, that is the percentage of the signal increase with respect to the initial value (Figure 15). A linear regression between the signal $\Delta I/I_0$(%) and the logarithm of Lyz concentration

([Lyz]/pM) was obtained in the range 70 – 7*10^5 pM described by the following equation: $\Delta I/I_0$(%) = 20.23 log[Lyz](pM) ±0.84 – 31.97±1.6 with a correlation coefficient of R^2 = 0.996. A LOD of 2 pM was calculated as 3 times the standard deviation of the regression equation divided by its slope (3 σ/slope). The obtained limit of quantification (LOQ) was 70 pM.

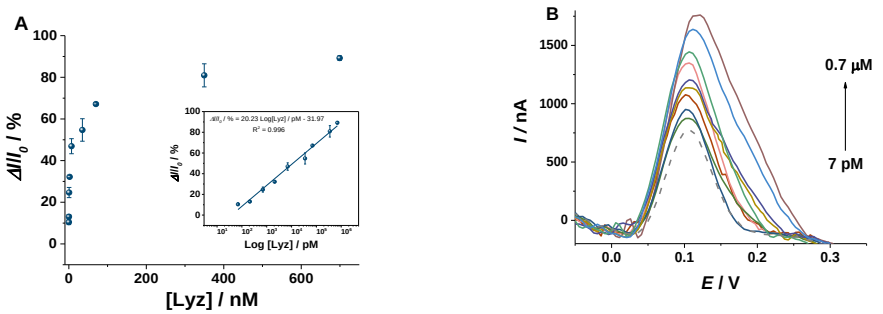

Figure 15 A *Lyz dose-response curve where the points correspond to ΔI/I0(%) ± RSD. Inset: Variation of ΔI/I0 (%) with the logarithm of Lyz concentration;* ***B*** *Variation of DPV α-Naphthol oxidation peak with the increase of Lyz concentration*

The analytical performance of the aptasensor developed in this work was compared with the ones obtained in other recently published papers. In terms of sensitivity, the developed aptasensor presents much better performance compared with other aptasensors tested in real wine samples[197,198], allowing the detection of Lyz even after a 1:100 sample dilution, minimising the matrix effect. Hence, having a wide linear range of 4 magnitude orders, allowed the detection of Lyz in ultralow and high levels with a high degree of confidence despite the comparable LODs reported for other aptasensors as presented in Table 4

Table 4 *Comparison of analytical performances with other Lyz recent developed aptasensors*

Sensor configuration	**Detection method**	**LOD (pM)**	**Linearity (pM)**	**Real samples**	**Ref.**
LBA/Diazonium salt/PGE	EIS	1.67 *10^6	1.67 *10^6 – 5 *10^6	Wine	[199]
LBA/ Cu_2O/rGO/PpPG	DPV	60	10^2 – 2*10^5	Saliva	[200]
dsDNA/AuNPs-CNPE	DPV	2	10 – 10^6	Urine	[201]
LBA/AuNC/GCE	SWV	0.1	0.1 – 10^4	Egg white	[202]

LBA/AuNP/SPAuE	CV	$2.3*10^4$	$7*10^4 – 7*10^5$	Wine	[203]
Biot-LBA/Lys/SH-LBA/AuNSs/Poly-L-Lys/SPCE	DPV	2	$70 – 7*10^5$	Wine	This work

AuNC – Gold nanocluster, AuNP – gold nanoparticles, AuNS – Gold nanostructures, GCE – Glassy carbon electrode, LBA – Lyz binding aptamer, Lyz – Lysozyme, PGE – Pencil Graphite Electrode, Poly-L-Lys – Poly-L-Lysine, PpPG - plasma-polymerized propargylamine, rGO – reduced graphene oxide, SPAuE – Screen printed gold electrode, SPCE – Screen-printed carbon electrode.

2.3.6 Selectivity and applications

Selectivity of the aptasensor was tested in the presence of molecules that are often found in the same matrices with Lyz (Glu, BSA) or that have a similar molecular structure (IL-6) with potential applications in biological samples. Recovery studies were performed using 0.15 nM BSA, 0.5 nM IL-6 and 560 nM Glu solutions in Buffer B, alone and in the presence of 7 nM Lyz. Tests were performed for each interferent individually as well as with a mix of all interferents in the presence and absence of Lyz. No significant signal differences were observed, proving the selectivity of the aptasensor (Figure 16A).

The applicability of the aptasensor was tested in 3 different types of commercial wine: dry and sweet white wine and rose wine. The samples were first spiked with different concentrations of Lyz and then a 1:100 dilution with Buffer B was performed. The final concentration of Lyz in the diluted samples ranged from 70 pM to 350 nM. A minimum of 5 samples with different amounts of Lyz were spiked and the calibration curves were obtained for all wines (Figure 16B) were compared with the one obtained for Lyz in Buffer B. The following equations were obtained for the 3 wines:

A. Dry white wine: $\Delta I/I_0(\%) = 20.68 \log[Lyz](pM) \pm 0.32 – 33.15 \pm 1.28$, $R^2 = 0.999$
B. Sweet white wine: $\Delta I/I_0(\%) = 20.70 \log[Lyz](pM) \pm 0.36 – 32.57 \pm 1.41$, $R^2 = 0.998$
C. Rose dry wine: $\Delta I/I_0(\%) = 20.77 \log[Lyz](pM) \pm 0.35 – 33.32 \pm 1.38$, $R^2 = 0.999$

The equations obtained in wine samples are almost similar to the ones obtained in Buffer B, proving that the aptasensor presents no interference in wine samples. The sweet white wine has a Glu concentration of around 140 mM, before dilution, while the dry white wine a Glu concentration of only 20 mM. Having so similar calibration curve equations for the 2 types of white wine proves the response of the aptasensor is not influenced regardless the concentration of Glu. A rose wine sample was tested, rich in

tannins and other acidic compounds that can modify the pH of the assay during the incubation time. The results showed no significant influence in the aptasensor response.

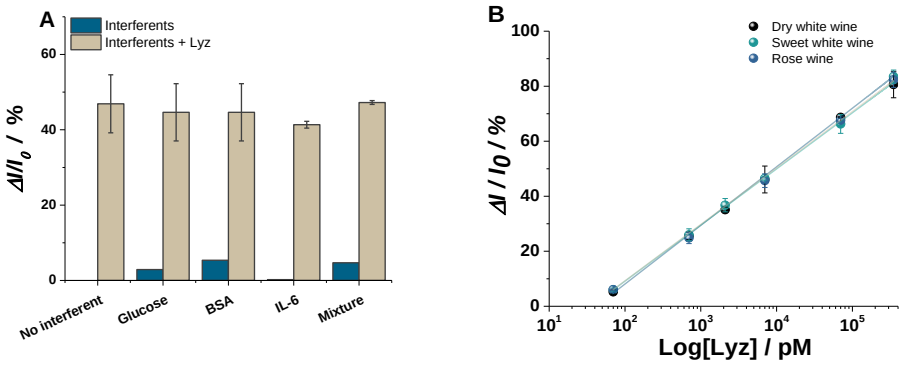

***Figure 16 A**) Histograms representing ΔI/I₀ (%) values obtained by testing the aptasensor in solutions containing the interferents alone (navy) and in mixture with Lyz (beige). **B-D**: Lyz dose-response curves obtained in different wine samples represented as ΔI/I₀*

The applicability of the newly developed aptasensor was compared with a standard fluorescence protein detection method. For this, rose wine, dry white wine and sweet white wines were spiked with 35 µM Lyz, the highest allowed concentration in wine. The results obtained by the aptasensor were compared with a Qubit® Fluorescence Protein Assay Kit. Table 5 shows that there is no significant difference between the electrochemical aptasensor and the fluorescence detection method. The recovery rates were in the range between 97.4 % and 109.7 %, which is an acceptable range for an electrochemical aptasensor, proving the utility of this method in the wine industry.

***Table 5** Comparison of the recovery rates of the aptasensor developed in this work and the Qubit fluorescence protein assay*

	Spiked Lyz (µM)	Electrochemical aptasensor			Qubit® Protein Assay kit		
		Found (µM)	RSD (%)	Recovery (%)	Found (µM)	RSD (%)	Recovery (%)
Dry white wine	35	34.9	4.8	99.7	36.0	1.4	102.8

Sweet white wine	38.4	2.8	109.7	34.4	1.0	98.2
Rose wine	34.1	3.6	97.4	34.1	2.3	97.5

2.4 Conclusions

A voltammetric sandwich aptasensor was developed for Lyz determination. First, a platform based on AuNSs/Poly-L-Lys was optimised for a good SH-Apt immobilisation efficiency. The sensing properties were greatly improved by combining the polymer film with AuNSs; hence, AuNSs(II)@PEG/Poly-L-Lys/SPCE demonstrated a higher catalytic effect and optimal anchoring platform for the apta-assay development. In the second part of the study, Lyz was quantified using a sandwich-structured assay and enzymatic signal amplification. The assay detected Lyz with a LOD of 2 pM in the wide linear range between 70 to $7^{*}10^{5}$ pM. The aptasensor has proven its selectivity in the presence of commonly found interferents and was applied successfully in wine samples. The results were compared with those obtained using a commercial protein fluorescence detection method.

III. Metallic nanostructures based electrochemical platforms

1. Nickel foam modified copper wires for glucose amperometric determination (Study 4)

1.1 Introduction

According to WHO, more than 422 million people are suffering from diabetes. A very large part of these people live in underdeveloped countries where access to traditional detection methods is more difficult and, therefore, there are lower chances of early disease detection[204]. Fast and affordable Glu detection methods are extremely necessary in order to detect diabetes in its early stages and implement an effective treatment since the first signs of diabetes development.

Electrochemical sensors are very good tools in this direction. By optimising them, good sensitivity, high reproducibility with an increased simplicity towards Glu determination can pe obtained, all these at a low cost of production[205]. Non-enzymatic Glu electrochemical sensors based on transition metals respect all the above characteristics, particularly those containing Cu^{2+} or Ni^{2+} oxides that can not only acting as good promoters for Glu oxidation but they also offer an increased catalytic effect, extremely important for low LODs[206]. Moreover, by functionalising nanoporous materials with other metals coatings can significantly increase the electrocatalytic effect[207].

All these considered, in this study a novel sensing platform for the non-enzymatic detection of Glu using 3D copper nanostructures was developed. The electrodes were characterised by electrochemical techniques and they were applied for selective Glu detection in real samples.

1.2 Materials and methods

1.2.1 Materials

Sodium hidroxyde (NaOH), Nickel chloride ($NiCl_2$* $6H_2O$), ammonium chloride (NH_4Cl), copper sulfate ($CuSO_4$* $5H_2O$), H_2SO_4, paracetamol, ascorbic acid (AAc), Glu,

Rhamnose and uric acid (UA) were purchased from Sigma-Aldrich and used without further purification. Milli-Q ultrapure water (18 MΩ cm^{-1}) was used for solutions preparation. Electrochemical studies were performed on Autolab PGSTAT302N and Palmsens EmStat Blue potentiostats, using a three-electrode cell composed of a platinum wire (BASi) as a counter electrode and a Ag/AgCl electrode as reference electrode. As a working electrode, Cu strips of different Cu nanoporous morphologies like Cu modified with Ni foam (Cu/Nif) with a geometrical area of 0.05 cm^2 were used.

1.2.2. Electrochemical assessment of the 3D Cu nanoporous electrodes

Cu nanoporous electrodes were characterised in EIS and CV. For the EIS studies, a 5 mM $[Fe(CN)_6]^{3-/4-}$ in 0.1 M KCl solution was used as a redox probe. A 0.01 – 10^5 Hz frequency window was used at open circuit potential. Fittings of the obtained EISs were performed using Nova 1.10 software. For the CV analysis, 0.1 M NaOH was used as a supporting electrolyte, and the potential was scanned 2 times from 0 – 0.8 V at a scan rate of 10 mV s^{-1}. Analyses were performed in solutions free of Glu and in the presence of 0.225 mM Glu in 0.1 M NaOH.

Glu detection was performed by CA at a working potential of +0.55 V vs. Ag/AgCl in 0.1M NaOH under continuous stirring at 500 rpm (interval time 0.1s, analysis time: up to 1200-1600s), with successive Glu solutions additions after every 100 s using 2.5 mM solutions and different volumes: 4 additions of 12.5 µL that were followed by 25 µL.

The interference experiments were performed using CA at +0.55 V vs. Ag/AgCl in the presence of several electroactive species, respectively: paracetamol, AAc Rhamnose and uric acid (UA). The additions of the interfering species were alternated with those of the analyte to confirm the selectivity of the platform.

1.3 Results and discussions

1.3.1 Electrochemical characterisation of 3D Cu nanoporous electrodes

EIS studies were performed in order to study the interfacial charge-transfer phenomena. In Figure 17 a comparison between the Cu/Ni_f electrodes and Cu strips from the point of view of R_{ct} is presented.

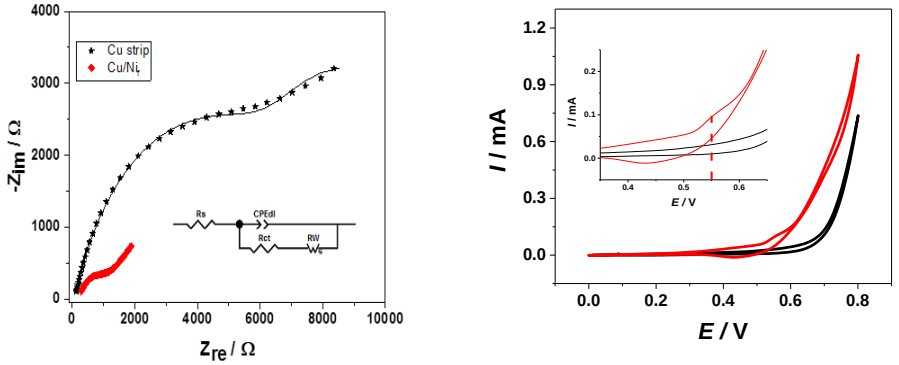

Figure 17 A *EIS data recorded in 5mM [Fe (CN)$_6$]$^{3-/4-}$ in 0.1M KCl solution for Cu strip and Cu/Nif electrodes as Nyquist plots; inset: the proposed equivalent circuit to fit the measured points;* ***B*** *CV of the Cu/Nif working electrode in the absence (black line) and in the presence of 0.225 mM Glu (red line) in 0.1 M NaOH aqueous solution*

As shown in Figure 17, the value of the R_{ct} corresponding to the Cu strip electrode significantly decreased after the Ni foam deposition (6800 -> 1100 Ω), showing a better electron transfer rate and a better electrocatalytical effect.

From the calculated double-layer capacitances C_{dl} and taking into consideration the average double–layer capacitance of a smooth metal surface of 20 μF.cm^{-2}, the real surface area may be calculated as:

$$A_{real} = \frac{C_{dl}}{20} \text{ [cm}^2\text{]} \quad (2)$$

The roughness factor, σ, which is related to the ratio between the real and geometrical surface area, was calculated as:

$$\sigma = \frac{A_{real}}{A_{geometric}} \quad (3)$$

In Table 6 a comparison regarding the double layer capacitance, real surface area and corresponding surface roughness is presented. Cu/Nif surface has a higher roughness that has a positive influence on the overall electroanalytical characteristics of the electrode by increasing the active area.

Table 6. *Double-layer capacitance, real surface area and corresponding surface roughness values for the investigated Cu electrodes calculated from the EIS data*

Working electrode type	CPE_{dl} / µF	A_{real}/cm^2	σ
Cu strip	26.2	1.31	14.55
Cu/Ni$_f$	73.4	3.67	40.77

The properties of the Cu/Ni$_f$ electrodes were evaluated in the presence of Glu, as a model molecule. Figure 17 B presents the obtained CVs in a 0.1 M NaOH solution with and without 0.225 mM Glu at a 10 mV s^{-1} scan rate. An anodic peak was observed in the presence of Glu at +0.55 V, peak that was absent in the absence of the target analyte.

1.3.2. Analytical performances

As a result, this potential was chosen in CA analysis for the evaluation of Cu/Ni$_f$ electrodes towards Glu quantification. As seen in Figure 18A and C, a stable signal was obtained after 400 s. Next, standard additions of 2.5 mM Glu (12.5 – 25µL) and 25 mM Glu (50 µL) solutions in 0.1M NaOH were performed every 100 s. The signal corresponding to the electrochemical oxidation of Glu followed a stair-like augmentation trend. The signal was stabilised at about 5 s after Glu addition, suggesting that the porous morphology of Cu/Ni$_f$ electrodes increased the electrochemical transfer rate allowing fast oxidation of the analyte.

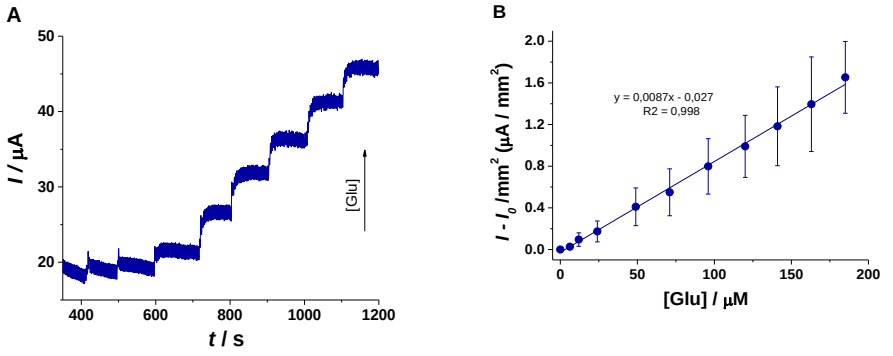

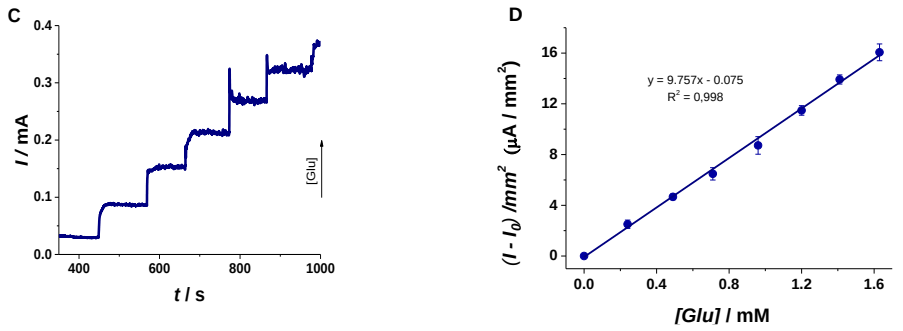

Figure 18 A. *CA of $CuNi_f$ electrodes in 0.1M NaOH with standard additions of 2.5 mM Glu solution every 100 s (4 times of 12.5 µL to reach a small concentration difference and then 25 - 50 µL until the end of analysis), under continuous stirring at 500 rpm (+0.55 V, 0.1 s step potential, 1200 s analysis time);* ***B****. The calibration curve in the range of 6 – 185 µM Glu;* ***C.*** *CA of $CuNi_f$ electrodes in 0.1M NaOH with standard additions of 25 mM Glu solution every 100s (50 µL) under continuous stirring at 500 rpm (+0.55 V, 0.1 s step potential);* ***D****. The calibration curve in the range of 0.24 - 1.63 mM Glu*

By plotting $I-I_0/mm^2$ against the concentration of Glu in the chronoamperometry studies, a proportional increase in the signal was observed, and two calibration curves were obtained (Figure 18 B and D):

(i) The first one in the range of 6 - 206 µM defined by the equation: $y(\mu A/mm^2) = 0.0087*Glu(mM)-0.027$ ($R^2=0.998$) has a lower LOD and demonstrates the good analytical performances of the sensor: LOD calculated as signal/noise ratio of 2 µM and a LOQ of 6 µM .

(ii) For the second one, a linear range of 0.24–1.63 mM was defined by the following equation: $y(\mu A/mm^2) = 9.757*Glu(mM) - 0.075$ ($R^2=0.996$), and it shows the possible applicability of the sensor real scenarios.

1.3.3. Specificity and applications

In order to prove the specificity of this method toward Glu detection in complex matrixes, interferences studies were carried. For this, analytes that are commonly found together with Glu in biological fluids were used: UA, Paracetamol, AAc and sugars like Rhamnose. First, CV analyses were performed in a 0.1 M NaOH solution with 150 µM interfering agent and in the presence or absence of 150 µM Glu (Figure 19 A-B). No peak was observed for UA and Paracetamol in the 0.5 – 0.6 V potential domain, showing that there are no potential false-positive results in their presence.

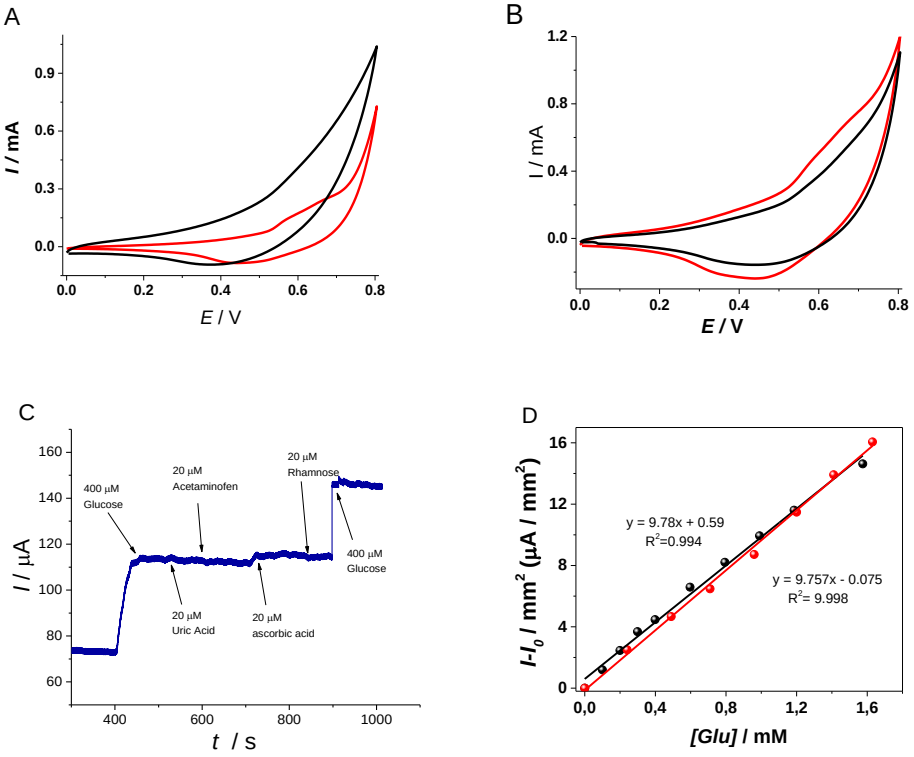

***Figure 19 A-B**. CVs in 0.1 M NaOH solution in the presence of 150 µM UA (A) and 150 µM P (B) as interfering agents in the absence (black line)/presence (red line) of 150 µM Glu; **C.** Amperometric responses in 0.1 M NaOH solution with standard additions every 100 s of 400 µM Glu, 20 µM UA, P, AA, R and 400 µM Glu; **D**. Calibration curve for the Cu/Nif on Cu electrode in the range of 0.24 - 1.63 mM Glu (red line) performed on standard solutions and on commercial human serum spiked with 0.1 M Glu (black line)*

CA studies were also performed in the same conditions as previously described. The current responses of Glu, UA, Paracetamol, AAc, and Rhamnose were registered at a constant potential of +0.55 V *vs*. Ag/AgCl and the results are presented in Figure 19C. After the signal stabilisation, Glu was added in the 0.1 M NaOH solution in order to achieve 400 µM total concentration. Next, different volumes of interfering agents were added every 100s in order to achieve 20 µM of each interferent. In the end, after all interferents were added to the detection solution, a standard addition of Glu was performed again in order to reach a total of 800 µM Glu in the solution. There was no influence observed from P and UA as expected from the CV studies. A small signal modification, a slight anodic peak increase was observed when AA was added in the detection solution. All in all, it can be said that the above-mentioned compounds have

no significant influence in the CA detection of Glu at Cu/Ni_f electrode, showing that de developed methods has a significant potential for Glu detection in complex matrices.

The Cu/Ni_f electrodes were also tested in commercial human serum spiked with different Glu concentrations. First, the serum sample was diluted 1:100 with 0.1 M NaOH. No further filtration or pretreatment steps were necessary. The $I\text{-}I_0/mm^2$ was plotted against Glu concentration and a proportional increase of the signal was observed. A calibration curve was plotted and compared with the one obtained in 0.1 M NaOH solution (Figure 19D). No significant differences were observed, showing the good applicability of this sensor in real Glu samples detection. Moreover, the 1:100 dilution is a step that helps reaching the linearity domain of Glu in blood samples.

1.4 Conclusions

3D electrochemical Cu/Ni_f electrodes and Cu sticks have been successfully electrochemically characterised and applied for Glu detection. An extra step of Cu sticks functionalisation with an additional Ni foam layer enhanced the electroanalytical response related to the non-enzymatic detection of Glu in 0.1 M NaOH and in serum samples. Cu/Ni_f 3D Cu nanostructures can successfully act as electrode material for Glu sensing with a promising potential for real samples analysis.

2. Modified Glassy carbon electrodes with gold nanovoids for selective Tetracycline detection (study 5)

2.1 Introduction

According to a data overview regarding antibiotic consumption in the last 12 years, an increase of 30% in antibiotic use was observed, with a prevalence in low and middle-income countries[208]. WHO classified antimicrobial resistance as one of the major challenges in human and animal health, expecting it to keep growing if prevention measures are not taken as soon as possible[209].

Tetracyclines are the widely employed antibiotics for human and animal treatment and have been widely investigated by aptasensors in veterinary residues. TET is the first discovered representative and the most used. It is absorbed in small amounts through the animal intestinal tract and remains in important concentrations in veterinary wastes that will further accumulate in environmental samples[210,211].

In the last years, TET has been widely used in livestock in order to assure the fast and healthy growth of the animals leading to large TET residues in animal-derived food as well as in wastewaters and wastewater treatment plants. Hence, residuals from pharmaceutical manufacturing or hospital wastewaters are not negligible, all contributing to the appearance of TET-resistant bacteria isolates in the environment [162,212]. Therefore, finding fast, low-cost and reliable solutions for TET detection in water is of primary importance. TET detection in water with the help of electrochemical aptasensors attracts more and more attention considering the increased accumulation in residual water[213] even though, for the moment, HPLC[214] and capillary electrophoresis[215] represent the gold standards in TET concentration in water determination.

The integration of gold nanostructures into the electrochemical aptasensors development can help increase the conductivity and electrochemical area, creating more sites for aptamer immobilisation, while at the same time offering a reactive surface that can immobilise aptamers using the Au-SH bond preserving aptamers bioactivity[216].

In this study, a new nanostructured gold platform with application in the development of a TET specific electrochemical aptasensor at glassy carbon electrodes (GCE) was developed and optimised. The nano-scale morphologies and topographies of the gold nanostructures (nanovoids) were evaluated using electrochemical techniques and surface characterisation methods like scanning electron microscopy, atomic force microscopy and X-ray photoelectron spectroscopy. A thiol-tethered DNA aptamer was

immobilised at gold nanovoids electrodeposited on GCE (AuNVs/GCE) by different strategies for simple and fast analysis but selective, sensitive, and cost-efficient detection of TET. The affinity reaction between the target and its specific aptamer led to conformational and structural changes in the recognition layer that was directly quantified by the redox reaction obtained in DPV, which occurred at the aptamer redox label, Ferrocene (Scheme 4).

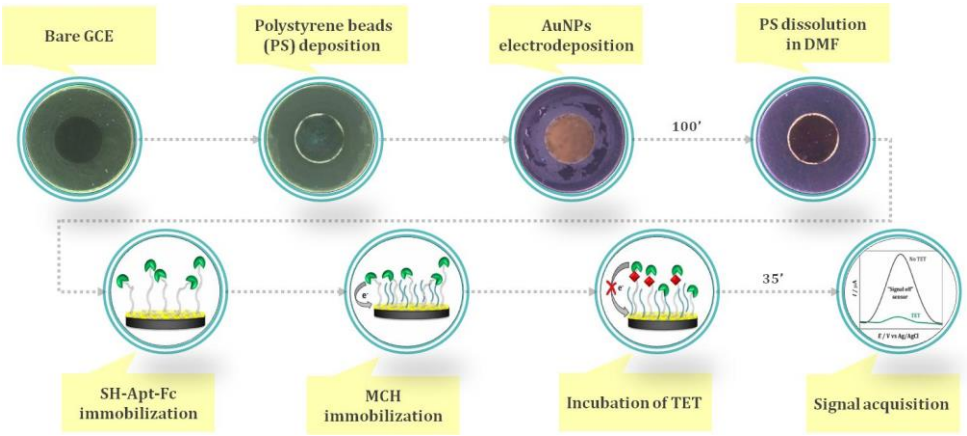

Scheme 4 *Ferrocene-aptamer-based sensor assay for tetracycline detection*

2.2 Materials and methods

2.2.1. Materials

TET, Ampicillin trihydrate, Oxytetracycline hydrochloride (OxyTET), Amoxicillin, Vancomycin hydrochloride, Gentamicin sulphate, polystyrene latex beads (0.3 and 0.6 μm), KCl, NaCl, $HAuCl_4$, H_2SO_4, tris(hydroxymethyl)aminomethane, *N,N*-dimethylformamide (DMF), potassium monohydrogen phosphate, potassium dihydrogen phosphate were purchased from Sigma Aldrich. Nuclease-free water was purchased from ThermoFisher (USA).

The aptamers used were purchased from Alpha DNA (Canada) and modified (SH-$(CH_2)_6$- at the 5'-end and Fc redox label at 3'-end:

- The TET specific aptamer (76-oligonucleotide sequence, 5'-CGT ACG GAA TTC GCT AGC CCC CCG GCA GGC CAC GGC TTG GGT TGG TCC CAC TGC GCG TGG ATC CGA GCT CCA CGT G-3') selected from a previous reported study (K_d = 63.6 nM) (217).
- The OxyTET specific aptamer (71-oligonucleotide sequence 5'- GGA ATT CGC TAG CAC GTT GAC GCT GGT GCC CGG TTG TGG TGC GAG TGT GTG GAT CCG AGC TCC ACG TG -3')

The buffers used in this study were:

- TRIS buffer pH 8 containing 10 mM TRIS-HCl, 100 mM NaCl, 100 mM KCl and 5 mM $MgCl_2*6H_2O$;
- PBS buffer 0.02 M pH 7.4 containing 0.02 M K_2HPO_4/KH_2PO_4 and 0.1 M NaCl.

The reagents were of analytical grade and used without additional purification. All other aqueous solutions were prepared using Mili-Q water (≥18 MΩ·cm).

2.2.2 Instrumentation

All electrochemical experiments were performed using an Autolab potentiostat with NOVA 1.11 software. Electrochemical characterisation of the electrodes was performed by CV, DPV, SWV and EIS in 5 mM $[Fe(CN_6)]^{4-/3-}$ in 0.1M KCl.

Different electrochemical cells were used for gold electrodeposition: SPCE, and gold-based screen printed electrodes (AuSPE) purchased from DropSens, GCE and gold electrodes (AuE) purchased from BASi.

Surface characterization in terms of topography and morphology was performed by Atomic Force Microscope (Cypher S, Asylum Research, Santa Barbara, CA. The morphology of the polystyrene nanospheres monolayer and AuNPs was observed using a scanning electron microscope (GeminiSEM 300; Zeiss) with primary electron energy of 1 kV, respectively 15 kV. All of the XPS spectra were obtained on a Thermo Scientific™ ESCALAB™ 250Xi+ X-ray Photoelectron Spectrometer (XPS). The optical images were taken using the stereomicroscope M250Leica A.

2.2.3 Platform development

AuNPs were electrochemically deposited at the GCE and SPCE surfaces from a solution containing 1.2 mM $HAuCl_4$ in 0.5 M H_2SO_4 using a pulse assisted procedure: 10 potential pulses between -1.4 V *vs.* Ag/AgCl/3 M KCl for 50 ms and open-circuit potential for 1 s followed by a 60 s at -0.75 V chronoamperometry to obtain a sufficient Au thickness.

In order to obtain a more nanostructured gold platform, a new approach was designed, namely gold nanovoids (AuNVs). Firstly, 2.5 % (wt %) of 300 nm polystyrene latex beads (PS) suspension was prepared in a hydroalcoholic mixture ($EtOH:H_2O$=1:1) containing 2 % (v/v) Tween 20. Prior to the use, the suspension was kept in the ultrasonication bath for 10 minutes, then thoroughly vortexed for 2 minutes. 7 µL of PS suspension was deposited onto the GCE surface and left for 30 s followed by a two-step spin-coating procedure : 900 rpm for 60 s, followed by 2000 rpm for 180s. After the PS deposition, the modified GCE was washed three times with 100 µL distilled water. Secondly, the PS/GCE was subjected to the electrochemical deposition of gold

nanoparticles from a 1.2 mM $HAuCl_4$ solution in 0.5 M H_2SO_4 followed by the PS dissolution in DMF for 90 minutes, under stirring (800 rpm). Finally, the modified electrodes were rinsed three times with 100 µL distilled water and kept at 4 °C for further use.

2.2.4 Aptasensor developement

The as prepared nanostructured gold platform (AuNVs/GCE) was further used for the immobilisation of the 5' thiolated-aptamer at the modified electrode surface as follows: 0.5 µM Fc-aptamer solution was prepared in TRIS buffer and subjected to a potential pulse-assisted method as immobilisation protocol. The immobilisation procedure was adapted from a previously published study[218] and consisted in switching the potential applied to the electrode surface between 0.5 V and -0.2 V *vs.* Ag/AgCl/3M KCl with a 10ms pulse duration for 32 s in a 0.5 µM Fc-Aptamer solution in TRIS buffer. The electrodes were further washed 3 times with 200 µM TRIS buffer in order to remove the unbound 5' thiolated aptamer molecules. In order to block the free active gold binding sites an unspecific short-thiol was used. To this end, 0.05 mM MCH was prepared in 0.02 M PBS pH 7.4 containing 30 % (v/v) absolute ethanol and was immobilized at the Apt/AuNVs/GCE by the same immobilization procedure for a total of 20s.

In order to assess the analytical performance of the developed aptasensor, DPV measurements were performed to trigger the oxidation reaction of the Ferrocene moiety labelled at the aptamer-modified AuNVs/GCE. First, the potential was swept from - 0.1 to + 0.5 V in 0.1M KCl at the MCH/Fc-Apt/AuNVs/GCE in order to assess the Fc initial peak current intensity (I_0) and then swept back to -0.1 V in order to reverse the redox reaction.

After the incubation with TET for 30 minutes, a new DPV measurement was performed to determine the Fc anodic peak current after the affinity reaction (I). TET incubation time was optimised by keeping a fixed TET concentration and incubating for different time periods: 15-60min. The signal change was observed, and the highest modification was chosen.

2.2.5 Selectivity and applications

The selectivity of the aptasensor for TET in complex matrices was evaluated against five antibiotics, namely OxyTET, Ampicillin, Amoxycillin, Vancomycin, and Gentamicin. The aptasensing protocol of the analogues was carried out in the same manner as for TET at a fixed concentration of 50 nM alone and in combination with TET in 1:1 ratio. Hence, a mixture of all five antibiotics was prepared to a total concentration

of 25 nM of each antibiotic. This mixture was also tested alone and in the presence of 25 nM TET.

The applicability of the aptasensor was proven by analysing water samples with different grades of purification using the standard addition methods. Two samples of water were collected from the local water treatment plant: before the primary decantation and after the primary purification. The 3rd sample was collected directly from the laboratory, being normal tap water. Firstly, the samples were filtered using a 0.45 μM syringe filter in order to remove any solid waste, then a dilution of 1:10 with PBS was performed. Next, the samples were spiked with 50 – 150 nM Tet and analysed using the same protocol described for TET analysis in buffer solution. The concentration of TET found in the samples was calculated according to the calibration equation, and then the recovery rates were calculated.

2.3 Results and discussions

2.3.1 Platform optimisation

To obtain a high surface area for the immobilisation of the thiolated-aptamer, polystyrene latex beads were firstly deposited onto GCE. The gold nanostructure was electrochemically obtained by gold electrodeposition by means of CV or multipulse amperometry, followed by removal of the PS by means of an organic solvent. This electrochemical deposition of Au at modified PS/GCE resulted in the formation of gold nanovoids (AuNVs/GCE). For comparison reasons, gold was also electrodeposited at bare GCE in the same experimental conditions obtaining the platform AuNPs/GCE. Next, polystyrene beads of different sizes and concentration suspensions were evaluated in order to obtain the nanostructured gold platform with the best analytical performance. Therefore, beads of 300 and 600 nm and concentration solutions of 2.5 and 5.0 wt% were analysed. To verify the quality and reproducibility of the prepared electrode surfaces, the electrodes were further by means of CV (-0.4 V - 0.8 V , 100 mV s^{-1}). The 2nd cycle was used to evaluate the anodic and cathodic current peak intensities and an average current intensity was calculated (*n=3*).

2.3.1.1 Gold electrodeposition by means of cyclic voltammetry

Depending on the parameters involved in the electrodeposition of AuNPs at GCE surface by CV, different electrocatalytic properties were obtained. Although the S-Au immobilization strategy has several advantages as gold-based nanostructures platforms involve fewer steps in their elaboration compared with other approaches while preserving the bioelement bioactivity there are also some disadvantages regarding this strategy which are mainly linked to the use of Au as a substrate. The Au layer can be oxidized by the oxygen from the air, limiting its reactivity. Additionally, the use of Au increases the costs for the production of the platform. However, our work directly aimed

to remedy these disadvantages by optimizing the concentration of the $HAuCl_4$ and using a smaller amount of Au and, therefore, exposing a smaller Au surface for a shorter period of time during the electrodeposition procedure.

Table 7 *Optimization of the parameters involved in the development of the gold nanopatterned platform*

Platform		PS beads (nm)	$HAuCl_4$ conc. (mM)	CV scans
AuNPs/GCE	**(b)**	-	0.6	10
	(c)	-	1.2	10
AuNVs/GCE	**(d)**	300	0.6	10
	(e)	300	1.2	10
	(f)	300	1.2	15
	(g)	600	1.2	10
	(h)	600	1.2	15

Firstly, a 5.0 % (wt %) PS latex beads suspension of two sizes were tested in the design of the nanovoids gold platform, namely 300 nm (platforms d –e) and 600 nm (platforms g, h) (Table 7). It can be seen an electrocatalytic effect of both AuNPs/GCE and AuNVs/GCE compared to bare GCE which varies depending on the parameters used in the design of the gold platform. Generally, higher current values were obtained when using 300 nm PS beads size compared to the one of 600 nm PS which could be due to a more controlled gold platform formation when using PS beads of smaller size. In all cases, when comparing the $HAuCl_4$ solution concentration from which the electrodeposition of the AuNPs was performed either at bare GCE or PS/GCE, 1.2 mM $HAuCl_4$ solution concentration showed to provide the best response in terms of current intensity of the redox probe $[Fe(CN_6)]^{4-/3-}$ solution. For example, both **(b)** AuNPs(-;0.6,10)/GCE and **(d)** AuNVs(300;0.6,10)/GCE platforms exhibited lower current values of 51.8 μA and 82.0 μA, respectively when using the 0.6 mM $HAuCl_4$ solution concentration compared to the platforms **(c)** AuNPs(-;1.2;10)/GCE (92.5 μA) and **(e)** AuNVs(300;1.2;10)/GCE (102.2 μA), respectively.

Next, the number of cycles involved in the CV electrodeposition procedure was modulated. When sweeping the potential for 10 cycles - platform **(e)** AuNVs(300;1.2;10)/GCE - a higher current value (102.2 μA) was obtained compared to the one of platform **(f)** AuNVs(300;1.2;15)/GCE (91.0 μA) when the potential was cycled

for 15 times. The platform with the best performance using this procedure was platform **(e)** AuNVs(300;1.2;10)/GCE obtained starting from 5 % wt PS beads of 300 nm, and by cycling the potential in the range between - 0.2 V to + 1.2 V for 10 cycles from a solution containing 1.2 μM $HAuCl_4$ in 0.5 M H_2SO_4.

2.3.1.2 Gold electrodeposition by means of multi-pulse assisted amperometry

As the analytical performance in terms of redox peak currents intensity of the redox probe $[Fe(CN_6)]^{4-/3-}$ of platform **(e)** AuNVs(300;1.2;10)/GCE was slightly improved compared to the response of bare GCE, another procedure for gold electrodeposition was studied.

The electrochemical Au deposition between the beads was adjusted using the 1.2 mM $HAuCl_4$ solution as optimized previously by adapting procedure reported in the literature[219]. Firstly, Au nuclei formation for homogeneous Au deposition (10 potential pulses at - 1.4 V *vs.* Ag/AgCl/3 M KCl with 50 ms pulse duration; between each pulse the electrode was kept at open-circuit potential for 1 s) followed by Au growth to obtain a sufficient Au thickness for optimal surface enhancement (- 0.57 V applied for different time periods). The Au growth was controlled by following the shape of the chronoamperogram. Next, as described in the previous section, PS nanospheres were further removed from the electrode surface by dissolution in DMF.

Next, different 300 nm PS concentrations of 2.5 and 5.0 wt% suspension were electrodeposed using the pulse assisted procedure described above modifying the chronoamperometry time (60, 120, 180 s) and the results were evaluated in order to obtain the nanostructured gold platform with the best analytical performance (Figure 20 A). It can be seen that no matter what platform was used, a growth of the analytical signal was obtained up to 120 s of applied potential, followed by a signal decrease after 60 more seconds. This signal change can be corelated with a continuous increase of gold deposition up to 120 s on the electrode free sites, which will lead to a signal increase after the PS dissolution. After the 120 s multiple layers of gold can be formed, that can cover the PS and that in the end will hinder their dissolution, resulting in a decrease of the electrochemical signal.

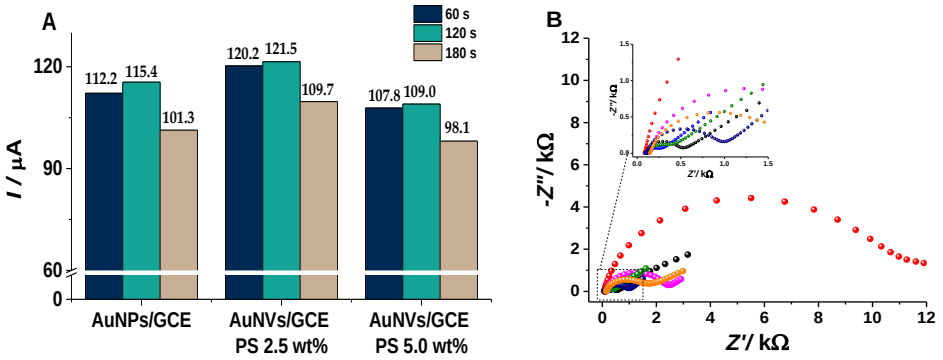

***Figure 20 A**.Peak current intensities at AuNPs/GCE, AuNVs/GCE, AuNVs/GCE platforms obtained by CV in 5 mM [Fe(CN)6]4-/3- in 0.1 M KCl solution; **B.** EIS measurements in 5 mM $[Fe(CN)_6]^{3-/4-}$ in 0.1 M KCl of TET specific aptasensor after each development step: Bare GCE (black), 300 nm 2.5% PS beads suspension/GCE (red), 1.2 mM AuNPs/PS/GCE (green), AuNVs/GCE (blue), Apt/AuNVs/GCE (dark blue), MCH/ Apt/AuNVs/GCE (orange), TET/MCH/Apt/AuNVs/GCE (pink)*

In order to choose the platform most suitable for further modification, the CV oxidation peak of 5 mM $[Fe(CN)_6]^{-3/-4}$ in 10 mM PBS pH 7.4 was studied. The platform using a concentration of PS suspension of 2.5 wt% offered a higher current intensity for $[Fe(CN)_6]^{-3/-4}$ oxidation then the AuNP based platform and that of the one using 5.0 wt% PS suspension. This proves that the nanostructured platform presented in this study has a higher active area then the AuNPs based platform and that by using a 2.5 wt% concentration of PS suspension the surface formation is more controlled than in the case of a 5.0 wt% concentration of PS suspension where PS conglomerations can be formed.

The assembling of the aptasensor and the electron transfer rate of the $[Fe(CN)_6]^{3-/4-}$ redox probe at different development stages were investigated by EIS. As shown in the Nyquist plots from Figure 20 B and its inset, a semi-circular portion in high frequency section and a linear portion in low frequency section indicates a mixed process controlled by the R_{ct} and the diffusion process respectively. The semicircle diameter was used as the probe to calculate the Rct values at the modified electrode surface and to evaluate the influence of every modification step in the development of the TET specific aptasensor. The differences in R_{ct} can be determined by the diffusion and adsorption process at the electrode surface. A high increase of the R_{ct} can be observed, as expected, after the deposition of polystyrene nanobeads, increase explained by their adsorption on the GCE surface and by their lack of electric conductivity. After the gold electrodeposition and considerable decrease of R_{ct} is noticed, following another decrease after the next step, proving the dissolution of the

polystyrene beads and a 3 times better conductivity of AuNVs/GCE compared with the bare GCE (0.14 *vs* 0.43 kΩ**).**

Moreover, the optimized nanostructured gold surface was characterized by Atomic force microscopy (AFM) and Scanning electron microscopy (SEM) techniques. Both techniques reveal a gold nanostructured film formation of 300 nm diameter nanovoids - assisted deposition of AuNPs (Figure 21). A honeycomb formation of the gold nanovoids was observed in atomic force microscopy studies with regular voids of 300 nm diameter and 3D gold layers electrodeposed around them. All this led to the development of a 3D platform with a high surface and an increased electroactive area, as proven by the electrochemical studies.

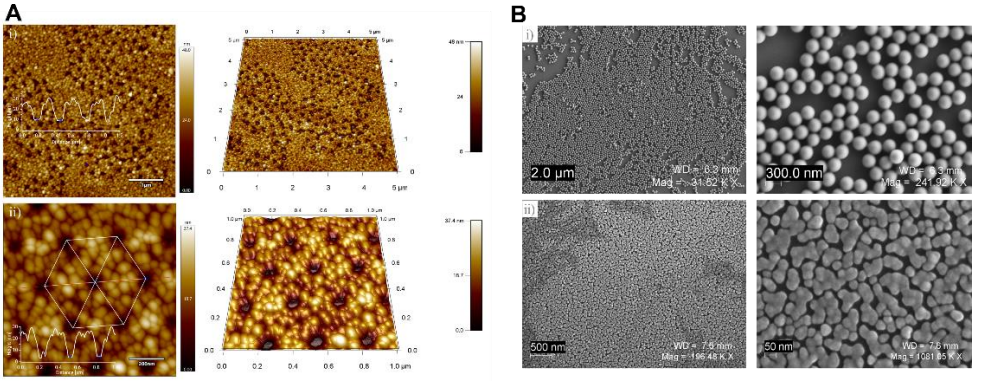

Figure 21 A *AFM images of the gold platform after the dissolution of polystyrene beads (300 nm, 2.5 wt%)***,** *2D topographic images and section profiles along the red line and 3D images. Scan area i) 5×5 µm² and ii) 1×1 µm² . The holes in the Au layer are arranged in a regular hexagonal lattice (a = 300 nm), which indicates the release of spherical objects (polystyrene beads) with diameters of pitch size;* ***B*** *SEM images of i) polystyrene deposited through spin coating on the glassy carbon electrode surface and ii) gold nanostructured platform (AuNVs/GCE) after the dissolution of polystyrene beads (300 nm, 2.5 wt%)*

2.3.2 Aptasensor developement

The optimized AuNVs/GCE platforms were further used as support for the covalent binding of the thiol tethered Fc-Apt. The S-Au immobilization strategy allows the creation of self-assembled monolayers , which presents several advantages like the uniformity of the monolayer, the resistance to non-specific adsorption of interfering molecules, the ability to include multiple aptamers or other moieties and also the ease of preparation and integration in sensing platform. Drop casting over-time incubation (60 min) and electrochemical potential pulse-assisted technique were envisaged as immobilization protocols at AuNVs/GCE platform. The MPA procedure was optimized with respect to the overall duration (16, 32, 90, 180 and 360 s) and Fc-Apt concentration

solutions (0.1, 0.5, 1.0 and 5.0 μM) in TRIS buffer (Table 8). After the aptamer immobilization, the electrodes were tested by DPV in 0.1 M KCl to trigger the anodic Fc signal and, therefore, the efficiency of the immobilization. First, the immobilization by the MPA method was tested due to the fast and tailored ssDNA immobilization. The DPV signal after the immobilization of a 1.0 μM Fc-Apt solution was tested for different periods (90, 180 and 360 s). It can be seen an increase in the Fc anodic signal from 90 s to 180 s, but a slight decrease when MPA was applied for a total time duration of 360 s. Hence, the current intensities were relatively low (~ 0.1 – 0.2 μA). Although longer immobilization time could provide augmented ssDNA strands available for the affinity reaction, one must also consider the density/homogeneity ratio, which could lead to a highly unorganized arrangement of the immobilized strands at lengthy exposure, that might hinder the aptamer binding capabilities. In order to enhance the electrochemical signal, a 5.0 μM Fc-Apt solution concentration was tested in the same conditions. Although the concentration of the Fc-Apt solution was higher, a quenching behaviour of the DPV signal was observed when applying the MPA method for longer periods. This might be explained by the immobilization of a high density of ssDNA strands at the AuNVs 3D nanostructured platform that hindered the electron transfer from the Fc label at the electrode surface. To verify the efficiency if the MPA immobilization method, the over time (60 min) chemisorption was evaluated, leading to a DPV response very close to the response after 90 s potential pulse overall duration.

Table 8 *Optimisation of the immobilisation procedure of the Fc-Apt at the AuNVs/GCE platform. The current values correspond to the Ferrocene oxidation peak signals obtained by DPV measurements in the potential range between -0.1 to 0.5 V at 10 mV s^{-1}.*

Immobilisation procedure		**Aptamer conc. (μM)**	**E (V)**	**I (μA)**	**Stdev (%)**
Procedure	**Time**				
Drop casting incubation	**60 min**		0.18	0.205	9.8
Potential pulse-assisted technique	**90 s**	**1**	0.01-0.15	0.089	78.7
	180s		0.16	0.236	42.4
	360s		0.17	0.187	10.7
	180s	**5**	0.13	0.060	50.0
	360s		0.05-0.16	0.085	47.1
	16 s	**0.5**	0.22	0.510	38
	32 s		0.22	1.190	35

	32 s	**0.1**	0.25	0.540	37

By far, the highest current intensities obtained for Fc electrochemical oxidations were after MPA immobilisation using a 0.5 μM aptamer solution for 16 and 32s. Having a fast analysis with low consumption of reagents is one of the main targets of electrochemical aptasensors development. An aptamer concentration of 0.5 μM immobilised using a 32s MPA procedure was chosen for further optimisations.

Following this, the surface was passivated with MCH for 3 min using the same potential pulse-assisted immobilization protocol (0.05 mM MCH solution in 0.02 M PBS containing 30% (v/v) ethanol).

2.3.3 Analytical performances

A concentration - response curve of tetracycline was obtained under the optimized conditions. The signal is reported as $\Delta I/I_0$ percent units, that is the percentage of the signal decrease with respect to the initial value. A decrease in the peak current height was recorded by increasing the concentration of the antibiotic in the range from 12.5 nM to 4 μM obtaining a logarithmic curve (Figure 22A). A linear regression between the signal $\Delta I/I_0$(%) and the logarithm of TET concentration ([TET]/nM) was obtained in the range 12.5 – 1000 nM described by the following equation: $\Delta I/I_0(\%)$ = 46.16 log[TET](nM) ±2.11 – 44.47±4.34 with a correlation coefficient of R^2 = 0.989. The obtained LOD and LOQ were 1.22 nM, and 4.23 nM, respectively. The LOD was calculated from 3 times the standard deviation of the regression equation divided by its slope and the LOQ as 10 times the standard deviation of the regression equation divided by its slope[191].

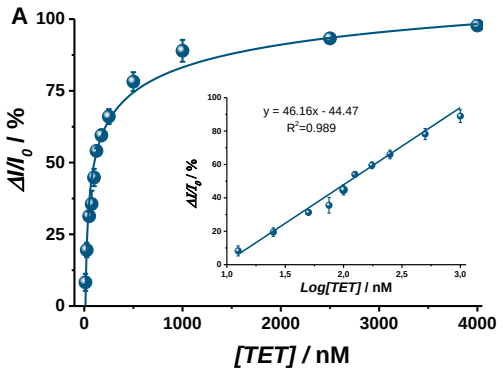

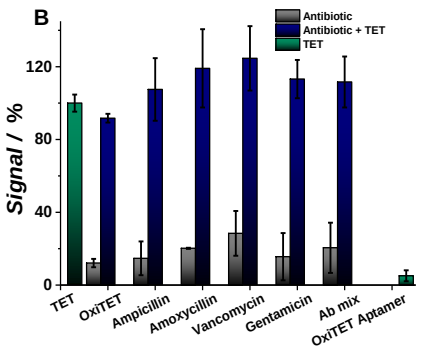

Figure 22 A Tetracycline dose-response curve where the points correspond to $\Delta I/I_0(\%)$ ± RSD. Inset: Variation of $\Delta I/I_0\%$ with the logarithm of TET concentration; B) The electrochemical signal change after incubating the aptasensor with 50 nM TET (black) 50 nM antibiotic (dark blue), 50nM Antibiotic+50nM TET (green), 25nM of each Antibiotic mix (dark blue) and 25 nM each antibiotic + 25 nM TET

2.3.4 Selectivity, stability and applications

The affinity of the sensing platform towards TET can be clearly seen by the comparison between the relative response between the antibiotic signal alone and in a mixture with TET. However, as displayed in Figure 22 B, Vancomycin was the only antibiotic that had led to a signal enhancement above 20% out of all antibiotics. This may be due to its high molecular weight (1485.7 g mol^{-1}), 3-fold of TET, that might lead to unspecific adsorption phenomena. There is a slight increase in the relative signal for Amoxycillin (119.2%) which can be attributed to the presence of a phenolic group in the antibiotic structure which can be part of the affinity binding site with the aptamer. Hence, in waste water samples, or in the bloodstream of antibiotic-treated animals, the concentration of TET could get to higher levels, therefore the analysis should not be considerably affected. In contrast, little difference in the signal intensity was observed when the analogues were presented alone or in a mixture with TET, which highlights that TET could be differentiated by the proposed aptasensing strategy. Further, a specific aptamer for OxyTET labelled with Fc was immobilized at the AuNVs-based platform and tested in the presence of 50 nM TET. Very little influence (5.1%) was found, proving thus satisfactory selectivity of the proposed aptasensor for tetracycline detection.

In terms of reproducibility, at least 3 analyses were performed for every concentration of TET used for the calibration curve calculation and the relative RSD was calculated. It varied from 0.89 to 4.63%, in every case, it is less than 5%, proving a good reproducibility and reliability for further developments.

Besides, the stability of the developed aptasensor was evaluated by storing the modified electrodes at 4 °C and performing different analyses (3 different days) under the same conditions. No significant signal difference (less than 6.0%) was observed, proving that the proposed aptasensor had a satisfying stability for TET detection.

The applicability of the aptasensor was proven by analysing water samples with different grades of purification using the standard addition methods. Two samples of water were collected from the local water treatment plant: before the primary decantation (water sample 2) and after the purification (water sample 1). The 3rd sample was collected directly from the laboratory, being normal tap water (water sample 3). After the filtration and dilution processes described in materials and methods, the

samples were spiked with 50, 100 and 150 nM TET and analysed. The found concentration was calculated according to the calibration plot equation.

Table 9 *Recovery rates of TET from spiked waste and tap water samples.*

	Added (nM)	**Found (nM)**	**Recovery (%)**	**RSD* (%)** *(n = 3)*
Water sample 1	50	46.59	93.18	1.89
	100	94.06	94.06	6.02
	150	152.72	101.81	6.05
Water sample 2	50	53.95	107.90	3.18
	100	100.15	100.15	2.14
	150	168.97	112.64	1.12
Water sample 3	50	52.39	104.79	5.57
	100	95.21	95.21	6.13
	150	143	95.33	2.34

As seen in Table 9, the recovery rates in all cases were in the range 93.18 - 112.64 %. This shows that there is no significant effect from the matrix and that TET can be detected using this aptasensor in wastewater or treated water, no matter its level of purification.

2.4 Conclusions

In this work, a novel gold-based platform for electrochemical sensing was developed and applied for the selective detection of TET traces in water samples. Novel gold nanostructures were synthesised by the electrodeposition of gold from a solution on $HAuCl_4$ on PS beads modified GCE. 3D Honeycombed-like gold platform was obtained by deposing gold in multilayer, followed by the dissolution of PS beads. A significantly higher electroactive surface area was obtained compared to the electrodeposition of gold nanoparticles in the absence of PS beads. The utility of the platform towards aptasensing was proven by immobilising a TET specific aptamer and the electrochemical detection of TET. The newly developed aptasensor showed good analytical performances in a linear range of 12.5 – 1000 nM with a LOD of 1.22 nM and LOQ of 4.23 nM. It has proven good selectivity in the presence of other antibiotics with similar molecular structures and no interferences from the matrix when tested in wastewater samples.

3. Gold-Platinum / Graphene oxide-based platform for AraH1 allergen determination (Study 6)

3.1 Introduction

Peanuts (Arachis hypogaea) are among the most common food products that cause allergic reactions. They are often introduced into the human diet due to their essential content of proteins, fats, iron, zinc, and niacin (vitamin B3)(174). Ara H1 is the most prevalent peanut allergen. It is considered one of the most severe, life-threatening food sensitivities since it triggers the highest frequency of severe and fatal reactions, even in trace amounts. It accounts for 35 to 95% of allergic reactions in peanut sensitive patients[175].

Currently, in the U.S, there are 32 million people suffering from food allergies, which roughly means 1 in 10 adults[176]. Moreover, there has been a 377% increase in the diagnosed anaphylactic food-induced reactions between 2007 and 2016[177]. Thus, it is extremely important to develop fast, accurate and sensitive methods for in situ detection of Ara H1. Electrochemical aptasensors represent a good alternative to traditional detection methods like liquid chromatography[221] or ELISA[222].

The ligands used for the immobilisation of aptamers on the surface of electrodes are of major importance for the sensitivity and reproducibility of the aptasensors [223–225]. Covalent bonds are mostly employed, whereas affinity interactions (i.e., using streptavidin-biotin, lectin-carbohydrates, metal cation-chelator, etc.) are of election for tailored orientation immobilisation[226]. Nanomaterials play a vital role in bioelements accumulation, assembly density controlling and electron transfer boosting at the interface of aptasensors[227]. GO are carbon-composed materials synthesised from graphite powder and strong oxidising agents. This oxidising process can produce numerous oxygen groups like hydroxyl or carboxyl that do not act only as catalytical active centres in the electrochemical processes but also offer good anchoring sites for covalent immobilisation[138]. Having the GO modified with carboxylic groups (GO-COOH), the platform becomes suitable for the immobilisation of -NH_2 tethered aptamers by using the strong interaction within the amidic generated covalent bonds. Despite these extremely important properties of GO, the main drawback originates from the formation of some structural defects and vacancies that break the sp^2 network and dramatically

decrease the electronic conductivity. For this reason, GO tends to be rather an insulating material. Materials like MNPs have been previously used in combinations with GO-COOH[140,141]. Noble metal-based nanoparticles, like gold and platinum, are ideal tools in increasing GO-COOH conductivity. They modify the electrochemical characteristics of the biosensor by offering high electrical conductivity that can significantly decrease the insulating effect of GO-COOH, larger surface-to-volume ratio and increased biocompatibility, all of these improving the sensor's overall performances[117].

In this work, two strategies were applied to develop an electrochemical platform based on GO-COOH and MNPs immobilised on SPCEs. Thanks to the affinity reaction between the specific DNA receptor and the target analyte, an electrochemical aptasensor with high specificity and good sensitivity towards Ara H1 was developed. The method was applied in peanut-free food samples with very good recoveries proving to be a promising tool for peanut allergy prevention (Scheme 5).

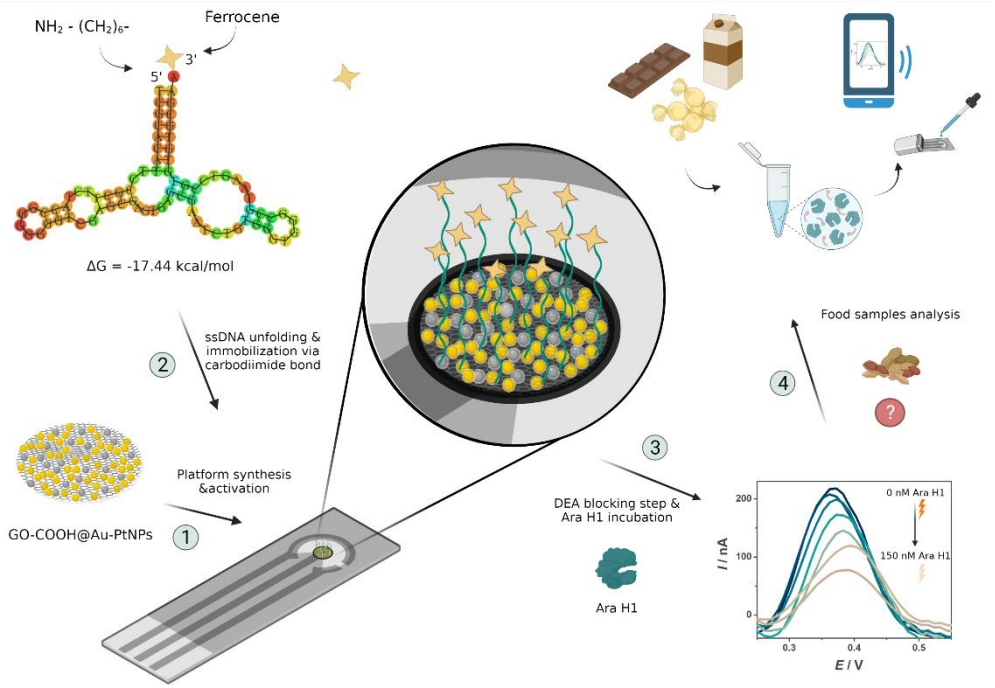

Scheme 5 *Schematic representation of the graphene-bimetallic based aptasensor for Ara H1 peanut allergen analysis*

3.2 Materials and methods

3.2.1. Materials

Ara H1 protein, GO-COOH, KCl, NaCl, Na_2HPO_4, NaH_2PO_4, TRIS, 1-ethyl-3-(3-dimethylaminopropyl) carbodiimide (EDC), *N*-hydroxysuccinimide (NHS), $K_3[Fe(CN_6]$, $K_4[Fe(CN_6]$, Hexaammineruthenium (II) chloride $[Ru(NH_3)_6]Cl_2$, Hexaammineruthenium (III) chloride $[Ru(NH_3)_6]Cl_3$, Ferrocene Dimethanol, DEA, 2-(N-Morpholino)ethanesulfonic acid (MES), $MgCl_2$, chicken egg white albumin (Ovalbumin) were purchased from Sigma Aldrich (Italy). H_2SO_4, $HAuCl_4$ and Chloroplatinic acid (H_2PtCl_6) were purchased from Merck (Germany).

The Ara H1 specific aptamer (K_d= 350±82 nM)[228] was bought from Biomers, (Italy) and had the following sequence:

5` - $NH_2$ - $(CH_2)_6$ - TCGCACATTCCGCTTCTACCGGGGGGGTCGAGCGAGTGAGCGAATCTGTGGGTGGGCCGTAAGTCCGTGTGTGCGAA – 3` Fc

The supporting electrolytes and buffers used in this study were:

- Electrolyte solution - 0.1 M KCl;
- Affinity buffer - 10 mM TRIS buffer pH 7.4 containing 10 mM TRIS, 100 mM NaCl, 100 mM KCl and 5 mM $MgCl_2$;
- Activation buffer - 0.1 M MES buffer pH 5.5 adjusted with 0.1 M NaOH;
- Blocking buffer – 2.5 mM DEA pH 9.8 containing 1 mM $MgCl_2$.

For the analysis of the real samples, chocolate cookies, a fondant chocolate bar with 70% cacao and a chocolate milk-based beverage, all free of peanuts traces were bought from the local supermarket.

All the electrochemical experiments were performed using a Methrom Autolab (Netherlands) and Nova 2.1 software was used for data acquisitions. Data analysis was performed using OriginLab analysis software.

After each development step, the platform was characterised in CV using 5 mM $[Fe(CN)_6]^{3-/4-}$ in 0.1 M KCl (-0.5 – 0.3 V, 100 mV s^{-1}) and 5 mM $[Ru(NH_3)_6]^{2+/3+}$ in 0.1 M KCl (-0.5 – 0.3 V, 100 mV s^{-1}) redox probes, respectively. EIS analyses were performed in 5 mM $[Fe(CN)_6]^{3-/4-}$ in 0.1 M KCl by applying 61 frequencies (100 MHz – 0.1 Hz) at a fixed potential of + 0.2 V. DPV analysis were performed in electrolyte solution and in 50 mM Ferrocene dimethanol in electrolyte solution (0 – 0.6 , 15 mV s^{-1}).

3.2.2. Platform development

Two different approaches were used for the development of a suitable platform for Ara H1 aptamer immobilisation. In both cases, the first step was represented by the ultrasonication for 60 min of a 2 mg mL^{-1} stock suspension of GO-COOH in water.

For the first approach, the electrochemical synthesis of MNPs, GO-COOH were vortexed until a homogenous suspension was obtained and 5 µL were dropped onto the working electrode surface. Next, on the GO-COOH modified SPCE platform, Au-PtNPs were electrodeposited via CV (-0.2 – 1.2 V, 50 mV s^{-1}, 10 scans) from a solution containing 5 mM $HAuCl_4$ and 5 mM H_2PtCl_6 in 0.5 M H_2SO_4 to generate the GO-COOH/Au-PtNPs/SPCE and Au-PtNPs/GO-COOH/SPCE platforms, respectively.

For the second approach, the chemical synthesis method of particles in GO suspension was employed to obtain GO-COOH@Au-PtNPs/SPCE platforms. To this, 1 mL of suspension containing 1 mg mL^{-1} GO-COOH, 5 mM $HAuCl_4$ and 5 mM H_2PtCl_6 was ultrasonicated for 30 min. Next, 300 µL of 5 mg mL^{-1} $NaBH_4$ was added, and the solution was kept under stirring for 2h 30 min. After that, the suspension was centrifuged at 13000 rpm for 5 min, and the supernatant was removed. 1 mL of water was added to wash the particles, followed by 5 min centrifugation and supernatant removal. This washing step was performed three times. Next, the particles were kept at 80 ^oC until completely drying. 1 mg of particles were suspended in 1 mL of water and ultrasonicated for 90 min before use.

3.2.3. Aptasensor development

For the NH_2-ssDNA-Fc (Apt) immobilisation, a 5 µM Apt solution in affinity buffer was used. Prior to the immobilisation, a solution containing NHS/EDC 0.2 M/0.4 M in activation buffer was dropped on the working electrode surface and left to react for 90 min at 4 °C, in a humid atmosphere. Next, the electrodes were washed three times with 100 µL activation buffer and incubated overnight with 5 µL Apt solution at 4 °C, in a humid atmosphere. After the incubation, the electrodes were washed three times with 100 µL affinity buffer and tested by EIS and DPV.

Next, a 2.5 mM blocking buffer solution was dropped on the electrode and left to react for 15 min, followed by a washing step with 3*100 µL affinity buffer. A 20.1 mM Ara H1 stock solution was prepared in affinity buffer and diluted to the desired concentrations. 5 µL were dropped on the working electrode surface and left to react for 90 min, in a humid atmosphere, at 20 ^oC. For the quantification of Ara H1 concentration, the oxidation peak intensity of the Fc moiety from the NH_2-ssDNA-Fc was measured by performing DPV measurement in electrolyte solution after the blocking step and after the incubation with the protein. The ratio of the current intensities (I/I_0) was calculated and correlated with the Ara H1 concentration.

3.2.4. Applications

In order to assess the selectivity of the developed aptasensor for Ara H1 allergen, analysis was performed in the presence of molecules commonly found in the same food products like Ovalbumin and *β*-lactoglobulin milk major allergen. For this, solutions containing an equimolar mixture of 100 nM of interferent and Ara H1 and solutions containing 100 nM interferent free of Ara H1 were tested.

For the analysis of the real samples, chocolate cookies, a fondant chocolate bar with 70% cacao and a chocolate milk-based beverage were used in order to prove the applicability of this method. An extraction was performed using a procedure adapted from[229]. Briefly, 0.1 g of homogenised cookie and chocolate sample or 0.1 mL of milk-based beverage was mixed with 2 mL of 10 mM PBS buffer pH 7.4, followed by incubation under stirring at 60 °C for 15 min. After being cooled down at room temperature, the solution mixture was centrifuged at 4000 rpm for 5 min. The supernatant of the mixture was filtered through a filter syringe with 0.2 μm diameter pores and diluted 10 times. The precision of this method in terms of recovery rate was evaluated by spiking Ara H1 standard solutions of 0 – 150 nM into the food samples and calculating the Ara H1 found concentration from the standard calibration curve.

3.3 Results and discussions

3.3.1. Platform optimisation

For this step, a 2 mg mL^{-1} GO-COOH stock suspension in water was diluted to desired concentrations. The final suspensions were ultrasonicated for 45 min before being deposited on the electrode surface. For the deposition, the GO-COOH particles were vortexed and 5 μL were dropped on the working electrode. After the complete drying of the GO-COOH, the electrodes were tested by CV and EIS in $[Fe(CN)_6]^{3-/4-}$ redox probe. Concentration in the range of 0.1 – 1 mg mL^{-1} GO-COOH were immobilised.

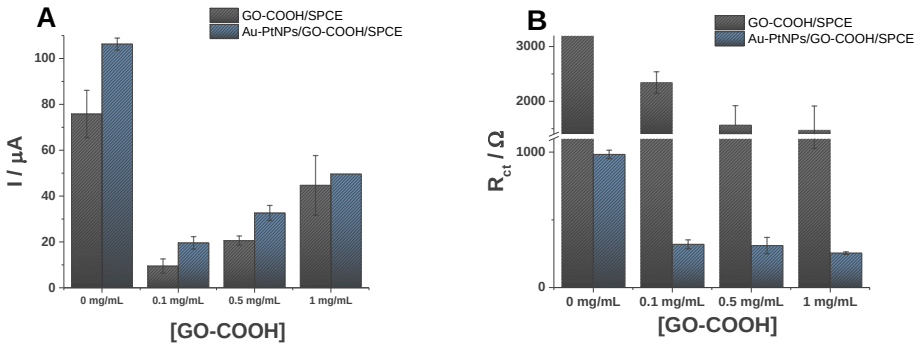

Figure 23 A: *Average current intensities of the CV oxidation/reduction of a 5 mM $[Fe(CN)_6]^{3-/4-}$ in 0.1 M KCl solution at the surface of GO-COOH modified electrodes;* ***B:*** *R_{ct} obtained in EIS using 5 mM $[Fe(CN)_6]^{3-/4-}$ in 0.1 M KCl redox probe at the surface of GO-COOH modified electrodes*

From the CV studies (Figure 23A) a significant decrease in current intensity can be observed after GO-COOH deposition on the SPCE working electrode. A higher concentration of GO-COOH shows a higher average current intensity, 1 mg mL^{-1} proving to be the concentration with the best conductivity of the three concentrations deposed. In contrast, the EIS studies (Figure 23B) showed a decrease in charge transfer resistance (R_{ct}) after the deposition of GO-COOH on SPCE. Moreover, an increase in GO-COOH concentration led to a proportional decrease of R_{ct} and therefore, to better conductivity.

Next, on the GO-COOH platform, Au-PtNPs were electrodeposited (CV: -0.2 – 1.2 V, 50 mV s^{-1}, 10 scans) from a solution containing 5 mM $HAuCl_4$ and 5 mM H_2PtCl_6 in 0.5 M H_2SO_4. In both CV and EIS studies, the electrodeposition of Au-PtNPs led to increased conductivity, showing that the deposition of noble particles had a positive effect. The reduced average current intensities obtained in CV after the deposition of GO-COOH might be due to electrostatic repulsions that might appear between the negatively charged COO^- groups grafted on GO and the $[Fe(CN)_6]^{-3/-4}$ redox probe.

Further, two concentrations of GO-COOH were used for electrode deposition. 1 mg mL^{-1} and 0.1 mg mL^{-1} were also deposed on top of the Au-PtNPs and not only as the first layer. From CV (Figure 24A) and EIS (Figure 24B) studies it seems to be no significant difference in CV and EIS between the platforms with gold on top and GO-COOH as the first layer and the platform with GO-COOH as the top layer. So, since there is more probable to have a higher density of carboxylic groups, for further optimisations, the platform with GO-COOH on top of a 5 mM $HAuCl_4$ and 5 mM H_2PtCl_6 layer (GO-COOH/Au-PtNPs) will be further evaluated.

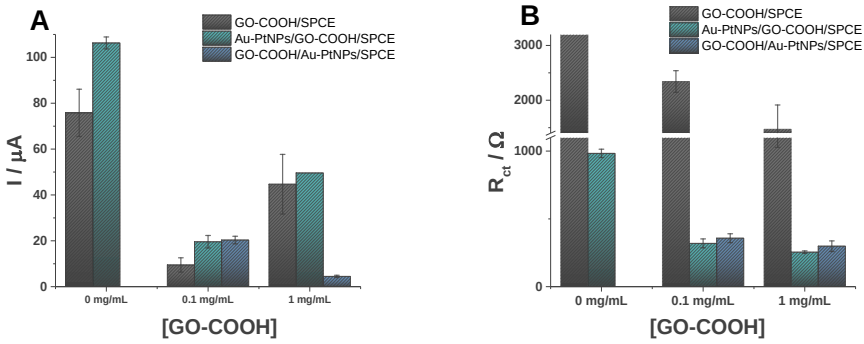

Figure 24 A: *Average current intensities of the CV oxidation/reduction of a 5 mM $[Fe(CN)_6]^{3-/4-}$ in 0.1 M KCl solution at the surface of GO-COOH (black), Au-PtNPs/GO-COOH (green) and GO/Au-PtNPs(blue) modified SPCE;* ***B:*** *R_{ct} obtained in EIS using 5 mM $[Fe(CN)_6]^{3-/4-}$ in 0.1 M KCl redox probe at the GO-COOH (black), Au-PtNPs/GO-COOH (green) and GO/Au-PtNPs (blue) modified SPCE*

3.3.2. Comparison between electrochemical (GO-COOH/Au-PtNPs) and chemical (GO-COOH@Au-PtNPs) syntheses of GO-COOH bimetallic platforms

A new protocol was employed for the synthesis of a new type of GO-COOH and noble metals particles by chemically reducing different concentrations of $HAuCl_4$ and H_2PtCl_6 in a suspension containing 1 mg mL^{-1} GO-COOH particles, according to the procedure described in materials and methods. Two types of chemically synthesised particles were obtained: GO-COOH@AuNPs and GO-COOH@Au-PtNPs. The newly synthesised particles were resuspended in water, in a concentration range of 0.1 – 1.0 mg mL^{-1} and then immobilised on the SPCEs working electrode surface and left to dry before being tested in CV and EIS in 5 mM $[Fe(CN)_6]^{3-/4-}$ in 0.1 M KCl, 5 mM $[Ru(NH_3)_6]^{2+/3+}$ in 0.1 M KCl and in DPV using a 50 µM Fc dimethanol solution in 0.1 M KCl. All results were compared with the ones obtained by the immobilisation of GO-COOH on the surface of electrodeposited AuNPs and Au-PtNPs on the SPCE working electrode surface, namely GO-COOH/AuNPs and GO-COOH/Au-PtNPs.

From the CV studies (Figure 25A), higher current intensities can be observed on the platforms where the MNPs were chemically synthesised directly in GO-COOH particles suspension. However, due to the electrostatic repulsions between the negatively charged $[Fe(CN)_6]^{3-/4-}$ and the high density of $-COO^-$ groups at the GO-COOH@MNPs/SPCE surface, the highest current intensities were obtained when a smaller concentration of particles was dropped on the working electrode. In contrast, in

EIS the electric repulsions are smaller and therefore the surface conductivity is more accurately characterised. As it can be observed, in the case of chemically synthesised particles, there is a decrease in R_{ct} with the increase of particles concentration showing an increase in conductivity from 0.1 mg mL^{-1} particles concentration up to 2 mg mL^{-1} particles concentration. In all cases, the 2 mg mL^{-1} concentration of particles showed the best conductivity in EIS with very small variations between the types of platforms. Looking at the voltammograms obtained for each platform when 2 mg mL^{-1} particles were immobilised (Figure 25C) a much better conductivity can be observed for the GO-COOH@AuNPs and GO-COOH@Au-PtNPs platforms, indicating to be better alternatives for a more sensitive aptasensors than GO-COOH/AuNPs and GO-COOH/Au-PtNPs platforms.

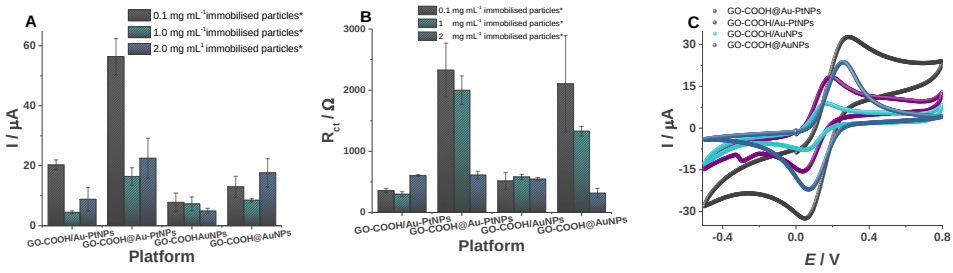

* Immobilised particles concentration: GO-COOH for electrodeposited metallic platforms

GO-COOH@metallic-composite for chemically synthesised particles

Figure 25 A *Average current intensities of the CV oxidation/reduction of a 5 mM $[Fe(CN)_6]^{3-/4-}$ in 0.1 M KCl after the immobilisation of 0.1 mg mL^{-1} (black), 1 mg mL^{-1} (green) and 2 mg mL^{-1} (blue) particles;* ***B*** *R_{ct} obtained in EIS using 5 mM $[Fe(CN)_6]^{3-/4-}$ in 0.1 M KCl redox probe KCl after the immobilisation of 0.1 mg mL^{-1} (black), 1 mg mL^{-1} (green) and 2 mg mL^{-1} (blue) particles.* ***C:*** *CVs obtained in 5 mM $[Fe(CN)_6]^{3-/4-}$ in 0.1 M KCl after the immobilisation of 2 mg mL^{-1} of particles on the SPCE surface*

But, since the signal that was going to be detected and correlated with Ara H1 concentration was the electrochemical oxidation of the Ferrocene moieties grafted on the aptamer's 3' end, it was very important to assess directly its oxidation at all platforms . For this, a 50 µM Fc methanol in 0.1 M KCl was dropped on the electrode surface and a DPV (-0.2 – 0.5 V, 10 mV s^{-1}) was performed. The peak current intensities and the RSDs were considered when choosing the best platforms for Fc oxidation and Apt immobilisation. Regarding the GO-COOH/Au-PtNPs platforms, even though they showed very conductivity in $[Fe(CN)_6]^{-3/-4}$ in 0.1 M KCl analyses, for the Fc dimethanol oxidation, low peak current intensities were obtained (0.41 (24% RSD) µA for 0.1 mg mL^{-1} GO-COOH, and 0.03 µA for 1 mg mL^{-1} GO-COOH). Higher intensities with good

reproducibility were obtained for 2 mg mL^{-1} GO-COOH/AuNPs (1.16 mg mL^{-1}), 1 and 2 mg mL^{-1} GO-COO@AuNPs (0.38 and 0.40 µA) and 2 mg mL^{-1} GO-COOH@Au-PtNPs (0.88 µA). As a result, the last 4 mentioned platforms were chosen for the next optimisation steps.

3.3.3. Aptasensor development

For the NH_2-ssDNA-Fc (Apt) immobilisation protocol a 5 µM Apt in affinity buffer solution was used. Before the immobilisation, a solution containing NHS/EDC 0.2 M/0.4 M in affinity buffer was dropped on the working electrode surface and left to react for 90 min at 4 °C in a humid atmosphere in order to activate the GO-COOH platform. Next, the electrodes were washed with 3*100 µL affinity buffer and incubated overnight with 5 µL Apt solution at 4 °C in a humid atmosphere. After the incubation, the electrodes were washed with 3*100 µL affinity buffer and tested in DPV and EIS.

For the EIS analysis, the R_{ct} was read before the aptamer immobilisation and after. The results were compared in order to see the modification of the electrode surface. In DPV, the Apt immobilisation was quantified as the Fc oxidation peak height.

The platforms that showed the best conductivity in the previous platform analysis, were chosen for aptamer immobilisation.

- 2 mg mL^{-1} GO-COOH@Au-PtNPs
- 1 mg mL^{-1} GO-COOH@AuNPs
- 2 mg mL^{-1} GO-COOH@AuNPs
- 1 mg mL^{-1} GO-COOH/AuNPs

The results presented in Table 10 were used to choose the most suitable platform for aptamer immobilisation. As it can be seen, the only platforms that showed an increase in R_{ct} are 2 mg mL^{-1} GO-COOH@Au-PtNPs and 2 mg mL^{-1} GO-COOH@AuNPs showing that on the other 2 platforms there might be a very low or no immobilisation at all. Therefore, these 2 platforms were used further for the aptamer concentration and incubation time optimisation.

Table 10 . *R_{ct} obtained in EIS in 5 mM $[Fe(CN)_6]^{3-/-4}$ in 0.1 M KCl before and after the Apt immobilisation*

Platform	EIS				
	Rct (p) Ω	Rct (a) Ω	Rct (a-p) Ω	Rct (a/p)	RSD %

2 mg mL^{-1} GO-COOH@Au-PtNPs	203	661	458	*3.25*	*3.5*
2 mg mL^{-1} GO-COOH@AuNPs	320.3	336	16	*1.05*	*1.5*
1 mg mL^{-1} GO-COOH@AuNPs	1305	1003	302	*0.81*	*43.4*
1 mg mL^{-1} GO-COOH/AuNPs	461	456	4.71	*0.99*	*19.1*

For this, Apt solutions of 0, 2 and 5 μM in affinity buffer were incubated in a humid atmosphere at 4° C for 1, 3 and 18 h. Next, the electrodes were washed 3 times with 100 μL affinity buffer to remove the unbound strands and tested in DPV with affinity buffer. On both platforms there is no Fc oxidation peak when the incubation was performed in the solution free of Apt. When the concentration was optimised, on both platforms and after 1, 3 or 18 h of incubation, the solution containing 5 μM Apt showed high current intensities corresponding to the Fc oxidation. The reproducibility was a very important factor to be considered when choosing the best Apt immobilisation protocol. The platform containing 2 mg mL^{-1} GO-COOH@AuNPs yielded very high RSDs between 12 and 34.6% (*n=4*). In comparison, at the bimetallic platform, more reproducible results were obtained with RSDs in the range of 3.6 – 13.2 % (*n=4*). As a result, for further optimisation, the platforms obtained by chemical synthesis were used.

An important parameter that had to be optimised in order to obtain the best aptamer immobilisation is the NHS/EDC couple buffer. The NHS/EDC reacts differently at different pH and salts concentrations with different reaction efficiencies. Therefore, activation and affinity buffers were used as media for the two reactants and to wash the electrodes after the 90 min of reaction. After the reaction, different concentrations of Apt were immobilised using 3h or overnight incubation periods and the Fc oxidation peak was read afterwards in order to assess which buffer and immobilisation method are more suitable for our platform.

In Figure 26A higher Fc oxidation peak values can be observed for 2 and 5 μM Apt concentrations with a 3h and overnight incubation period, when activation buffer was used. In Figure 26B the DPVs obtained after the immobilisation of 0 - 5 μM Apt incubated overnight and a previous activation with NHS/EDC in activation buffer are represented. No peak was observed when the incubation was performed in the solution free of Apt, a small peak of around 15 nA when 2 μM Apt solution was incubated and an oxidation peak of 232 nA was obtained after the overnight incubation of a 5 μM Apt solution. For further optimisations, activation buffer was used as NHS/EDC reaction solvent and 5 μM aptamer was incubated overnight.

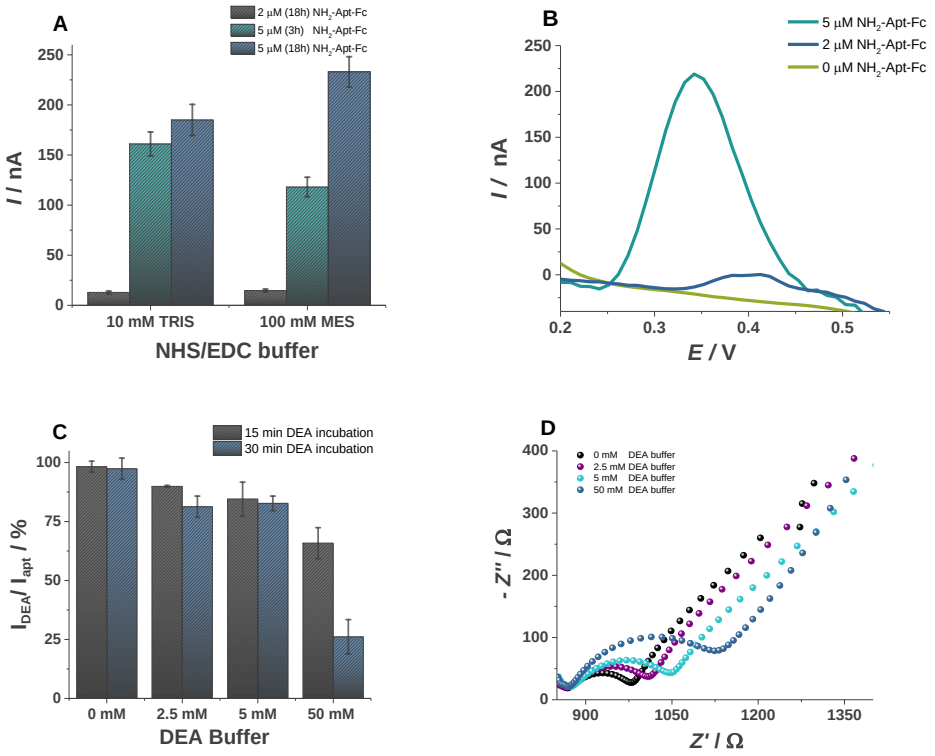

Figure 26 A *Current intensities (nA) corresponding to Fc oxidation in DPV (-0.2 – 0.55 V, 15 mV s^{-1}) in 10 mM TRIS buffer pH 7.4 after the Apt immobilisation and a previous COOH groups activation using NHS/EDC (0.2 M/0.4 M) solutions in affinity buffer and activation buffer;* ***B*** *DPVs curves in affinity buffer after different Apt concentrations immobilisation;* ***C*** *I/I_0(%) obtained in DPV in affinity buffer after 15 and 30 min of incubation with different concentrations of blocking buffer;* ***D*** *Nyquist plots obtained by EIS in 5 mM $[Fe(CN)_6]^{-3/-4}$ in 0.1 M KCl after 15 min of incubation with different concentrations of blocking buffer*

In order to block the remaining free activated carboxyl groups, blocking buffer was used. Concentrations in the range of 0 – 50 mM DEA were incubated for 15 min to 30 min and the electrodes were tested in EIS (Figure 26D) and DPV (Figure 26C), respectively, before and after the DEA incubation. In impedance, the increase of the R_{ct} was evaluated, whereas in DPV, the Apt label, Fc oxidation peak signal recovery.

When choosing the optimum blocking agent concentration and incubation time, two aspects were considered. A high concentration of DEA buffer or a longer immobilisation period could block the current charge transfer and decrease the Fc oxidation intensity. However, if the concentration is not high enough, there is the

possibility that the activated free -COOH groups are not blocked and could lead to an increased non-specific adsorption effect. Therefore, from the DPV tests, the percentage of Fc oxidation peak recovery was analysed by comparing the oxidation peak obtained after the blocking step (I_0) with the one obtained before. Incubations with 0 mM DEA were performed also as control. It can be observed that the best recovery was obtained generally when 15 minutes were used as incubation time. Regarding the concentration when 2.5 mM DEA was incubated, a recovery of 89.9 % with an RSD of 0.4 % after 15 min and 81.3 % with an RSD of 5.5 % after 30 min. From the impedance studies (Figure 26D) it can be observed an increase of R_{ct} with the increase of DEA concentration (15 min incubation), proving the immobilisation of the blocking agent. For further studies, a 2.5 mM blocking buffer incubated for 15 minutes at 25 ^{o}C was used for the blocking step.

3.3.4 Analytical performances

For the detection of Ara H1 allergen, first, the incubation time was optimised. 100 nM of protein was incubated for 30 to 90 min, and the Fc oxidation peak was evaluated in DPV and compared with the current peak intensity (I_0) obtained after the blocking step. After 30 min incubation time, a signal decrease, calculated as I/I_0 (%), of 83.3 ± 4.5 ($n=3$) was obtained, 77.5 ± 1.7 % ($n=3$) after 60 min and 60.3 ± 3.5 % after 90 min, respectively. The highest decrease in the Fc peak intensity I/I_0 (%) was observed after 90 min of Ara H1 incubation, choosing this parameter for the affinity assay. In order to characterise each development step, EIS analysis in 5 mM $[Fe(CN)_6]^{3-/4-}$ in 0.1 M KCl was performed. As shown in Figure 27A, an increase in the R_{ct} values was obtained after each step, with the GO-COOH@Au-PtNPs platform having the best conductivity. This demonstrates the successful immobilisation of the aptamer, the good blocking of the remaining active COOH groups and the successful aptamer - analyte interaction.

For the quantification of the protein, a calibration curve calculated as I/I_0 (%) was obtained in the 0 - 150 nM range with a LOD (estimated based on the signal/noise ratio of three, S/N=3) of 1.66 nM and a limit of quantification (LOQ) of 4.98 nM. The equation describing the linearity curve is I/I_0 (%) = − 0.363 ± 0.01 [Ara H1] (nM) + 96.95 ± 0.11 with a correlation coefficient R^2=0.995 (Figure 27B and 27C).

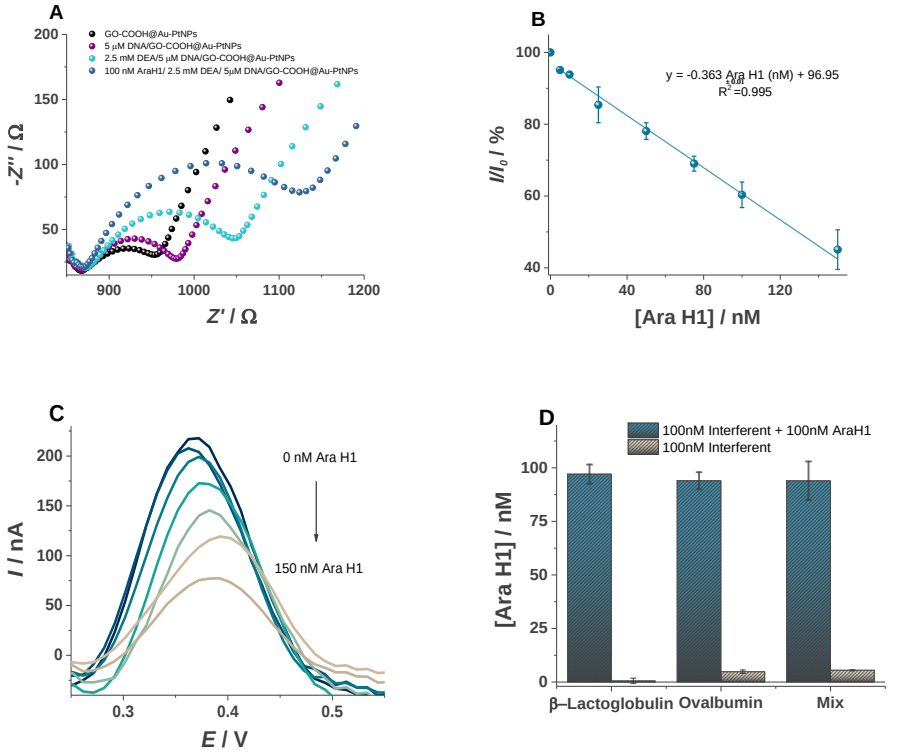

Figure 27 A *Nyquist plots obtained in a 5 mM $[Fe(CN)_6]^{3-/4-}$ in 0.1 M KCl solution after each step in the aptasensor development;* ***B*** *Ara H1 dose-response curve where the points correspond to I/I_0 (%) variation with Ara H1 concentration (nM);* ***C*** *Signal "off" variation of Fc oxidation DPVs with the increase of Ara H1 concentration;* ***D*** *Histograms representing the recovery of Ara H1 after the analysis of solutions containing equimolar mixture solutions of interferent and Ara H1 allergen (blue) and interferent solution free of Ara H1 allergen (grey)*

3.3.5. Specificity and applications

In order to assess the selectivity of the developed aptasensor for Ara H1 allergen, analysis was performed in the presence of molecules commonly found in food products, like Ovalbumin and β-lactoglobulin milk major allergen. For this, solutions containing equimolar (100 nM) mixture solutions interferent and Ara H1 allergen and solutions containing 100 nM interferent free of Ara H1 were tested. The signal recovery was calculated based on the calibration curve obtained in standard conditions (Figure 27D). The results showed that in the presence of Ara H1 allergen, the detected concentration is very close to the one added in the solution (93.94 – 97.04 nM), while in the absence of

Ara H1 very little interference was observed from Ovalbumin and in the mix of the interferents, where signals corresponding to 4.81 nM and 5.48 nM, respectively, were detected. These results show that there is no significant interference in the analysis of Ara H1 from proteins commonly found in peanut-based food products. The overall good selectivity shown by the signal "off" aptasensor is attributed to the specific recognition ability of the Ara H1 aptamer, which can specifically recognise and capture the target with self-conformation change and to the GO-COOH@Au-PtNPs platform's ability to reduce the non-specific adsorption rate in the presence of large proteins.

In order to prove the applicability of the aptasensor, peanut-free food samples were tested. Chocolate cookies, a bar of fondant chocolate with 70% cacao and a chocolate-based milk drink were tested by the standard addition method, in the range of 0 – 150 nM. The food samples were subjected to extraction and dilution (1:10) prior the analysis. The electrodes were tested before and after the incubation with the real samples and the concentration of allergen was calculated using the standard calibration curve obtained in the affinity buffer. As observed in Table 11, the obtained recovery values were in the range between 94.4 % and 104.8 % with small RSDs, proving the high performance of the GO-COOH@Au-PtNPs based aptasensor for Ara H1 allergen detection in real samples. Moreover, calibration curves were plotted for all three real samples using the obtained I/I_0 (%), and their slope was compared with the one obtained in the affinity buffer. In all cases, the resulted slope was in the range of ±10 % from the slope obtained in the affinity buffer (− 0.352 ± 0.007 for chocolate cookies, − 0.352 ± 0.018 for the chocolate bar and − 0.397 ± 0.010 for the chocolate milk).

Table 11 *Real samples applications*

Sample	Spiked Ara H1 (nM)	Found Ara H1 (nM)	RSD (%) (*n≥3*)	Recovery (%)
Chocolate cookies	0	1.6	1.5	
	50	47.8	3.9	95.7
	100	100.1	8.4	100.1
	150	141.8	8.9	94.6
70% Cacao chocolate bar	0	1.8	14.4	
	50	50.1	2.4	100.2
	100	100.9	1.7	101
	150	141.6	1.3	94.4
Chocolate milk	0	1.8	0.4	
	50	52.4	5.5	104.8

	100	99.8	3.3	99.8

Even though peanut allergy is one of the major allergies and is life-threatening, only a very small number of aptasensors have been developed so far, the one proposed in this work being one of the first Ara H1 electrochemical aptasensor ever to be published. The analytical performances shown by our method are comparable with the ones obtained by the only recently published electrochemical aptasensor published lately (175), with a wider linear range and a higher number of real sample applications proved in this work. All in all, our developed method shows an improvement compared with the previous work and has the capacity for *in situ* determination of Ara H1 allergen from food samples.

3.4 Conclusions

In this study, we demonstrated the sensitivity and selectivity of a GO-COOH and MNPs-based platform towards the *in situ* detection of Ara H1 allergen in food products at disposable electrodes. Taking advantage of the high number of aptamers anchoring sites of the GO-COOH combined with the good electroconductivity and large surface area of Au-PtNPs, the aptasensor demonstrated enhanced performance towards aptamer – antigen interaction, quantified as an electrochemical aptasensor with a wide linear range of 0 – 150 nM and a LOD of 1.66 nM. Proteins found in high concentrations in milk and egg-based products have a little impact on the Ara H1 detection, showing very good specificity. The aptasensor was also effective in determining Ara H1 peanut allergen in spiked chocolate cookies, 70% cacao chocolate bar and chocolate milk samples with acceptable recovery rates and very good standard deviations, providing a promising alternative for the decentralised electrochemical detection of food allergens.

IV General conclusions

The aim of this thesis was to develop new electrochemical platforms suitable for medical and environmental targets analysis. Several detection strategies like direct detection or indirect detection using a bioreceptor were employed.

In the studies presented, the first important goal is the development and characterisation of different nanostructures modified platforms suitable for electrochemical detection. The second goal was to demonstrate their applicability in real samples analysis. For this, different analytes with a common characteristic: their impact over the human health were detected from complex matrixes.

The personal contribution added to this thesis was divided into three main chapters and a total of 6 studies. Since one of the main goals of the thesis was to develop platforms using nanomaterials as building blocks for electrochemical sensors, the type of materials used for electrode modification was chosen in order to divide the studies into chapters.

Therefore, in the first chapter, the synthesis of polymeric platforms was presented. Cone like shapes were obtained by the electropolymerisation of poly-pyrrole on the surface of a working electrode of a screen-printed carbon electrochemical cell. The polymerisation conditions and the additives from the monomer solutions were optimised before deciding on the most suitable platform. With analytical performances that allow the detection of FA in biological fluids (LR 2.5 – 200 μM and LOD of 0.8 μM), its applicability was demonstrated by detecting FA in human serum and commercially available tablets.

For the second chapter, two different platforms that combine de advantages of polymeric structures and noble metals nanostructures were developed. In a first study, gold and platinum nanostructures were electrodeposited on a screen-printed carbon electrode after a previous polymerisation of aniline. In this way, a structured platform was obtained, with a high electrical conductivity and good reproducibility. The platform was applied toward arsenic fingerprinting. A linear range of arsenic detection was obtained in the range 2.5 – 15 ppb with a very good selectivity in the presence of interfering metals.

On the second study presented in this chapter, poly-L-Lys was first electropolymerized on the working electrode of a screen-printed carbon electrochemical cell in order to decrease the variability of the carbon electrodes and then AuNSs were electrodeposited. In this case, not only the good catalytic effect of the

gold structures was taken into consideration but also its affinity toward Au-SH reaction that helped the immobilisation of a Lyz specific aptamer. After the interaction between the aptamer and Lyz, an enzymatic quantification of the analyte was performed with analytical performances that allowed the detection of Lyz in the range from 70 to $7*10^5$ pM and its quantification from three different wine types. The method was compared with a commercially available protein quantification assay and very similar results were obtained.

The last chapter focuses only on metallic structures and their applications in medical and environmental targets detection. The first study demonstrates the good electroconductivity of copper wires dopped with nickel foam and their selectivity toward Glu amperometric detection in the range of 6 µM to 1.63 mM. The sensor showed a good response towards Glu detection in serum.

The second and the third studies presented in the last chapter focus on the development of noble metals nanostructures used in aptamer immobilisation and their applicability towards aptasensing of TET in wastewater and Ara H1 allergen in milk and chocolate-based food products. In the case of AraH1 specific aptasensor, a linear range of 0 – 150 nM was obtained with a LOD of 1.66 nM, while the TET specific aptasensor detected the antibiotic in the 12.5 – 1000 nM range.

All the studies presented in this thesis proved the applications of different nanomaterials towards electrochemical sensing, with good selectivity, analytical performances and results in real samples.

V Originality of the thesis

This thesis originality consists in the study and development of novel approaches and methods for the design of several nanomaterials based electrochemical sensors suitable for the detection of a broad range of molecules. Sensitive platforms were obtained by the deposition of metallic particles, polymers or functionalised GO on the surface of different electrochemical cells.

In order to increase the general surface of the electrode and their electroconductivity, different nanostructures containing in situ synthesised nanostructures were synthesised. Polymers like poly-pyrrole, poly-L-Lys and PANI were used to enhance the conductivity and reproducibility of carbon-based surfaces. In all cases the polymerisation procedure was not just reproduced but adapted from other studies and improved in order to create new and better polymeric nanostructured surfaces compared with the ones already published. Moreover, the Poly-pyrrole surface was optimised in order to be able to selectively detect FA in biologic fluids and from pharmaceutical samples using a direct detection method suitable for in field analysis at a very low cost of production.

A novel aptasensor was developed for the detection of Lyz allergen in wine, this method being one of the few reported methods of wine contamination control. Novel AuNSs with very high conductivity were developed at the surface of SPCE. The aptasensor, developed on portable electrochemical cells, showed good result in different types of wine so therefore in different matrixes and it is a promising tool towards *in situ* wines analyses and less contaminated wine.

Another element of originality is represented by the development of a low cost, enzymeless sensor for Glu detection in serum, based on copper wired dopped with nickel foam. The sensor presents a linear range that allows the detection of normal Glu blood values but also hyper- and hypo-glycemia.

Novel AuNSs were developed by using polystyrene beads as shape controllers, obtaining nanovoids like shapes and a high electroactive area. The nanostructures were used for aptamer immobilization and the detection of tetracycline residues in waster waters, being one of the first ever aptasensor that can selectively detect TET in such low concentrations as the one found in water samples.

Even though the peanuts allergy is one of the major allergies with millions of people proned to develop, there are very few analytical methods able to detect the Ara H1 allergen fast, with a low cost and little or no sample pretreatment. In this thesis, a

novel material was developed based on the gold-platinum nanoparticles and GOs. The novel material benefits from the very good conductivity of AuNPs and PtNPs and the high number of aptamer anchoring sites of GOs. Its applicability was demonstrated by developing one of the very few electrochemical aptasensors able to detect low concentrations of Ara H1 allergen in chocolate, milk and cookies, without the need of complicated sample pretreatment or long waiting times.

All in all, the studies presented in this thesis will be an important asset for the future development of novel electrochemical sensors and analytical devices thanks to the multitude of novel nanomaterials and nanostructures that were obtained or to the improvement of the ones already published. The sensors and aptasensors obtained will bring the *in situ* detection of some analytes of medical importance one step closer to successful accomplishment.

BIBLIOGRAPHY

1. The A Venot DR, Toth K, Durst RA, Wilson GS, Avenot DRT, Buck RP, et al. INTERNATIONAL UNION OF PURE AND APPLIED CHEMISTRY PHYSICAL CHEMISTRY DIVISION, COMMISSION ON BIOPHYSICAL CHEMISTRY ANALYTICAL CHEMISTRY DIVISION, COMMISSION ON ELECTROANALYTICAL CHEMISTRY ELECTROCHEMICAL BIOSENSORS: RECOMMENDED DEFINITIONS AND CLASSIFICATION Prepared for publication by Electrochemical biosensors: Recommended defnitions and classification (Technical Report). Pure Appl Chem. 1999;71(12):2333–48.
2. Turner APF. Biosensors : Fundamentals and Applications. Biosensor adn Bioelectronics Centre [Internet]. 1987 [cited 2021 Nov 9];(January):40. Available from: http://urn.kb.se/resolve?urn=urn:nbn:se:liu:diva-92007
3. Fraden J. Handbook of Modern Sensors. Handbook of Modern Sensors. 2010;
4. Madhura TR, Devi KSS, Ramaraj R. Introduction to electrochemical sensors for the detection of toxic chemicals. Metal Oxides in Nanocomposite-Based Electrochemical Sensors for Toxic Chemicals. 2021 Jan 1;1–18.
5. Simões FR, Xavier MG. Electrochemical Sensors. Nanoscience and its Applications. 2017 Jan 1;155–78.
6. Ensafi AA. An introduction to sensors and biosensors. Electrochemical Biosensors. 2019 Jan 1;1–10.
7. Thévenot DR, Toth K, Durst RA, Wilson GS. Electrochemical biosensors: recommended definitions and classification. Biosensors and Bioelectronics. 2001 Jan 1;16(1–2):121–31.
8. Villalonga A, Sánchez A, Mayol B, Reviejo J, Villalonga R. Electrochemical biosensors for food bioprocess monitoring. Current Opinion in Food Science. 2022 Feb 1;43:18–26.
9. Song Y, Xu M, Li Z, He L, Hu M, He L, et al. Ultrasensitive detection of bisphenol A under diverse environments with an electrochemical aptasensor based on multicomponent AgMo heteronanostructure. Sensors and Actuators B: Chemical. 2020 Oct 15;321:128527.
10. Karunakaran R, Keskin M. Biosensors: components, mechanisms, and applications. Analytical Techniques in Biosciences. 2022 Jan 1;179–90.
11. Huang X, Zhu Y, Kianfar E. Nano Biosensors: Properties, applications and electrochemical techniques. Journal of Materials Research and Technology. 2021 May 1;12:1649–72.
12. Xie J, Wen D, Liang L, Jia Y, Gao L, Lei J. Evaluating the Validity of Current Mainstream Wearable Devices in Fitness Tracking Under Various Physical Activities: Comparative Study. JMIR Mhealth Uhealth 2018;6(4):e94 https://mhealth.jmir.org/2018/4/e94 [Internet]. 2018 Apr 12 [cited 2021 Nov 26];6(4):e9754. Available from: https://mhealth.jmir.org/2018/4/e94

13. Zuo C, Chen Q, Tian L, Waller L, Asundi A. Transport of intensity phase retrieval and computational imaging for partially coherent fields: The phase space perspective. Optics and Lasers in Engineering. 2015 Aug 1;71:20–32.

14. Gaffney EM, Lim K, Minteer SD. Breath biosensing: using electrochemical enzymatic sensors for detection of biomarkers in human breath. Current Opinion in Electrochemistry. 2020 Oct 1;23:26–30.

15. Xie Y, Liu T, Chu Z, Jin W. Recent advances in electrochemical enzymatic biosensors based on regular nanostructured materials. Journal of Electroanalytical Chemistry. 2021 Jul 15;893:115328.

16. Updike SJ, Hicks GP. The Enzyme Electrode. Nature 1967 214:5092 [Internet]. 1967 Jun 1 [cited 2021 Nov 26];214(5092):986–8. Available from: https://www.nature.com/articles/214986a0

17. Putzbach W, Ronkainen NJ. Immobilization Techniques in the Fabrication of Nanomaterial-Based Electrochemical Biosensors: A Review. Sensors 2013, Vol 13, Pages 4811-4840 [Internet]. 2013 Apr 11 [cited 2021 Dec 2];13(4):4811–40. Available from: https://www.mdpi.com/1424-8220/13/4/4811/htm

18. Revathi C, Rajendra Kumar RT. Enzymatic and Nonenzymatic Electrochemical Biosensors. Fundamentals and Sensing Applications of 2D Materials. 2019 Jan 1;259–300.

19. Hu H, Pan D, Xue H, Zhang M, Zhang Y, Shen Y. A photoelectrochemical immunoassay for tumor necrosis factor-α using a GO-PTCNH2 nanohybrid as a probe. Journal of Electroanalytical Chemistry. 2018 Sep 1;824:195–200.

20. Karimzadeh A, Hasanzadeh M, Shadjou N, Guardia M de la. Peptide based biosensors. TrAC Trends in Analytical Chemistry. 2018 Oct 1;107:1–20.

21. Lakshmanan A, Zhang S, Hauser CAE. Short self-assembling peptides as building blocks for modern nanodevices. Trends in Biotechnology. 2012 Mar 1;30(3):155–65.

22. Vanova V, Mitrevska K, Milosavljevic V, Hynek D, Richtera L, Adam V. Peptide-based electrochemical biosensors utilized for protein detection. Biosensors and Bioelectronics. 2021 May 15;180:113087.

23. Xu S, Ma W, Bai Y, Liu H. Ultrasensitive Ambient Mass Spectrometry Immunoassays: Multiplexed Detection of Proteins in Serum and on Cell Surfaces. J Am Chem Soc [Internet]. 2019 Jan 9 [cited 2021 Dec 2];141(1):72–5. Available from: https://pubs.acs.org/doi/full/10.1021/jacs.8b10853

24. Wink T, van Zuilen SJ, Bult A, van Bennekom WP. Self-assembled Monolayers for Biosensors. Analyst [Internet]. 1997 Jan 1 [cited 2021 Dec 2];122(4):43R-50R. Available from: https://pubs.rsc.org/en/content/articlelanding/1997/an/a606964i

25. Liu Q, Wang J, Boyd BJ. Peptide-based biosensors. Talanta. 2015 May 1;136:114–27.

26. Florea A, Melinte G, Simon I, Cristea C. Electrochemical Biosensors as Potential Diagnostic Devices for Autoimmune Diseases. Biosensors 2019, Vol 9, Page 38 [Internet]. 2019 Mar 4 [cited 2021 Dec 2];9(1):38. Available from: https://www.mdpi.com/2079-6374/9/1/38/htm

27. Takeuchi T, Sunayama H. Molecularly Imprinted Polymers. Encyclopedia of Polymeric Nanomaterials [Internet]. 2014 [cited 2021 Dec 3];1–5. Available from: https://link.springer.com/referenceworkentry/10.1007/978-3-642-36199-9_126-1

28. Mostafa AM, Barton SJ, Wren SP, Barker J. Review on molecularly imprinted polymers with a focus on their application to the analysis of protein biomarkers. TrAC Trends in Analytical Chemistry. 2021 Nov 1;144:116431.

29. Ahmed S, Shaikh N, Pathak N, Sonawane A, Pandey V, Maratkar S. An overview of sensitivity and selectivity of biosensors for environmental applications. Tools, Techniques and Protocols for Monitoring Environmental Contaminants. 2019 Jan 1;53–73.

30. Fang L, Liao X, Jia B, Shi L, Kang L, Zhou L, et al. Recent progress in immunosensors for pesticides. Biosensors and Bioelectronics. 2020 Sep 15;164:112255.

31. Jia M, Liao X, Fang L, Jia B, Liu M, Li D, et al. Recent advances on immunosensors for mycotoxins in foods and other commodities. TrAC Trends in Analytical Chemistry. 2021 Mar 1;136:116193.

32. Marco MP, Gee S, Hammock BD. Immunochemical techniques for environmental analysis I. Immunosensors. TrAC Trends in Analytical Chemistry. 1995 Aug 1;14(7):341–50.

33. Felix FS, Angnes L. Electrochemical immunosensors – A powerful tool for analytical applications. Biosensors and Bioelectronics. 2018 Apr 15;102:470–8.

34. Tertiş M, Melinte G, Ciui B, Şimon I, Ştiufiuc R, Săndulescu R, et al. A Novel Label Free Electrochemical Magnetoimmunosensor for Human Interleukin-6 Quantification in Serum. Electroanalysis [Internet]. 2019 Feb 1 [cited 2022 May 31];31(2):282–92. Available from: https://onlinelibrary.wiley.com/doi/full/10.1002/elan.201800620

35. Suri CR, Raje M, Varshney GC. Immunosensors for pesticide analysis: Antibody production and sensor development. Critical Reviews in Biotechnology. 2002;22(1):15–32.

36. Holford TRJ, Davis F, Higson SPJ. Recent trends in antibody based sensors. Biosensors and Bioelectronics. 2012 Apr 15;34(1):12–24.

37. Rebelo TSCR, Ribeiro JA, Sales MGF, Pereira CM. Electrochemical immunosensor for detection of CA 15-3 biomarker in point-of-care. Sens Biosensing Res. 2021 Aug 1;33:100445.

38. Ştefan G, Hosu O, de Wael K, Lobo-Castañón MJ, Cristea C. Aptamers in biomedicine: Selection strategies and recent advances. Electrochimica Acta. 2021 Apr 20;376:137994.

39. Hianik T. Aptamer-Based Biosensors. Encyclopedia of Interfacial Chemistry: Surface Science and Electrochemistry. 2018 Jan 1;11–9.

40. Bruno JG. A Review of Therapeutic Aptamer Conjugates with Emphasis on New Approaches. Pharmaceuticals 2013, Vol 6, Pages 340-357 [Internet]. 2013 Mar 19 [cited 2021 Dec 13];6(3):340–57. Available from: https://www.mdpi.com/1424-8247/6/3/340/htm

41. Hermann T, Patel DJ. Adaptive recognition by nucleic acid aptamers. Science (1979) [Internet]. 2000 Feb 4 [cited 2021 Dec 13];287(5454):820–5. Available from: https://www.science.org/doi/abs/10.1126/science.287.5454.820

42. Patel DJ, Suri AK. Structure, recognition and discrimination in RNA aptamer complexes with cofactors, amino acids, drugs and aminoglycoside antibiotics. Reviews in Molecular Biotechnology. 2000 Mar 1;74(1):39–60.

43. Melinte G, Selvolini G, Cristea C, Marrazza G. Aptasensors for lysozyme detection: Recent advances. Talanta. 2021 May 1;226:122169.

44. Girolamo A de, McKeague M, Pascale M, Cortese M, DeRosa MC. Immobilization of Aptamers on Substrates. Aptamers for Analytical Applications [Internet]. 2018 Oct 26 [cited 2021 Dec 22];85–126. Available from: https://onlinelibrary.wiley.com/doi/full/10.1002/9783527806799.ch3

45. Lai Q, Chen W, Zhang Y, Liu Z. Application strategies of peptide nucleic acids toward electrochemical nucleic acid sensors. Analyst [Internet]. 2021 Sep 27 [cited 2021 Dec 22];146(19):5822–35. Available from: https://pubs.rsc.org/en/content/articlehtml/2021/an/d1an00765c

46. Kurup CP, Tlili C, Nurul S, Zakaria A, Ahmed MU. Recent Trends in Design and Development of Nanomaterial-based Aptasensors. 2021 [cited 2021 Dec 22];11(6):14057–77. Available from: https://biointerfaceresearch.com/

47. Blidar A, Hosu O, Feier B, Ştefan G, Bogdan D, Cristea C. Gold-based nanostructured platforms for oxytetracycline detection from milk by a "signal-on" aptasensing approach. Food Chemistry. 2022 Mar 1;371:131127.

48. Kumar S, Kalkal A. Electrochemical detection: Cyclic voltammetry/differential pulse voltammetry/impedance spectroscopy. Nanotechnology in Cancer Management. 2021 Jan 1;43–71.

49. Rusling JF, Kumosinski TF. Voltammetric Methods. Nonlinear Computer Modeling of Chemical and Biochemical Data. 1996 Jan 1;177–205.

50. PLETCHER D, GREFF R, PEAT R, PETER LM, ROBINSON J. Potential sweep techniques and cyclic voltammetry. Instrumental Methods in Electrochemistry. 2010 Jan 1;178–228.

51. Manivel P, Dhakshnamoorthy M, Balamurugan A, Ponpandian N, Mangalaraj D, Viswanathan C. Conducting polyaniline-graphene oxide fibrous nanocomposites: preparation, characterization and simultaneous electrochemical detection of ascorbic acid, dopamine and uric acid. RSC Advances [Internet]. 2013 Aug 5 [cited 2022 Jan 21];3(34):14428–37. Available from: https://pubs.rsc.org/en/content/articlehtml/2013/ra/c3ra42322k

52. Venton BJ, DiScenza DJ. Voltammetry. Electrochemistry for Bioanalysis [Internet]. 2020 Jan 1 [cited 2022 Jan 21];27–50. Available from: https://linkinghub.elsevier.com/retrieve/pii/B978012821203500004X

53. Núñez-Bajo E, Fernández Abedul MT. Chronoamperometric determination of ascorbic acid on paper-based devices. Laboratory Methods in Dynamic Electroanalysis. 2020 Jan 1;75–83.

54. Wang J, Zeng H. Recent advances in electrochemical techniques for characterizing surface properties of minerals. Advances in Colloid and Interface Science. 2021 Feb 1;288:102346.

55. Patel BA. Amperometry and potential step techniques. Electrochemistry for Bioanalysis. 2020 Jan 1;9–26.

56. Amatore C, Arbault S, Bouton C, Coffi K, Drapier JC, Ghandour H, et al. Monitoring in Real Time with a Microelectrode the Release of Reactive Oxygen and Nitrogen Species by a Single Macrophage Stimulated by its Membrane Mechanical Depolarization. ChemBioChem [Internet]. 2006 Apr 3 [cited 2022 Jan 21];7(4):653–61. Available from: https://onlinelibrary.wiley.com/doi/full/10.1002/cbic.200500359

57. Current Trends in Electrolytes. Electrochemical Society Interface. 2019 Jan 1;28(2):47.

58. Sacco A. Electrochemical impedance spectroscopy: Fundamentals and application in dye-sensitized solar cells. Renewable and Sustainable Energy Reviews. 2017 Nov 1;79:814–29.

59. Bigdeli IK, Yeganeh M, Shoushtari MT, Zadeh MK. Electrochemical impedance spectroscopy (EIS) for biosensing. Nanosensors for Smart Manufacturing. 2021 Jan 1;533–54.

60. Ananda Murthy HC, Wagassa AN, Ravikumar CR, Nagaswarupa HP. Functionalized metal and metal oxide nanomaterial-based electrochemical sensors. Functionalized Nanomaterial-Based Electrochemical Sensors. 2022 Jan 1;369–92.

61. Ernst H, Knoll M. Electrochemical characterisation of uric acid and ascorbic acid at a platinum electrode. Analytica Chimica Acta. 2001 Dec 10;449(1–2):129–34.

62. Kamal Eddin FB, Wing Fen Y. Recent Advances in Electrochemical and Optical Sensing of Dopamine. Sensors (Basel) [Internet]. 2020 Feb 14 [cited 2022 Feb 7];20(4). Available from: /pmc/articles/PMC7071053/

63. Sajid M, Nazal MK, Mansha M, Alsharaa A, Jillani SMS, Basheer C. Chemically modified electrodes for electrochemical detection of dopamine in the presence of uric acid and ascorbic acid: A review. TrAC Trends in Analytical Chemistry. 2016 Feb 1;76:15–29.

64. Song J, Xu L, Xing R, Li Q, Zhou C, Liu D, et al. Synthesis of Au/Graphene Oxide Composites for Selective and Sensitive Electrochemical Detection of Ascorbic Acid. Scientific Reports 2014 4:1 [Internet]. 2014 Dec 17 [cited 2022 Feb 7];4(1):1–7. Available from: https://www.nature.com/articles/srep07515

65. Du J, Yue R, Yao Z, Jiang F, Du Y, Yang P, et al. Nonenzymatic uric acid electrochemical sensor based on graphene-modified carbon fiber electrode. Colloids and Surfaces A: Physicochemical and Engineering Aspects. 2013 Feb 20;419:94–9.

66. Yang C, Trikantzopoulos E, Nguyen MD, Jacobs CB, Wang Y, Mahjouri-Samani M, et al. Laser Treated Carbon Nanotube Yarn Microelectrodes for Rapid and Sensitive Detection of Dopamine in Vivo. ACS Sensors [Internet]. 2016 May 27 [cited 2022 Feb 7];1(5):508–15. Available from: https://pubs.acs.org/doi/full/10.1021/acssensors.6b00021

67. Wu Y, Deng P, Tian Y, Feng J, Xiao J, Li J, et al. Simultaneous and sensitive determination of ascorbic acid, dopamine and uric acid via an electrochemical sensor based on PVP-graphene composite. Journal of Nanobiotechnology [Internet]. 2020 Aug 10 [cited 2022 Feb 7];18(1):1–13. Available from: https://jnanobiotechnology.biomedcentral.com/articles/10.1186/s12951-020-00672-9

68. Díaz-Fernández A, Lorenzo-Gómez R, Miranda-Castro R, de-los-Santos-Álvarez N, Lobo-Castañón MJ. Electrochemical aptasensors for cancer diagnosis in biological fluids – A review. Analytica Chimica Acta. 2020 Aug 8;1124:1–19.

69. Reta N, Saint CP, Michelmore A, Prieto-Simon B, Voelcker NH. Nanostructured Electrochemical Biosensors for Label-Free Detection of Water- and Food-Borne Pathogens. ACS Applied Materials and Interfaces [Internet]. 2018 Feb 21 [cited 2022 Feb 7];10(7):6055–72. Available from: https://pubs.acs.org/doi/full/10.1021/acsami.7b13943

70. Hai X, Li Y, Zhu C, Song W, Cao J, Bi S. DNA-based label-free electrochemical biosensors: From principles to applications. TrAC Trends in Analytical Chemistry. 2020 Dec 1;133:116098.

71. Malvano F, Pilloton R, Albanese D. Label-free impedimetric biosensors for the control of food safety – a review. https://doi.org/101080/030673192019166709 6 [Internet]. 2019 Mar 15 [cited 2022 Feb 7];100(4):468–91. Available from: https://www.tandfonline.com/doi/abs/10.1080/03067319.2019.1667096

72. Zaccari I, Davies AG, Walti C, Laurenson SX. Label-free electrochemical biosensors for clinical diagnostic. Proceedings of the 7th Cairo International Biomedical Engineering Conference, CIBEC 2014. 2015 Jan 23;15–8.

73. Zhang J, Oueslati R, Cheng C, Zhao L, Chen J, Almeida R, et al. Rapid, highly sensitive detection of Gram-negative bacteria with lipopolysaccharide based disposable aptasensor. Biosensors and Bioelectronics. 2018 Jul 30;112:48–53.

74. Waller DF, Hew BE, Holdaway C, Jen M, Peckham GD. Rapid Detection of Bacillus anthracis Spores Using Immunomagnetic Separation and Amperometry. Biosensors 2016, Vol 6, Page 61 [Internet]. 2016 Dec 20 [cited 2022 Feb 7];6(4):61. Available from: https://www.mdpi.com/2079-6374/6/4/61/htm

75. Tertis M, Leva PI, Bogdan D, Suciu M, Graur F, Cristea C. Impedimetric aptasensor for the label-free and selective detection of Interleukin-6 for colorectal cancer screening. Biosensors and Bioelectronics. 2019 Jul 15;137:123–32.

76. Manzano M, Viezzi S, Mazerat S, Marks RS, Vidic J. Rapid and label-free electrochemical DNA biosensor for detecting hepatitis A virus. Biosensors and Bioelectronics. 2018 Feb 15;100:89–95.

77. Ma C, Liu H, Zhang L, Li H, Yan M, Song X, et al. Multiplexed aptasensor for simultaneous detection of carcinoembryonic antigen and mucin-1 based on metal ion electrochemical labels and Ru(NH3)63+ electronic wires. Biosensors and Bioelectronics. 2018 Jan 15;99:8–13.

78. Sattarahmady N, Rahi A, Heli H. A signal-on built in-marker electrochemical aptasensor for human prostate-specific antigen based on a hairbrush-like gold nanostructure. Scientific

Reports 2017 7:1 [Internet]. 2017 Sep 11 [cited 2022 Feb 7];7(1):1–8. Available from: https://www.nature.com/articles/s41598-017-11680-5

79. Wei B, Mao K, Liu N, Zhang M, Yang Z. Graphene nanocomposites modified electrochemical aptamer sensor for rapid and highly sensitive detection of prostate specific antigen. Biosensors and Bioelectronics. 2018 Dec 15;121:41–6.

80. Wen W, Huang JY, Bao T, Zhou J, Xia HX, Zhang XH, et al. Increased electrocatalyzed performance through hairpin oligonucleotide aptamer-functionalized gold nanorods labels and graphene-streptavidin nanomatrix: Highly selective and sensitive electrochemical biosensor of carcinoembryonic antigen. Biosensors and Bioelectronics. 2016 Sep 15;83:142–8.

81. Wang Y, Luo J, Liu J, Sun S, Xiong Y, Ma Y, et al. Label-free microfluidic paper-based electrochemical aptasensor for ultrasensitive and simultaneous multiplexed detection of cancer biomarkers. Biosensors and Bioelectronics. 2019 Jul 1;136:84–90.

82. Díaz-Fernández A, Lorenzo-Gómez R, Miranda-Castro R, de-los-Santos-Álvarez N, Lobo-Castañón MJ. Electrochemical aptasensors for cancer diagnosis in biological fluids – A review. Analytica Chimica Acta. 2020 Aug 8;1124:1–19.

83. Sun L, Chen Y, Chen F, Ma F. Peptide-based electrochemical biosensor for matrix metalloproteinase-14 and protein-overexpressing cancer cells based on analyte-induced cleavage of peptide. Microchemical Journal. 2020 Sep 1;157:105103.

84. Cardoso RM, Pereira TS, Facure MHM, dos Santos DM, Mercante LA, Mattoso LHC, et al. Current progress in plant pathogen detection enabled by nanomaterials-based (bio)sensors. Sensors and Actuators Reports. 2022 Nov 1;4:100068.

85. Xiao Y, Lai RY, Plaxco KW. Preparation of electrode-immobilized, redox-modified oligonucleotides for electrochemical DNA and aptamer-based sensing. Nat Protoc [Internet]. 2007 [cited 2022 Feb 8];2(11):2875–80. Available from: https://pubmed.ncbi.nlm.nih.gov/18007622/

86. Schoukroun-Barnes LR, Macazo FC, Gutierrez B, Lottermoser J, Liu J, White RJ. Reagentless, Structure-Switching, Electrochemical Aptamer-Based Sensors. http://dx.doi.org/101146/annurev-anchem-071015-041446 [Internet]. 2016 Jun 15 [cited 2022 Feb 8];9:163–81. Available from: https://www.annualreviews.org/doi/abs/10.1146/annurev-anchem-071015-041446

87. Villalonga A, Pérez-Calabuig AM, Villalonga R. Electrochemical biosensors based on nucleic acid aptamers. Analytical and Bioanalytical Chemistry [Internet]. 2020 Jan 1 [cited 2022 Feb 8];412(1):55–72. Available from: https://link.springer.com/article/10.1007/s00216-019-02226-x

88. Pividori MI, Merkoçi A, Alegret S. Electrochemical genosensor design: immobilisation of oligonucleotides onto transducer surfaces and detection methods. Biosensors and Bioelectronics. 2000 Aug 1;15(5–6):291–303.

89. Vanova V, Mitrevska K, Milosavljevic V, Hynek D, Richtera L, Adam V. Peptide-based electrochemical biosensors utilized for protein detection. Biosensors and Bioelectronics. 2021 May 15;180:113087.

90. Melinte G, Hosu O, Ştefan G, Bogdan D, Cristea C, Marrazza G. Poly-L-Lysine@gold nanostructured hybrid platform for Lysozyme aptamer sandwich-based detection. Electrochimica Acta [Internet]. 2022 Jan 20 [cited 2022 Jan 27];403:139718. Available from: https://linkinghub.elsevier.com/retrieve/pii/S0013468621020028

91. Selvolini G, Lettieri M, Tassoni L, Gastaldello S, Grillo M, Maran C, et al. Electrochemical enzyme-linked oligonucleotide array for aflatoxin B1 detection. Talanta. 2019 Oct 1;203:49–57.

92. Gao S, Zheng X, Hu B, Sun M, Wu J, Jiao B, et al. Enzyme-linked, aptamer-based, competitive biolayer interferometry biosensor for palytoxin. Biosensors and Bioelectronics. 2017 Mar 15;89:952–8.

93. Tian J, Liang Z, Hu O, He Q, Sun D, Chen Z. An electrochemical dual-aptamer biosensor based on metal-organic frameworks MIL-53 decorated with Au@Pt nanoparticles and enzymes for detection of COVID-19 nucleocapsid protein. Electrochimica Acta. 2021 Aug 10;387:138553.

94. Lim MC, Kim YR. Analytical Applications of Nanomaterials in Monitoring Biological and Chemical Contaminants in Food. J Microbiol Biotechnol [Internet]. 2016 Sep 28 [cited 2021 Dec 9];26(9):1505–16. Available from: https://www.jmb.or.kr/journal/view.html?doi=10.4014/jmb.1605.05071

95. Zhang N, Li J, Liu B, Zhang D, Zhang C, Guo Y, et al. Signal enhancing strategies in aptasensors for the detection of small molecular contaminants by nanomaterials and nucleic acid amplification. Talanta. 2022 Jan 1;236:122866.

96. Ramalingam S, Collier CM, Singh A. A Paper-Based Colorimetric Aptasensor for the Detection of Gentamicin. Biosensors 2021, Vol 11, Page 29 [Internet]. 2021 Jan 21 [cited 2021 Dec 9];11(2):29. Available from: https://www.mdpi.com/2079-6374/11/2/29/htm

97. Liu LB, Ye J. Ren-de agency in international faculty professional development: a China case study of glocal identity integration. https://doi.org/101080/1366453020191611628 [Internet]. 2019 Aug 8 [cited 2021 Dec 9];23(4):447–68. Available from: https://www.tandfonline.com/doi/abs/10.1080/13664530.2019.1611628

98. Gu M, Liu J, Li D, Wang M, Chi K, Zhang X, et al. Development of Ochratoxin Aptasensor Based on DNA Metal Nanoclusters. Nanoscience and Nanotechnology Letters. 2019 Sep 18;11(8):1139–44.

99. Jin H, Sun Y, Sun Z, Yang M, Gui R. Zero-dimensional sulfur nanomaterials: Synthesis, modifications and applications. Coordination Chemistry Reviews. 2021 Jul 1;438:213913.

100. Fan L, Zhang C, Liang G, Yan W, Guo Y, Bi Y, et al. Highly sensitive photoelectrochemical aptasensor based on MoS2 quantum dots/TiO2 nanotubes for detection of atrazine. Sensors and Actuators B: Chemical. 2021 May 1;334:129652.

101. Geng H, Chen X, Sun L, Qiao Y, Song J, Shi S, et al. ZnCuInSe/Au/TiO2 sandwich nanowires-based photoelectrochemical biosensor for ultrasensitive detection of kanamycin. Analytica Chimica Acta. 2021 Feb 15;1146:166–73.

102. He D, Wu Z, Cui B, Xu E. Aptamer and gold nanorod–based fumonisin B1 assay using both fluorometry and SERS. Microchimica Acta [Internet]. 2020 Apr 1 [cited 2021 Dec

9];187(4):1–8. Available from: https://link.springer.com/article/10.1007/s00604-020-4192-0

103. Jiang YY, Zhao X, Chen LJ, Yang C, Yin XB, Yan XP. Persistent luminescence nanorod based luminescence resonance energy transfer aptasensor for autofluorescence-free detection of mycotoxin. Talanta. 2020 Oct 1;218:121101.

104. Kou J, Nguyen EP, Merkoçi A, Guo Z. 2-dimensional materials-based electrical/optical platforms for smart on-off diagnostics applications. 2D Materials [Internet]. 2020 Jun 10 [cited 2021 Dec 9];7(3):032001. Available from: https://iopscience.iop.org/article/10.1088/2053-1583/ab896a

105. Sinha S, Kim H, Robertson AW. Preparation and application of 0D-2D nanomaterial hybrid heterostructures for energy applications. Materials Today Advances. 2021 Dec 1;12:100169.

106. Nodehi M, Baghayeri M, Behazin R, Veisi H. Electrochemical aptasensor of bisphenol A constructed based on 3D mesoporous structural SBA-15-Met with a thin layer of gold nanoparticles. Microchemical Journal. 2021 Mar 1;162:105825.

107. Mekonnen MM, Hoekstra AY. Sustainability: Four billion people facing severe water scarcity. Science Advances [Internet]. 2016 Feb 1 [cited 2022 Jan 27];2(2). Available from: https://www.science.org/doi/abs/10.1126/sciadv.1500323

108. Gopalan AI, Lee KP, Manesh KM, Santhosh P, Kim JH, Kang JS. Electrochemical determination of dopamine and ascorbic acid at a novel gold nanoparticles distributed poly(4-aminothiophenol) modified electrode. Talanta. 2007 Mar 15;71(4):1774–81.

109. Picciani PHS, Shimizu FM, Olimpio QG, Michel RC. Sensing Materials: Organic Polymers. Reference Module in Biomedical Sciences. 2021 Jan 1;

110. Grzeszczuk M. Polymer Electrodes: Preparation, Properties, and Applications. Encyclopedia of Interfacial Chemistry: Surface Science and Electrochemistry. 2018 Jan 1;838–48.

111. Stejskal J, Cz SC. Interaction of conducting polymers, polyaniline and polypyrrole, with organic dyes: polymer morphology control, dye adsorption and photocatalytic decomposition. Chemical Papers 2019 74:1 [Internet]. 2019 Nov 16 [cited 2022 Jan 27];74(1):1–54. Available from: https://link.springer.com/article/10.1007/s11696-019-00982-9

112. Zarrintaj P, Khalili R, Vahabi H, Saeb MR, Ganjali MR, Mozafari M. Polyaniline/metal oxides nanocomposites. Fundamentals and Emerging Applications of Polyaniline. 2019 Jan 1;131–41.

113. Taghizadeh A, Taghizadeh M, Jouyandeh M, Yazdi MK, Zarrintaj P, Saeb MR, et al. Conductive polymers in water treatment: A review. Journal of Molecular Liquids. 2020 Aug 15;312:113447.

114. Xie Y, Account P. Electrochemical Performance of Transition Metal-Coordinated Polypyrrole: A Mini Review. The Chemical Record [Internet]. 2019 Dec 1 [cited 2022 Jan

27];19(12):2370–84. Available from: https://onlinelibrary.wiley.com/doi/full/10.1002/tcr.201800192

115. Amor-Gutiérrez O, Giulia SM, Fernández-Abedul T, de La A, Muñiz E, Marrazza G. Folding-Based Electrochemical Aptasensor for the Determination of β-Lactoglobulin on Poly-L-Lysine Modified Graphite Electrodes. Sensors 2020, Vol 20, Page 2349 [Internet]. 2020 Apr 20 [cited 2022 Jan 27];20(8):2349. Available from: https://www.mdpi.com/1424-8220/20/8/2349/htm

116. Yang L, Liu S, Zhang Q, Li F. Simultaneous electrochemical determination of dopamine and ascorbic acid using AuNPs@polyaniline core–shell nanocomposites modified electrode. Talanta. 2012 Jan 30;89:136–41.

117. Daniel MC, Astruc D. Gold Nanoparticles: Assembly, Supramolecular Chemistry, Quantum-Size-Related Properties, and Applications toward Biology, Catalysis, and Nanotechnology. 2004 [cited 2022 Jan 28]; Available from: https://pubs.acs.org/sharingguidelines

118. Aralekallu S, Sannegowda LK. Metal nanoparticles for electrochemical sensing applications. Handbook of Nanomaterials for Sensing Applications. 2021 Jan 1;589–629.

119. Brown KR, Walter DG, Natan MJ. Seeding of Colloidal Au Nanoparticle Solutions. 2. Improved Control of Particle Size and Shape. 2000 [cited 2022 Jan 28]; Available from: https://pubs.acs.org/sharingguidelines

120. Blidar A, Hosu O, Feier B, Ştefan G, Bogdan D, Cristea C. Gold-based nanostructured platforms for oxytetracycline detection from milk by a "signal-on" aptasensing approach. Food Chemistry. 2022 Mar 1;371:131127.

121. Negahdary M. Electrochemical aptasensors based on the gold nanostructures. Talanta. 2020 Aug 15;216:120999.

122. Madianos L, Tsekenis G, Skotadis E, Patsiouras L, Tsoukalas D. A highly sensitive impedimetric aptasensor for the selective detection of acetamiprid and atrazine based on microwires formed by platinum nanoparticles. Biosensors and Bioelectronics. 2018 Mar 15;101:268–74.

123. Liu Y, Xu Q, Zhang Y, Ren B, Huang L, Cai H, et al. An electrochemical aptasensor based on AuPt alloy nanoparticles for ultrasensitive detection of amyloid-β oligomers. Talanta. 2021 Aug 15;231.

124. Gupta J, Arya S, Verma S, Singh A, Sharma A, Singh B, et al. Performance of template-assisted electrodeposited Copper/Cobalt bilayered nanowires as an efficient glucose and Uric acid senor. Materials Chemistry and Physics. 2019 Dec 1;238:121969.

125. Valentina Mihai G, Rosoiu S, Costovici S, Anicai L, Mihai G, Roşoiu S, et al. SYNTHESIS OF COPPER NANOWIRES USING AQUEOUS AND IONIC LIQUID ELECTROLYTES FOR ELECTROCHEMICAL DETECTION. Bull, Series B [Internet]. 2019 [cited 2022 Jan 28];81(2). Available from: https://www.researchgate.net/publication/335033637

126. Eugénio S, Silva TM, Carmezim MJ, Duarte RG, Montemor MF. Electrodeposition and characterization of nickel-copper metallic foams for application as electrodes for supercapacitors. Journal of Applied Electrochemistry [Internet]. 2014 Apr 1 [cited 2022 Jan 31];44(4):455–65. Available from: https://link.springer.com/article/10.1007/s10800-013-0646-y

127. Tappan BC, Steiner Iii SA, Luther EP, Tappan BC, Iii SAS, Luther EP. Nanoporous Metal Foams. Angewandte Chemie International Edition [Internet]. 2010 Jun 21 [cited 2022 Jan 31];49(27):4544–65. Available from: https://onlinelibrary.wiley.com/doi/full/10.1002/anie.200902994

128. Gao Z, Chen L, Chang J, Wang Z, Wu D, Xu F, et al. Bare Ni foam electrode-ferricyanides redox electrolyte system with high capacitive performance. International Journal of Hydrogen Energy. 2019 Apr 23;44(21):10554–60.

129. Golgovici F, Pumnea A, Petica A, Manea AC, Brincoveanu O, Enachescu M, et al. Ni–Mo alloy nanostructures as cathodic materials for hydrogen evolution reaction during seawater electrolysis. Chemical Papers [Internet]. 2018 Aug 1 [cited 2022 Jan 31];72(8):1889–903. Available from: https://link.springer.com/article/10.1007/s11696-018-0486-7

130. Guo MM, Wang PS, Zhou CH, Xia Y, Huang W, Li Z. An ultrasensitive non-enzymatic amperometric glucose sensor based on a Cu-coated nanoporous gold film involving co-mediating. Sensors and Actuators B: Chemical. 2014 Nov 1;203:388–95.

131. Smart A, Crew A, Pemberton R, Hughes G, Doran O, Hart JP. Screen-printed carbon based biosensors and their applications in agri-food safety. TrAC Trends in Analytical Chemistry. 2020 Jun 1;127:115898.

132. Kanagavalli P, Andrew C, Veerapandian M, Jayakumar M. In-situ redox-active hybrid graphene platform for label-free electrochemical biosensor: Insights from electrodeposition and electroless deposition. TrAC Trends in Analytical Chemistry. 2021 Oct 1;143:116413.

133. Lawal AT. Synthesis and utilization of carbon nanotubes for fabrication of electrochemical biosensors. Materials Research Bulletin. 2016 Jan 1;73:308–50.

134. Beluomini MA, da Silva JL, de Sá AC, Buffon E, Pereira TC, Stradiotto NR. Electrochemical sensors based on molecularly imprinted polymer on nanostructured carbon materials: A review. Journal of Electroanalytical Chemistry. 2019 May 1;840:343–66.

135. Zeng Y, Zhou Y, Kong L, Zhou T, Shi G. A novel composite of SiO2-coated graphene oxide and molecularly imprinted polymers for electrochemical sensing dopamine. Biosensors and Bioelectronics. 2013 Jul 15;45(1):25–33.

136. Rivas GA, Rodríguez MC, Rubianes MD, Gutierrez FA, Eguílaz M, Dalmasso PR, et al. Carbon nanotubes-based electrochemical (bio)sensors for biomarkers. Applied Materials Today. 2017 Dec 1;9:566–88.

137. Chaudhuri A, Chaudhuri A, Joydhar A. Graphene nanocomposites and applications in electrochemical energy storage materials. Materials Today: Proceedings. 2022 Feb 25;

138. Xu J, Wang Y, Hu S. Nanocomposites of graphene and graphene oxides: Synthesis, molecular functionalization and application in electrochemical sensors and biosensors. A review. Microchimica Acta 2016 184:1 [Internet]. 2016 Nov 12 [cited 2022 Jan 31];184(1):1–44. Available from: https://link.springer.com/article/10.1007/s00604-016-2007-0

139. Dreyer DR, Todd AD, Bielawski CW. Harnessing the chemistry of graphene oxide. Chemical Society Reviews [Internet]. 2014 Jul 7 [cited 2022 Jan 31];43(15):5288–301. Available from: https://pubs.rsc.org/en/content/articlehtml/2014/cs/c4cs00060a

140. Guo S, Wen D, Zhai Y, Dong S, Wang E. Platinum nanoparticle ensemble-on-graphene hybrid nanosheet: One-pot, rapid synthesis, and used as new electrode material for electrochemical sensing. ACS Nano [Internet]. 2010 Jul 27 [cited 2022 Jan 31];4(7):3959–68. Available from: https://pubs.acs.org/doi/full/10.1021/nn100852h

141. Luo JH, Li BL, Li NB, Luo HQ. Sensitive detection of gallic acid based on polyethyleneimine-functionalized graphene modified glassy carbon electrode. Sensors and Actuators B: Chemical. 2013 Sep 1;186:84–9.

142. Cinti S, Politi S, Moscone D, Palleschi G, Arduini F. Stripping Analysis of As(III) by Means of Screen-Printed Electrodes Modified with Gold Nanoparticles and Carbon Black Nanocomposite. Electroanalysis [Internet]. 2014 May 1 [cited 2022 Feb 3];26(5):931–9. Available from: https://onlinelibrary.wiley.com/doi/full/10.1002/elan.201400041

143. Das N, Sengupta S. Arsenicosis: diagnosis and treatment. Indian J Dermatol Venereol Leprol [Internet]. 2008 Nov 1 [cited 2022 Feb 3];74(6):571–81. Available from: https://pubmed.ncbi.nlm.nih.gov/19171979/

144. Yogarajah N, Tsai SSH. Detection of trace arsenic in drinking water: challenges and opportunities for microfluidics. Environmental Science: Water Research & Technology [Internet]. 2015 Jul 8 [cited 2022 Feb 3];1(4):426–47. Available from: https://pubs.rsc.org/en/content/articlehtml/2015/ew/c5ew00099h

145. National Research Council (U.S.). Subcommittee on Arsenic in Drinking Water. Arsenic in drinking water. 1999;310.

146. Argos M, Kalra T, Rathouz PJ, Chen Y, Pierce B, Parvez F, et al. Arsenic exposure from drinking water, and all-cause and chronic-disease mortalities in Bangladesh (HEALS): a prospective cohort study. The Lancet. 2010 Jul 24;376(9737):252–8.

147. Barbieri M, Nigro A, Sappa G. Arsenic contamination in groundwater system of Viterbo area (Central Italy). Senses and Sciences [Internet]. 2014 Sep 30 [cited 2022 Feb 3];1(3):101–6. Available from: https://sensesandsciences.com/index.php/Senses/article/view/39

148. Reghunath R, devi K, Singh KK. Recent advances in graphene based electrochemical glucose sensor. Nano-Structures & Nano-Objects. 2021 Apr 1;26:100750.

149. Wu T, Rayner CK, Jones KL, Xie C, Marathe C, Horowitz M. Role of intestinal glucose absorption in glucose tolerance. Current Opinion in Pharmacology. 2020 Dec 1;55:116–24.

150. Steiner MS, Duerkop A, Wolfbeis OS. Optical methods for sensing glucose. Chemical Society Reviews [Internet]. 2011 Aug 15 [cited 2022 Feb 4];40(9):4805–39. Available from: https://pubs.rsc.org/en/content/articlehtml/2011/cs/c1cs15063d

151. Pfützner A, Caduff A, Larbig M, Schrepfer T, Forst T. Impact of posture and fixation technique on impedance spectroscopy used for continuous and noninvasive glucose monitoring. Diabetes Technology and Therapeutics. 2004 Aug;6(4):435–41.

152. Adeel M, Rahman MM, Caligiuri I, Canzonieri V, Rizzolio F, Daniele S. Recent advances of electrochemical and optical enzyme-free glucose sensors operating at physiological conditions. Biosensors and Bioelectronics. 2020 Oct 1;165:112331.

153. Dong Q, Ryu H, Lei Y. Metal oxide based non-enzymatic electrochemical sensors for glucose detection. Electrochimica Acta. 2021 Feb 20;370:137744.

154. Pitkin RM. Folate and neural tube defects. The American Journal of Clinical Nutrition [Internet]. 2007 Jan 1 [cited 2022 Feb 4];85(1):285S-288S. Available from: https://academic.oup.com/ajcn/article/85/1/285S/4649476

155. Argyridis S. Folic acid in pregnancy. Obstetrics, Gynaecology & Reproductive Medicine. 2019 Apr 1;29(4):118–20.

156. Mida LA, della Zazzera V, Fontaine-Bisson B. Knowledge, attitude and practice of physicians regarding periconceptional folic acid for women at low risk of a neural tube defect affected pregnancy. Preventive Medicine Reports. 2021 Jun 1;22:101327.

157. De-Regil LM, Peña-Rosas JP, Fernández-Gaxiola AC, Rayco-Solon P. Effects and safety of periconceptional oral folate supplementation for preventing birth defects. Cochrane Database of Systematic Reviews. 2015 Dec 14;2015(12).

158. WHO | Periconceptional folic acid supplementation to prevent neural tube defects [Internet]. [cited 2022 Feb 4]. Available from: https://www.who.int/elena/titles/folate_periconceptional/en/

159. Cherlet M, Schelkens M, Croubels S, De Backer P. Quantitative multi-residue analysis of tetracyclines and their 4-epimers in pig tissues by high-performance liquid chromatography combined with positive-ion electrospray ionization mass spectrometry. Analytica Chimica Acta. 2003;492(1–2):199–213.

160. Zhan X, Hu G, Wagberg T, Zhan S, Xu H, Zhou P. Electrochemical aptasensor for tetracycline using a screen-printed carbon electrode modified with an alginate film containing reduced graphene oxide and magnetite (Fe3O4) nanoparticles. Microchimica Acta. 2016;183(2):723–9.

161. Kesavan S, Kumar DR, Lee YR, Shim JJ. Determination of tetracycline in the presence of major interference in human urine samples using polymelamine/electrochemically reduced graphene oxide modified electrode. Sensors and Actuators, B: Chemical. 2017;241:455–65.

162. Qian J, Xing C, Ge Y, Li R, Li A, Yan W. Gold nanostars-enhanced Raman fingerprint strip for rapid detection of trace tetracycline in water samples. Spectrochimica Acta - Part A: Molecular and Biomolecular Spectroscopy. 2020 May;232:118146.

163. Liu X, Huang D, Lai C, Zeng G, Qin L, Zhang C, et al. Recent advances in sensors for tetracycline antibiotics and their applications. TrAC - Trends in Analytical Chemistry [Internet]. 2018 Dec 1 [cited 2022 Feb 3];109:260–74. Available from: https://linkinghub.elsevier.com/retrieve/pii/S0165993618300888

164. Malekzad H, Jouyban A, Hasanzadeh M, Shadjou N, de la Guardia M. Ensuring food safety using aptamer based assays: Electroanalytical approach. TrAC - Trends in Analytical Chemistry. 2017 Sep;94:77–94.

165. Wu T, Jiang Q, Wu D, Hu Y, Chen S, Ding T, et al. What is new in lysozyme research and its application in food industry? A review. Food Chemistry. 2019;274(March 2018):698–709.

166. Callewaert L, Michiels CW. Lysozymes in the animal kingdom. Journal of Biosciences. 2010;35(1):127–60.

167. Porstmann B, Jung K, Schmechta H, Evers U, Pergande M, Porstmann T, et al. Measurement of lysozyme in human body fluids: Comparison of various enzyme immunoassay techniques and their diagnostic application. Clinical Biochemistry. 1989;22(5):349–55.

168. Weber P, Steinhart H, Paschke A. Investigation of the allergenic potential of wines fined with various proteinogenic fining agents by ELISA. Journal of Agricultural and Food Chemistry. 2007;55(8):3127–33.

169. Vasilescu A, Wang Q, Li M, Boukherroub R, Szunerits S. Aptamer-based electrochemical sensing of lysozyme. Chemosensors. 2016;4(2):1–20.

170. Park HS, Nahm DH. New occupational allergen in a pharmaceutical industry: Serratial peptidase and lysozyme chloride. Annals of Allergy, Asthma and Immunology. 1997 Feb 1;78(2):225–9.

171. Neethirajan S, Weng X, Tah A, Cordero JO, Ragavan K V. Nano-biosensor platforms for detecting food allergens – New trends. Sens Biosensing Res. 2018;18(February):13–30.

172. Neethirajan S, Weng X, Tah A, Cordero JO, Ragavan K V. Nano-biosensor platforms for detecting food allergens – New trends. Sens Biosensing Res. 2018;18(February):13–30.

173. Hosu O, Selvolini G, Marrazza G. Recent advances of immunosensors for detecting food allergens. Current Opinion in Electrochemistry. 2018;10:149–56.

174. Pi X, Wan Y, Yang Y, Li R, Wu X, Xie M, et al. Research progress in peanut allergens and their allergenicity reduction. Trends in Food Science & Technology. 2019 Sep 15;

175. Jiang H, Guo Q, Zhang C, Sun Z, Weng X. Microfluidic origami nano-aptasensor for peanut allergen Ara h1 detection. Food Chemistry. 2021 Dec 15;365:130511.

176. Gupta RS, Warren CM, Smith BM, Jiang J, Blumenstock JA, Davis MM, et al. Prevalence and Severity of Food Allergies Among US Adults. JAMA Network Open. 2019 Jan 4;2(1):e185630.

177. Food Allergy Research Education. Food Allergy Research Funding [Internet]. Mc Lean (VA). 2016. p. Education and awareness. Available from: http://www.foodallergy.org/advocacy/priorities/research-funding

178. Scherf KA, Poms RE. Recent developments in analytical methods for tracing gluten. Journal of Cereal Science. 2016;67:112–22.

179. FDA (Food and Drug Administration), WHO (World Health Organization). Codex Alimentarius. International Food Standards. 1963.

180. Zhang M, Wu P, Wu J, Ping J, Wu J. Advanced DNA-based methods for the detection of peanut allergens in processed food. TrAC Trends in Analytical Chemistry. 2019 May 1;114:278–92.

181. Wysocka-Żołopa M, Winkler K. Electrochemical synthesis and properties of conical polypyrrole structures. Electrochimica Acta. 2017 Dec 20;258:1421–34.

182. Cernat A, le Goff A, Holzinger M, Sandulescu R, Cosnier S. Micro- to nanostructured poly(pyrrole-nitrilotriacetic acid) films via nanosphere templates: Applications to 3D enzyme attachment by affinity interactions. Analytical and Bioanalytical Chemistry [Internet]. 2014 Feb 21 [cited 2022 Feb 21];406(4):1141–7. Available from: https://link.springer.com/article/10.1007/s00216-013-7135-3

183. Akbar S, Anwar A, Kanwal Q. Electrochemical determination of folic acid: A short review. Anal Biochem [Internet]. 2016 Oct 1 [cited 2022 Feb 21];510:98–105. Available from: https://pubmed.ncbi.nlm.nih.gov/27449133/

184. Metabolism and toxicity of arsenic: A human carcinogen on JSTOR [Internet]. [cited 2022 Mar 7]. Available from: https://www.jstor.org/stable/24105925?seq=1#metadata_info_tab_contents

185. Kempahanumakkagari S, Deep A, Kim KH, Kumar Kailasa S, Yoon HO. Nanomaterial-based electrochemical sensors for arsenic - A review. Biosensors and Bioelectronics. 2017 Sep 15;95:106–16.

186. Ravalli A, Rossi C, Marrazza G. Bio-inspired fish robot based on chemical sensors. Sensors and Actuators, B: Chemical. 2017 Feb 1;239:325–9.

187. Rapini R, Cincinelli A, Marrazza G. Acetamiprid multidetection by disposable electrochemical DNA aptasensor. Talanta. 2016;161:15–21.

188. Selvolini G, Băjan I, Hosu O, Cristea C, Săndulescu R, Marrazza G. DNA-based sensor for the detection of an organophosphorus pesticide: Profenofos. Sensors (Switzerland). 2018;18(7):1–12.

189. Saberi RS, Shahrokhian S, Marrazza G. Amplified electrochemical DNA sensor based on polyaniline film and gold nanoparticles. Electroanalysis. 2013;25(6):1373–80.

190. Rapini R, Marrazza G. Electrochemical aptasensors for contaminants detection in food and environment: Recent advances. Bioelectrochemistry. 2017;118:47–61.

191. Brett CMA, Brett AMO. Electrochemistry principles methods and applications. New York: Oxford University Press; 1993. 11 p.

192. Bu L, Liu J, Xie Q, Yao S. Anodic stripping voltammetric analysis of trace arsenic(III) enhanced by mild hydrogen-evolution at a bimetallic Au-Pt nanoparticle modified glassy carbon electrode. Electrochemistry Communications. 2015;59:28–31.

193. Negahdary M, Heli H. An ultrasensitive electrochemical aptasensor for early diagnosis of Alzheimer's disease, using a fern leaves-like gold nanostructure. Talanta. 2019 Jun 1;198:510–7.

194. Kayran YU, Jambrec D, Schuhmann W. Nanostructured DNA Microarrays for Dual SERS and Electrochemical Read-out. Electroanalysis. 2019 Feb;31(2):267–72.

195. Cheng TM, Huang TK, Lin HK, Tung SP, Chen YL, Lee CY, et al. (110)-Exposed gold nanocoral electrode as low onset potential selective glucose sensor. ACS Applied Materials and Interfaces. 2010;2(10):2773–80.

196. Trasatti S, Petrii OA. International Union of Pure and Applied Chemistry Physical Chemistry Division Commission on Electrochemistry: Real Surface Area Measurements in Electrochemistry. Pure and Applied Chemistry. 1991;63(5):711–34.

197. Ortiz-Aguayo D, del Valle M. Label-Free Aptasensor for Lysozyme Detection Using Electrochemical Impedance Spectroscopy. Sensors. 2018 Jan;18(2):354.

198. Titoiu AM, Porumb R, Fanjul-Bolado P, Epure P, Zamfir M, Vasilescu A. Detection of Allergenic Lysozyme during Winemaking with an Electrochemical Aptasensor. Electroanalysis. 2019 Nov;31(11):2262–73.

199. Ortiz-Aguayo D, del Valle M. Label-Free Aptasensor for Lysozyme Detection Using Electrochemical Impedance Spectroscopy. Sensors. 2018 Jan;18(2):354.

200. Fang S, Dong X, Ji H, Liu S, Yan F, Peng D, et al. Electrochemical aptasensor for lysozyme based on a gold electrode modified with a nanocomposite consisting of reduced graphene oxide, cuprous oxide, and plasma-polymerized propargylamine. Microchimica Acta. 2016;183(2):633–42.

201. Chen Z, Xu Q, Tang G, Liu S, Xu S, Zhang X. A facile electrochemical aptasensor for lysozyme detection based on target-induced turn-off of photosensitization. Biosensors and Bioelectronics. 2019 Feb;126:412–7.

202. Chen Z, Guo J, Li J, Guo L. Tetrahexahedral Au nanocrystals/aptamer based ultrasensitive electrochemical biosensor. RSC Advances. 2013;3(34):14385–9.

203. Titoiu AM, Porumb R, Fanjul-Bolado P, Epure P, Zamfir M, Vasilescu A. Detection of Allergenic Lysozyme during Winemaking with an Electrochemical Aptasensor. Electroanalysis. 2019 Nov;31(11):2262–73.

204. WHO Global Report on Diabetes. Global Report on Diabetes. Isbn [Internet]. 2016 [cited 2022 Apr 7];978:6–86. Available from: https://sci-hub.si/https://apps.who.int/iris/handle/10665/204874%0Ahttps://apps.who.int/iris/bitstream/handle/10665/204874/WHO_NMH_NVI_16.3_eng.pdf?sequence=1%0Ahttp://www.who.int/about/licensing/copyright_form/index.html%0Ahttp://www.who.int/about/licens

205. Palve YP, Jha N. A novel bilayer of copper nanowire and carbon nanotube electrode for highly sensitive enzyme free glucose detection. Materials Chemistry and Physics. 2020 Jan 15;240:122086.

206. Saei AA, Dolatabadi JEN, Najafi-Marandi P, Abhari A, de la Guardia M. Electrochemical biosensors for glucose based on metal nanoparticles. TrAC Trends in Analytical Chemistry. 2013 Jan 1;42:216–27.

207. Huang JF. Facile preparation of an ultrathin nickel film coated nanoporous gold electrode with the unique catalytic activity to oxidation of glucose. Chemical Communications [Internet]. 2009 Feb 24 [cited 2022 Apr 8];(10):1270–2. Available from: https://pubs.rsc.org/en/content/articlehtml/2009/cc/b819658c

208. Gelband H, Miller-Petrie M, Pant S, Gandra S, Levinson J, Barter D, et al. Executive summary: The state of the world's antibiotics. Center for Disease Dynamics, Economics and Policy. 2015.

209. World Health Organization. ANTIMICROBIAL RESISTANCE Global Report on Surveillance. 2014.

210. Cherlet M, Schelkens M, Croubels S, De Backer P. Quantitative multi-residue analysis of tetracyclines and their 4-epimers in pig tissues by high-performance liquid chromatography combined with positive-ion electrospray ionization mass spectrometry. Analytica Chimica Acta. 2003;492(1–2):199–213.

211. Zhan X, Hu G, Wagberg T, Zhan S, Xu H, Zhou P. Electrochemical aptasensor for tetracycline using a screen-printed carbon electrode modified with an alginate film containing reduced graphene oxide and magnetite (Fe3O4) nanoparticles. Microchimica Acta. 2016;183(2):723–9.

212. Jamal M, shareef M, Sajid S. Lincomycin and tetracycline resistance in poultry. Review. Matrix Science Pharma. 2017 Jan;1(1):33–8.

213. Alawad A, Istamboulié G, Calas-Blanchard C, Noguer T. A reagentless aptasensor based on intrinsic aptamer redox activity for the detection of tetracycline in water. Sensors and Actuators B: Chemical. 2019 Jun 1;288:141–6.

214. Peres GT, Rath S, Reyes FGR. A HPLC with fluorescence detection method for the determination of tetracyclines residues and evaluation of their stability in honey. Food Control. 2010 May 1;21(5):620–5.

215. Ibarra IS, Rodriguez JA, Miranda JM, Vega M, Barrado E. Magnetic solid phase extraction based on phenyl silica adsorbent for the determination of tetracyclines in milk samples by capillary electrophoresis. Journal of Chromatography A. 2011 Apr 22;1218(16):2196–202.

216. Heydari-Bafrooei E, Askari S. Ultrasensitive aptasensing of lysozyme by exploiting the synergistic effect of gold nanoparticle-modified reduced graphene oxide and MWCNTs in a chitosan matrix. Microchimica Acta. 2017;184(9):3405–13.

217. Han Q, Wang R, Xing B, Chi H, Wu D, Wei Q. Label-free photoelectrochemical aptasensor for tetracycline detection based on cerium doped CdS sensitized BiYWO6. Biosensors and Bioelectronics. 2018;106(January):7–13.

218. Jambrec D, Gebala M, La Mantia F, Schuhmann W. Potential-Assisted DNA Immobilization as a Prerequisite for Fast and Controlled Formation of DNA Monolayers. Angewandte Chemie International Edition. 2015 Dec 7;54(50):15064–8.

219. Kayran YU, Jambrec D, Schuhmann W. Nanostructured DNA Microarrays for Dual SERS and Electrochemical Read-Out. Electroanalysis. 2018;1–7.

220. Jambrec D, Gebala M, La Mantia F, Schuhmann W. Potential-Assisted DNA Immobilization as a Prerequisite for Fast and Controlled Formation of DNA Monolayers. Angewandte Chemie International Edition. 2015 Dec 7;54(50):15064–8.

221. Deng M, Wang H, Geng S, Guan X, Liang N. Application of an alkali destruction technique and natural deep eutectic solvent for greener extraction from peanut shells: optimization and extraction kinetics study. Analytical Methods [Internet]. 2022 [cited 2022 Apr 5]; Available from: http://xlink.rsc.org/?DOI=D1AY02033A

222. Montserrat M, Sanz D, Juan T, Herrero A, Sánchez L, Calvo M, et al. Detection of peanut (Arachis hypogaea) allergens in processed foods by immunoassay: Influence of selected target protein and ELISA format applied. Food Control. 2015 Aug 1;54:300–7.

223. Malecka K, Mikuła E, Ferapontova EE. Design Strategies for Electrochemical Aptasensors for Cancer Diagnostic Devices. Sensors (Basel) [Internet]. 2021 Feb 1 [cited 2022 Apr 27];21(3):1–41. Available from: https://pubmed.ncbi.nlm.nih.gov/33499136/

224. Girolamo A de, McKeague M, Pascale M, Cortese M, DeRosa MC. Immobilization of Aptamers on Substrates. Aptamers for Analytical Applications [Internet]. 2018 Oct 26 [cited 2022 Apr 27];85–126. Available from: https://onlinelibrary.wiley.com/doi/full/10.1002/9783527806799.ch3

225. Balamurugan S, Obubuafo A, Soper SA, Spivak DA. Surface immobilization methods for aptamer diagnostic applications. Analytical and Bioanalytical Chemistry [Internet]. 2008 Feb 23 [cited 2022 Apr 27];390(4):1009–21. Available from: https://link.springer.com/article/10.1007/s00216-007-1587-2

226. Riu J, Giussani B. Electrochemical biosensors for the detection of pathogenic bacteria in food. TrAC Trends in Analytical Chemistry. 2020 May 1;126:115863.

227. Farzin L, Shamsipur M, Sheibani S. A review: Aptamer-based analytical strategies using the nanomaterials for environmental and human monitoring of toxic heavy metals. Talanta. 2017 Nov 1;174:619–27.

228. Tran DT, Knez K, Janssen KP, Pollet J, Spasic D, Lammertyn J. Selection of aptamers against Ara h 1 protein for FO-SPR biosensing of peanut allergens in food matrices. Biosensors and Bioelectronics. 2013 May 15;43(1):245–51.

229. Jiang H, Guo Q, Zhang C, Sun Z, Weng X. Microfluidic origami nano-aptasensor for peanut allergen Ara h1 detection. Food Chemistry. 2021 Dec 15;365:130511.